Three-Site Kinetic Model for Selective Catalytic Reduction of NOx with Ammonia over a Commercial Catalyst for Calibration of Aftertreatment Systems in Diesel Powered Heavy Duty Vehicles

by

Gülden Hazal Karadağ

A Dissertation Submitted to the

Graduate School of Sciences and Engineering

in Partial Fulfillment of the Requirements for

the Degree of

Master of Science

in

Chemical and Biological Engineering

KOÇ UNIVERSITY

August 2017

Three-Site Kinetic Model for Selective Catalytic Reduction of NOx with Ammonia over a Commercial Catalyst for Calibration of Aftertreatment Systems in Diesel Powered Heavy Duty Vehicles

Koç University

Graduate School of Sciences and Engineering

This is to certify that I have examined this copy of a master's thesis by

Gülden Hazal Karadağ

and have found that it is complete and satisfactory in all respects,

and that any and all revisions required by the final

examining committee have been made.

Committee Members:

____
Prof. Can Erkey (Advisor)

____
Prof. Metin Türkay

____
Asst. Prof. Ayşe Bayrakçeken Yurtcan

Date: 24.08.2017

to my family; Ünal, Nurhan, Sibel, Deniz, Leo & Fındık

ABSTRACT

Selective catalytic reduction (SCR) of nitrogen oxides (NOx) with ammonia is an efficient process for NOx abatement in diesel powered heavy duty vehicles. In the first part of this study, mass transfer limitations for standard SCR reaction in a monolith reactor over a commercial copper-chabazite (Cu-CHA) washcoated catalyst were investigated using a single reaction model. Results revealed that the intrinsic kinetic parameters obtained at low temperatures cannot account for SCR activity at higher temperatures and external mass transfer limitations exist at temperatures above 350 ˚C. Accordingly, in the second part, a multi-site kinetic model, in combination with internal and external mass transfer effects, was developed for ammonia SCR of NOx over Cu-CHA. NH_3 adsorption & desorption, NH_3 oxidation, NO oxidation and standard SCR reactions as well as the N_2O formation reactions were studied separately in the temperature range of 100 to 600 °C using a monolith reactor. NH_3 adsorption and desorption profiles showed good agreement with a kinetic model based on three different sites for ammonia storage on Cu-CHA. These three sites are believed to be monocopper species located near/on 6-membered ring of the chabazite structure, copper oxide clusters or coppers which move to the large cages at high temperatures and sites on which ammonia binds loosely. Site densities and coefficients of the mass transfer coefficient correlation for square channeled cordierite honeycomb monoliths, ($Sh = A(1 + B(Re)(Sc)(d_h/L))^C$), were regressed from NH_3 adsorption breakthrough and temperature programmed desorption data. The activation energies and pre-exponential factors for NH_3 adsorption & desorption, NH_3 oxidation, NO oxidation, standard SCR, and N_2O formation reactions were also regressed from experimental data. The three site kinetic model is in excellent agreement with the experimental data at a wide temperature range (100 to 600 °C). The model also predicted very well standard SCR reactor effluent composition at different flow rates, which were not considered during the parameter estimation. Findings of this study revealed that correlations in the literature for estimation of mass transfer coefficients in monolith reactors were not appropriate for these systems (NH_3-SCR). Therefore, mass transfer coefficients should be regressed from experimental data at conditions of interest for accurate prediction of SCR activity.

ÖZET

Azot oksitlerin (NOx) amonyak ile seçici katalitik indirgenmesi (SCR) dizelle çalışan ağır iş araçlarında NOx azaltılması için etkili bir yöntemdir. Bu çalışmanın ilk kısmında, bakır-kabazit (Cu-CHA) ile kaplanmış monolit bir reaktör içerisinde gerçekleşen standart SCR reaksiyonunun kütle transferi sınırlandırmaları tek reaksiyon modeli kullanılarak incelenmiştir. Aldığımız sonuçlara göre, düşük sıcaklıkta elde edilen esas kinetik parametreleri kullanarak yüksek sıcaklıktaki SCR aktivitesi doğru hesaplanamamaktadır. Ayrıca dış kütle transfer kısıtlamaları 350 °C'nin üstünde etkilerini göstermeye başlamaktadır. Buna göre, çalışmanın ikinci kısımda, Cu-CHA katalizöründeki NOx'un amonyak SCR ile indirgenmesi için iç ve dış kütle transfer kısıtlamalarını da içeren çok siteli bir kinetik model geliştirilmiştir. Monolit reaktörde NH_3 adsorpsiyon ve desorpsiyon, NH_3 oksitlenmesi, NO oksitlenmesi, standart SCR reaksiyonu ve ek olarak N_2O oluşumu reaksiyonları 100 ila 600 °C arasında ayrı ayrı incelenmiştir. Cu-CHA üzerinde 3 farklı amonyak depolama sitesi olduğunu varsayan kinetik modelden elde edilen NH_3 adsorpsiyon ve desorpsiyon profili ile deneyden elde dilen profil iyi uyum göstermiştir. Bu 3 sitenin kabazitin 6-üyeli halkasının yakınına/üstüne bağlanan 1-bakır türleri, bakır-oksit kümelenmeleri ya da yüksek sıcaklıkta zeolitin daha büyük kısımlarına göç eden bakırlar ve amonyağın zayıf bağ ile bağlandığı yerler olduğu düşünülmektedir. NH_3 adsorpsiyon, breakthrough ve sıcaklık programlı desorpsiyon verisi kullanılarak site yoğunlukları ve kare kanallı kordirit arı kovanı tipi monoliti için kütle transfer katsayısı korelasyonundaki katsayılar, ($Sh = A(1 + B(Re)(Sc)(d_h/L))^C$), bulunmuştur. Ayrıca NH_3 adsorpsiyon & desorpsiyon, NH_3 oksitlenmesi, NO oksitlenmesi, standart SCR reaksiyonu ve de N_2O oluşumu reaksiyonlarının aktivasyon enerjileri ve pre-eksponensiyel katsayıları da deneysel verilerden elde edilmiştir. 3-siteli kinetik model sonuçları geniş bir sıcaklık aralığında (100 den 600 °C'ye) deneysel veriler ile mükemmel uyum göstermiştir. Parametre bulma esnasında kullanılmayan, farklı reaktör çıkışı akış hızlarına sahip standart SCR deneylerinin sonuçları da model sonuçları ile uyumlu bulunmuştur. Bu çalışmanın sonucunda literatürdeki monolit reaktörler için önerilen kütle transfer katsayısı korelasyonlarının bu tarz sistemler (NH_3-SCR) için uygun olmadığı gösterilmiştir.

ACKNOWLEDGEMENTS

I would like to express my sincere gratitude to my advisor Prof. Can Erkey for the continuous support during my master; for his patience, motivation, and immense knowledge. His guidance helped me all the time during the research. All of the discussions with him and brain storms we made in front of the white board helped me to shape my ideas about pursuing an academic carrier. I could not have imagined having a better advisor and mentor for my M.Sc. study.

I am also grateful to Dr. Selmi Erim Bozbağ for his precious guidance, suggestions, critical reviews, and above all his tolerance to my countless questions throughout the project. I would like to express my deepest gratitude for his timely advice which provided me the right direction whenever I felt confused.

I also would like to sincerely thank to my thesis committee members, Prof. Metin Türkay and Assoc. Prof. Ayşe Bayrakçeken for sparing their valuable time for me and for their insightful comments which incented me to widen my research from various perspectives. I would like to express my gratitude to Prof. Mehmet Somer and his lab for their generosity whenever I need a chemical or lab equipment. I am also grateful to İlyas Kızıloğlu for his unconditional help in the grammar check of my thesis.

I gratefully acknowledge the financial support from Koç University Graduate School of Science and Engineering and Ford Otosan.

I would like to thank all of my friends from Koç University and lab mates for sustaining quite peaceful and compatible research environment. I would particularly like to single out my dear friends Seçil Ünsal, Salim Şimşek, Ekin Eşen, Zeynep İnönü, Hande Güneş, Göktuğ Gönel and Ehsan Sarayloo for all the fun we have had in our coffee breaks at Koç University and also for the glorious events in Sariyer. Seçil is one of the people since I knew from the very beginning. We started our bachelor's degrees together and now we are getting our master degrees together. I cannot imagine a PhD life without her. I believe that we will continue to walk together. So many thanks also go to Salim for the sleepless thesis nights we were working together. You gave me strength in those desperate days, I probably could not complete this journey without you. I will definitely miss Ekin so much, he is the most compatible and friendly person I have ever met. Zeynep, you always gave me courage whenever I felt lost or helpless when struggling with a problem. She always has the best advices. Hande is one of the sweetest person I know, I regret that we met so late. I definitely wish to spend more time with her. I will miss all of you a lot and also our times at the engineering courtyard.

Many thanks go to my friends from Ankara for all the fun we had and for the amazing holidays and festivals. You have relieved me and gave me the strength whenever I felt alone in İstanbul.

I must express my very profound gratitude to my family for providing me with unfailing support and continuous encouragement throughout my endless years of study and research, and also during my entire life. This thesis is dedicated to you. None of my achievements have been possible without you, I love you so much!

I am deeply grateful to my dear friend Houman Bahmani Jalali for all the adventures, conversations and numerous dinners. You are one of the people who encourage me to continue for pursuing an academic career. But most importantly, you are the person who made this long two years in İstanbul easier, lovable and funnier. I am definitely sure that we will be there for each other whenever we need the most.

I am also grateful to Yalçın Kırkık for countless conversations, guidance and life experiences. I have been started to this academic journey under favour of your encouragement. Thank you for all the valuable lessons, they made me who I am today.

Last but not least, I would like to express my deepest gratitude to my girls; Ecem Boğatemur and Bilge Tunç. You are the people that I can always count on to share all of my thoughts without any hesitation. You inspired me during the difficult times when I needed words of encouragement. I am not good at expressing my emotions but you do not even know how much your help meant to me. I cannot even imagine a single day without talking with you. “You are my sisters and not by something as accidental as blood, by something much stronger. By choice.”

TABLE OF CONTENTS

LIST OF FIGURES

LIST OF TABLES

NOMENCLATURE

a_j	Active site density of reaction j (mol-site/m^3)
A	Channel geometry term in Sherwood Number correlation (dimensionless)
A_i	Pre-exponential factor (1/s)
A_k	Active site density for coverage k (mol-site/m^3)
B	Surface roughness term in Sherwood Number correlation (dimensionless)
C	Constant in Sherwood Number correlation (dimensionless)
D	Sutherland's constant (dimensionless)
D_{AB}	Binary diffusion coefficient of A in B (m/s^2)
C_1	Concentration at bulk phase (mol/m^3)
C_{1i}	Concentration at interphase (mol/m^3)
C_{NO}^b	Concentration of NO in the bulk gas phase (mol/m^3)
C_{NO}^w	Concentration of NO at the washcoat wall (mol/m^3)
C_{NO}^*	Concentration of NO in the washcoat (mol/m^3)
d_h	Hydraulic diameter of a channel (m)
$D_{eff,i}$	Effective diffusivity of species i (m^2/s)
$D_{eff,NO}$	Effective diffusivity of NO in the washcoat (m^2/s)
$D_{NO\text{-}air}$	Diffusivity of NO in air (m^2/s)
E_a	Activation energy for standard SCR reaction (J/mol)
E_i	Activation energy for reaction i (kJ/mol)
$E_{i,0}$	Activation energy for reaction i at zero coverage (kJ/mol)
f	Collision function (dimensionless)
f_c	Solid fraction of washcoat (dimensionless)
k	Boltzmann's constant (m^2.kg/s^2.K)
k_{app}	Apparent reaction rate constant (m/s)
k_i	Reaction rate constant of reaction i
k_m	External mass transfer coefficient (m/s)
$k_{m,i}$	Mass transfer coefficient for trace species i (kg/m^2.s)
k_{ov}	Overall reaction rate constant (m/s)
k_c^*	Intrinsic reaction rate constant per washcoat thickness (1/s)

L	Length of the monolith (m)
M_i	Molecular weight of species i (g/mol)
N_1	Molar flux to the interphase
$N_{NO,x}$	Molar flux of NO at x = 0 (mol/m^2.s)
p_t	Absolute pressure (Pa)
$r_{NO\text{-}air}$	Molecular separation of NO and air at collision (nm)
r_i	Molecular separation of species i at collision (nm)
r_j	Reaction rate for reaction j mol/(m^3.s)
$\overline{r_{NO}}$	Actual mean reaction rate within pore (mol/m^3.s)
r_{NO}	Reaction rate if not slowed by internal diffusion (mol/m^3.s)
R	Ideal gas constant (Pa.m^3/mol.K)
Re	Reynold's number (dimensionless)
R_i	Species mass rate (kg/m^3.s)
s_{ij}	Stoichiometric coefficient of species i for reaction j (dimensionless)
S	Surface area per reactor volume (m^{-1})
Sc	Schmidt number (dimensionless)
Sh	Sherwood number (dimensionless)
t_w	Washcoat thickness (m)
T	Temperature (°C, K)
T_0	Reference temperature (°C)
$T_{b,NO}$	Normal boiling point of species i (K)
u	Fluid velocity (m/s)
W_i^b	Mass fractions in the bulk gas phase (dimensionless)
W_i^w	Mass fractions at the washcoat wall (dimensionless)

Greek letters

α	Coverage dependence (dimensionless)
ε	void fraction of reactor (dimensionless)
$\varepsilon_{NO\text{-}air}$	Energy of molecular attraction between NO and air (K)
ε_i	Energy of molecular attraction of species i (K)

ρ	Fluid density (kg/m^3)
ρ_s	Density of gas at catalyst surface (kg/m^3)
δ	Washcoat thickness (m)
Υ	Thickness of the thin film on the catalyst surface (m)
φ	Thiele modulus (dimensionless)
ϕ	Tortuosity (dimensionless)
σ	Porosity (dimensionless)
σ	Constriction factor (dimensionless)
θ_k	Component of surface coverage (dimensionless)
μ	Fluid viscosity (Pa.s)
μ_0	Reference fluid viscosity (Pa.s)
η	Effectiveness factor (dimensionless)

Chapter 1

INTRODUCTION

Aftertreatment systems are used to convert harmful nitrogen oxides (NOx), carbon monoxide (CO), volatile hydrocarbons and particulate matters (PM) in the exhaust gas stream to the harmless forms. Strengthen emission standards for these gases reveal the necessity of better after treatment technologies. Nowadays, a combined system consisting of a diesel oxidation catalyst (DOC), a diesel particulate filter (DPF) and a selective catalytic reduction (SCR) unit has gained appreciable attention as an efficient process for heavy duty exhaust gas treatment. The main function of DOC is the oxidation of carbon monoxides (CO), unburned hydrocarbons and nitric oxides (NO), while the DPF is a type of wall-flow filter where exhaust gas enters channels are blocked at the end so that forcing the gas through filter wall but the particulate matters (or soot) are kept inside [1]. On the other hand, selective catalytic reduction (SCR) with ammonia is known as an efficient process for NOx abatement. In this process, NH_3, produced from on-board thermal decomposition of urea [2] is used as a reductant to reduce NOx in excess oxygen environment. Catalysts such as vanadia supported on titania (V_2O_5/TiO_2 promoted with WO_3) [3-7], Fe-exchanged [2, 8-12] and Cu-exchanged [2, 12-17] zeolites have been extensively studied for NH_3-SCR technology. Vanadia-based catalysts generally exhibit poor hydrothermal stability, generate N_2O at high temperatures, have high activity for the undesired oxidation of SO_2 to SO_3, formation of N_2O [18], and decrease in activity and selectivity at 550 °C [19, 20]. Toxic properties of vanadia are also an important issue [19, 20]. The high N_2 selectivity [21] and high NOx removal ability at high temperatures (>350 °C) [2] of iron-based catalysts are well known. However, at the same time, compared to copper-based catalysts, iron based catalysts have lower activity at low temperature range, relatively higher N_2O formation from the thermal decomposition of NH_4NO_3 [21] and lower ammonia uptake capacity [22]. These factors restrict the applicability of iron based catalysts.

Therefore, copper-zeolites with fairly good NH_3-SCR activity at low temperatures, N_2 selectivity [21] and ammonia uptake capacity [22] have received considerable attention in the past few years. A wide variety of copper containing zeolites with medium and large-pore sizes (i.e. Cu-MOR, Cu-BEA, and Cu-FAU) exist. Even though Cu-ZSM-5 has remarkable NO conversion activity and selectivity [14, 23], its low hydrothermal stability at high temperatures due to dealumination in the zeolite framework [24, 25] is a significant drawback. Recently, small-pore size zeolites with the chabazite (CHA) structure have been attracting increased attention due to their excellent catalytic activity for NO decomposition in exhaust gas streams and enhanced hydrothermal stability with high hydrocarbon resistance [26-30]. Especially, Cu-SSZ/13 and Cu-SAPO/34 (zeolites with the CHA structure) have been shown to demonstrate superior performance due to their excellent catalytic activity for NO decomposition in exhaust gas streams and enhanced hydrothermal stability with high hydrocarbon resistance [26-30]. These catalysts are washcoated inside the channels of honeycomb structured monoliths, such as cordierite, to prevent pressure drops, clogging of channels by ash and particulate matter, and also to increase the surface area for the SCR reactions [7]. Monolith reactors used in the after treatment technologies mostly operate in fully developed laminar flow regime. When flow passes through the monolith channels, species are transported to the thin washcoat catalyst on the surface of the monolith wall where the SCR reactions take place. The selective catalytic reduction includes a set of reactions which can be divided into three main sections:

1. Standard SCR reaction: Selective catalytic reduction of nitrogen oxides by ammonia on Cu-CHA catalysts is based on the reaction between NO and NH_3 in the presence of O_2 according to the following reaction called *standard SCR*:

$4NO + 4NH_3 + O_2 \longrightarrow 4N_2 + 6H_2O$, $\Delta H_{25°C} = -4.07x10^5$ J/mol NH_3 [2]

2. Fast SCR reaction: When the feed includes both NO and NO_2 at the same time, a much faster reaction takes place:

$$NO + 2NH_3 + NO_2 \longrightarrow 2N_2 + 3H_2O, \Delta H_{25°C} = -3.78x10^5 \text{ J/mol } NH_3 \text{ [2]}$$

3. NO_2 SCR reaction: When the feed includes just NO_2, a much slower reaction than Fast SCR takes place:

$$6NO_2 + 8NH_3 \longrightarrow 7N_2 + 12H_2O, \Delta H_{25°C} = -3.41x10^5 \text{ J/mol } NH_3 \text{ [2]}$$

In addition to these main reactions, many side reactions occur in the SCR reactor. Above 350°C, most of the ammonia is oxidized to nitrogen on the iron and copper exchanged catalysts. This is an undesired reaction since it competes with the standard SCR reaction for NH_3.

$$4NH_3 + 3O_2 \longrightarrow 2N_2 + 6H_2O, \Delta H = -3.12x10^5 \text{ J/mol } NH_3 \text{ [2]}$$

Moreover, nitric oxides are oxidized to nitric dioxides above 150°C which accelerate the reduction reaction (fast SCR).

$$NO + 1/2O_2 \longleftrightarrow NO_2, \Delta H = -5.6x10^4 \text{ J/mol } NH_3 \text{ [2]}$$

Existence of NO_2 species in the feed trigger the ammonium nitrate formation reaction and also above 200°C, ammonium nitrates are decomposed to N_2O.

$$2NH_3 + 2NO_2 \longrightarrow N_2 + NH_4NO_3 + H_2O, \Delta H = –2.91x10^5 \text{ J/mol } NH_3$$

$$NH_4NO_3 \longrightarrow N_2O + 2H_2O \ \Delta H = –3.66x10^4 \text{ J/mol } NH_4NO_3$$

SCR reactions over Cu-CHA are generally described by a complicated mechanism occurring on mono- or di-copper species [31-33] at temperatures below 300 °C. Above this temperature, however, the nature of the active sites have not yet been fully understood.

Development of a detailed reactor model for SCR is important for design and optimization of engine after treatment systems to meet stringent emissions standards. Although the kinetics of SCR reactions on Cu-zeolites have been extensively studied, there are very few reports on the effects of mass transfer limitations in SCR reactors. Besides, there is no comprehensive study of multi-site kinetic model in combination with mass transfer limitations for NH_3-SCR of NOx over Cu-CHA catalyst in the literature. Tronconi et al. showed that internal diffusion limitations in vanadia based washcoated catalysts were significant and most of the inner regions of the catalyst washcoat remained unused [7]. Presence of internal mass transfer limitations for standard SCR reaction on Fe-ZSM-5 at high temperature range (>350 °C) were also revealed by Metkar et al. but the effects of both internal and external diffusion limitations were not clarified for moderate temperatures [34]. Nova et al. investigated the diffusion limitations on Cu-exchanged zeolite catalysts at moderate to high temperatures by using three monoliths with different cell densities, loadings, lengths, and channel shapes [35]. They showed that NOx conversion decreased with decreasing monolith cell density above 350 °C due to both external and internal mass transfer limitations [35] but the individual contributions of the resistances were not explained clearly. In another study, Metkar et al. showed the existence of washcoat diffusion resistances on both Fe-ZSM-5 (>350 °C) and Cu-ZSM-5 (>250 °C) monolithic catalysts [2]. External mass transfer limitations were also found to exist [2]. A recent study by Hu et al. indicated the absence of pore diffusion limitations in standard SCR reactions catalyzed by Cu-SAPO-34 in the temperature range of 150 to 225 °C [27]. They showed that the kinetic parameters extracted from data in this temperature interval are free from pore diffusion effects within the zeolite crystal [27]. Effects of external diffusion limitation were ruled out because the higher temperatures were not considered.

To understand the effects of mass transfer resistances on overall system, external mass transfer coefficients should be estimated for entire temperature range of SCR reactions. Coefficients can be extracted from the correlations for monolith reactors. However, widely diverging results are obtained when different mass transfer correlations in the literature [36-43] are used. Therefore, in this study, we investigated the mass transfer limitations in a monolith reactor with a commercial Cu-CHA catalyst, extracted parameters for a Sherwood number correlation and developed a three-site kinetic model which is applicable for a variety of flow rates and temperatures. Chapter 2 presents a review of origins of automotive emissions, exhaust gas aftertreatment systems for diesel powered engines, selective catalytic reduction (SCR) process, SCR catalysts, kinetic modelling and mass transfer phenomena in monolith catalysts. In Chapter 3, experimental and computational methodology are covered. The methods applied in the experiments and the optimization part are presented in this chapter. Chapter 4 gives a comprehensive view on mathematical model used in this study. Chapter 5 includes experimental and computational results, and provides a detailed discussion of the results. Chapter 6 concludes the thesis by summarizing the work done.

Chapter 2

LITERATURE REVIEW

2.1. Automotive Emissions

Environmental protection is one of the most important subjects of our time. Civilization and rising living standards create a burden on the environment so great that it is having trouble renewing itself. One of the major environmental problems is the air pollution which is generated due to carbon monoxide (CO), sulphur dioxide (principally SO_2), nitrogen oxides (NOx), unburned hydrocarbons (HC), and particulate matter (PM) emissions since they are responsible for the formation of acid rain, photochemical smog, ozone depletion, thus resulting in global warming [44]. Sulphur oxides are normally not removed by the post-combustion or after treatment systems because the only effective way is to convert them into elemental sulphur, which would accumulate in the filtration system. Therefore, it is preferred to minimize the emissions originated from sulphur compounds by decreasing the sulphur content in the fuel [45]. Relative impacts of nitrogen oxides, carbon monoxides and unburned hydrocarbons on humans are estimated as 100 : 1 : 0.1, respectively [46]. Therefore, NOx gases can be thought of as the most harmful emission among those species. There are two major sources of nitrogen oxides which come from stationary sources like power plants, industrial heaters, cogeneration plants, [47] and mobile sources like internal combustion engines [48-50]. Figure 2.1 shows that nitrogen dioxides are formed mostly by transport, followed by the energy generation plants and heavy & light industries [46].

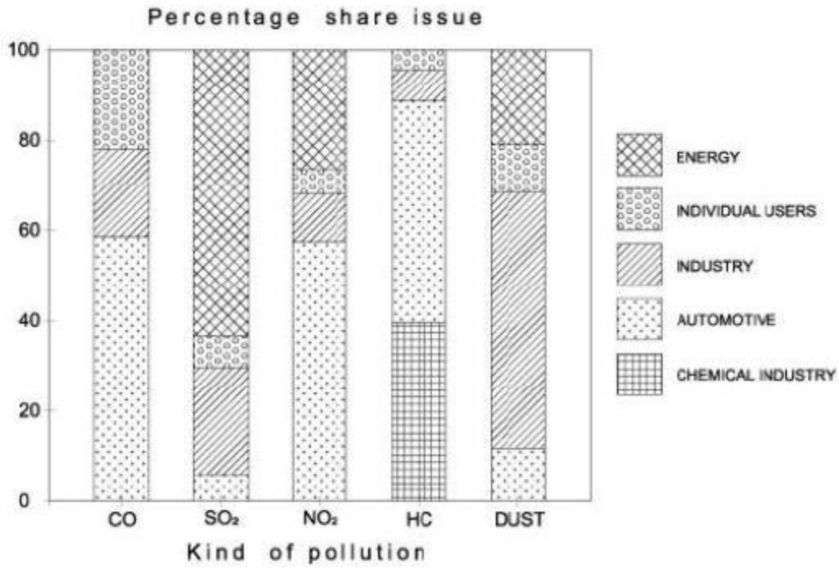

Figure 2. 1. Origin of air pollutants throughout the world, 2011 [46]

In the mobile sources, energy is obtained from the combustion of fossil fuels in the engine. Burning of crude oil theoretically generates only CO_2 and H_2O but this is not the case in reality due to incomplete combustion. High temperatures in the combustion chamber leads to formation of other harmful pollutants which need to be converted into harmless forms [45].

2.1.1. Gasoline and Diesel Engines

Chemical energy obtained from fuel is converted into mechanical energy by the combustion process both in the diesel and gasoline engines. The way of combustion is actually the major difference between these two systems. In a gasoline engine, fuel is mixed with air, mixture is compressed and then ignited by a spark from spark plug while in a diesel engine, air is not mixed with fuel in the intake stroke step. Instead, it is compressed and then ignited with a fuel injection rather than using a spark plug. Fuel auto ignition is generated by high temperatures and compression in the combustion chamber. Compression is around 2 times higher in a diesel engine (14:1 to 25:1) than a gasoline engine (8:1 to 12:1). High compression ratios in the gasoline engine can start fuel auto ignition which may result in engine knock or detonation [51]. Since this process creates excess heat, knocking can destroy engines. In other respects, higher compression ratios yield to higher thermal efficiencies and better fuel economies which makes diesel engine more desirable.

Mechanics are not the only difference between these engines as the fuel itself and the operating conditions also vary. Diesel fuel contains more carbon atoms (~14) than gasoline (~9), has higher energy density, emits less CO, CO_2 and NOx and is cheaper because it requires less refining. Restrictive emissions standards compel lean-burn engines to increase the amount of air in the air/fuel ratio, which can worsen the quality of the combustion but decreases the NOx emission. Lean-burn and direct injected common rail turbo-charged diesel engines are more efficient in terms of fuel economy and power density as opposed to rich-burn gasoline engines. This is because lean-burn and direct injected common rail turbo-charged engines operate with excess amounts of air (up to twice the amount needed for complete combustion). The excess air effectively cools down the combustion temperatures in the engine cylinder which decreases nitrogen oxide generation (by nearly half) and creates low engine exhaust emission without the need for an aftertreatment system in light duty vehicles (i.e. passenger cars). Fuel economy is also achieved, because the combustion process is more efficient since more air is available. Therefore, more power can be generated from the same amount of fuel in the lean-burn vehicles. On the other hand, rich burn engines operate under near stoichiometric air/fuel ratios which mean exactly enough air is sent to burn all of the fuel. They can provide lower emission levels with a single after treatment system (three-way catalyst), are more tolerant to ambient conditions, can operate on a broad variety of natural gas fuels, and usually have better transient load capability.

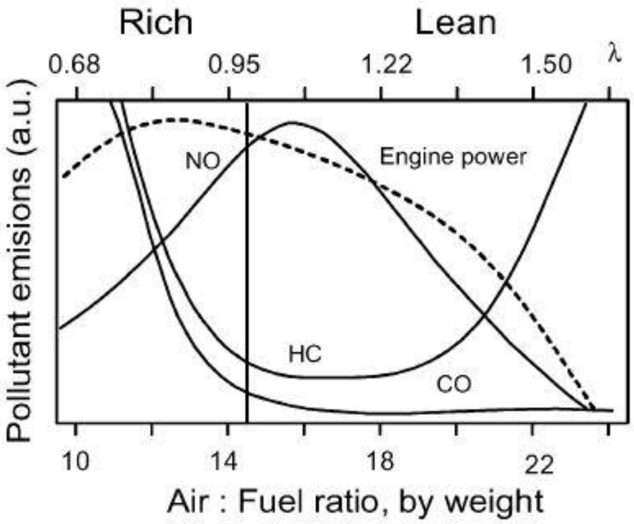

Figure 2. 2. Effect of A/F ratio (w/w) on engine emissions and engine power [45]

Combustion temperatures (≤800–850 °C for lean burn engine and ~1000 °C for rich burn engine) of lean burn condition seem to generate lower amounts of NOx. However, high air/fuel ratio result in engine misfire which yields high hydrocarbon emission [45]. Moreover, although lean-burn engines do not require an after treatment system in the beginning (they use an exhaust gas recirculation system), stricter emission standards reveal the necessity of additional systems for the effective removal of harmful emissions. A more complex after treatment system was already necessary for the heavy duty vehicles because they produce emissions untreatable with a single recirculation system. Thus, lean-burn engines are generally integrated with the combined system of diesel oxidation catalyst (DOC), diesel particulate filter (DPF) and selective catalytic reduction (SCR) to reach the lowest possible CO, HC, PM and NOx emission levels in the exhaust gas stream which will be explained in detail.

2.1.2. Emissions from the Diesel Engine

Diesel fuel is mostly composed of carbon and hydrogen. Ideally, at the end of complete combustion, only carbon dioxide and water are generated. However, many reasons like combustion temperature, ratio and concentration of air/fuel ratio, ignition time and fluctuations in the combustion chamber make complete combustion impossible and lead to the generation of harmful emissions. The emission of pollutants (CO, HC, NOx, PM) constitute less than 1% of the exhaust gas stream, the highest proportion of which belongs to nitrogen oxides (more than 50%). Particulate matters (i.e. soot) have the second highest amount since the lean burn operating condition of diesel engines minimizes the generation of other species. In addition, exhaust gas also includes some sulphur oxide species that depend on the quality and specifications of the fuel. Nowadays, harmful effects of sulphur oxides can be prevented by the usage of ultra-low sulphur diesel (ULSD) fuel [52].

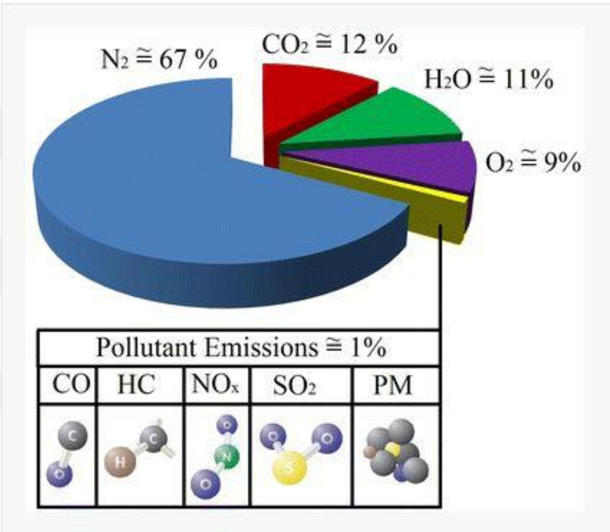

Figure 2. 3. Diesel exhaust gas composition [52]

2.1.3. Carbon Monoxide (CO) Emission

Incomplete combustion also results in carbon monoxide formation the amount of which is mostly dependent on air/fuel mixtures, maximized when the excess air factor is smaller than one (rich burn condition). Although the deficiency of air in the rich burn condition causes carbon monoxide formation, a small amount of CO is also produced under lean burn conditions due to kinetic effects [52]. Generation of carbon monoxide species increases when swirl or insufficient turbulences occur in the combustion chamber. CO is an odorless and colorless gas that can be inhaled and transmitted into the bloodstream of living organisms. Breathing air with a high concentration of CO reduces the amount of oxygen that can be transported in the blood stream to critical organs like the heart and brain by binding to hemoglobin and inhibiting its capacity to transfer oxygen. High CO concentrations in the air can cause asphyxiation, resulting in the slowing of reflexes, confusion, dizziness, unconsciousness, and even death [53].

2.1.4. Hydrocarbon (HC) Emission

Insufficient temperatures near the engine cylinder wall (lower than the temperature at the cylinder center) inhibit the burning of fuel, generating hydrocarbon emission. Lean burn operating conditions normally result in low amounts of hydrocarbons made up of alkanes, alkenes and aromatics. This pollutant is generally produced in light duty vehicles where combustion does not always occur due to low flame speeds[52].

Furthermore, the fuel type, engine adjustment and design, irregular operating conditions (such as instantaneous change in engine speed), fluctuations in injection, excessive nozzle cavity volumes, and injector needle bounce may result in formation of high amounts of unburned hydrocarbons. However, hydrocarbon emissions from tailpipes are lower than those leaving the engine because at over 600 °C, hydrocarbons continue to burn until they leave the tailpipe (if exposed to oxygen). Hydrocarbon emissions from tailpipes are around 50-60% of the total hydrocarbon emissions from vehicles. Hydrocarbon emissions can also occur from the crankcase, fuel system (responsible for 20–35 % of emissions), and from more indirect methods such as atmospheric venting of vapors during fuel distribution and dispensing (responsible for 15–25 % of emissions). These pollutants are harmful for both humans and environment, especially when they combine with other harmful gases. They can form ground level ozone and also are toxic with the potential to cause respiratory tract irritation and cancer [52].

2.1.5. Particulate Matter (PM) Emission

Particle composition of diesel exhaust gas typically includes 41% carbon, 7% unburned fuel, 25% unburned oil, 14% combination of sulfates & water, 13% ash and other species [54]. Particulate matter emission originate mostly from the incomplete combustion of fuel and lube oil but can also result from an agglomeration of very small particles of partially burned fuel, ash content of fuel oil & cylinder lube oil. Combustion temperature, exhaust gas cooling, and fuel and lubrication oil quality can also affect combustion quality and cause partial burning in the engine cylinder. In fact, PM emissions are around six to ten times higher in diesel engines than the gasoline ones. Diesel PM emissions can be classified into three major components: soot, soluble organic fraction (SOF), and inorganic fraction (IF). Soot is a granular particle which constitutes more than half of the total particulate matter emission. When heavy hydrocarbons are adsorbed or condensed on soot (especially at low exhaust gas temperatures), soluble organic fractions are observed in the exit stream.

Particulates matters are very small, spherical particles typically with a diameter of less than 1 μm. Inhaling these components can lead to premature death, asthma, lung cancer, and other cardiovascular problems. Moreover, they are pollutants to air, water, and soil because they can reduce visibility and impact agricultural productivity [52].

2.1.6. Nitrogen Oxide (NOx) Emission

The oxidation reaction of nitrogen in the air is thermodynamically difficult. However, because temperatures above 1600 C are reached in engine cylinders, nitrogen can react with oxygen easily. Therefore, the most important aspects of NOx formation are the temperature and oxygen concentrations during combustion. These two influences and the residence time are the parameters that determine the amount of NOx produced. The temperature of the flame is at its highest when the piston in the cylinder is near the top of its stroke. Most of the nitrogen oxides are formed during this time of the combustion process [52]. As this temperature increases, the amount of NOx increases by three fold for every 100 °C increase in the combustion chamber [55].

The main sources of nitrogen oxide emissions come from motor vehicles (55%) and industrial & commercial combustion processes (45%) [49]. Due to industrialization and rising living standards, fossil fuel usage has increased since the last century. It directly increases the amount of pollutants in the air originated from the combustion of fossil fuels. The other important source of nitrogen oxides is production and use of nitric acid (nitrification and oxidation of organic compounds) [49].

Natural sources of nitrogen oxides are known. An example of this is illustrated in the oxidation of ammonia, lightning, and volcanic activities. However, these are not as crucial as anthropogenic ones [49].

Several types of nitrogen oxides such as N_2O, NO, NO_2, N_2O_3, N_2O_4, NO_3, and N_2O_5 exist in the environment. The abbreviation NOx usually refers to nitrogen monoxide (NO), nitrogen dioxide (NO_2) and nitrous oxide (N_2O), which are called 'fresh' nitrogen oxides because they can reach atmosphere in these forms [49]. Most of the nitrogen oxides include NO (85-95%), which is gradually converted to nitrogen dioxide in the environment. Although nitrous oxide (N_2O), i.e. laughing gas, is also defined as a nitrogen oxide compound, there are no emission regulations related to it in the Europe region. However, recent studies show that nitrous oxides are one of the contributors of global warming therefore it is expected that the reduction technologies for N_2O will be studied in near future. N_2O adsorbs IR radiation 270 times more intensely than CO_2. In addition, it can contribute to ozone depletion by taking part in photochemical reactions in the stratosphere. Although nitrous oxide has a longer half-life (100-150 years) than nitrogen monoxide and dioxide, it is not as reactive as NO and NO_2 [49].

Transportation sources (light and heavy duty vehicles) are major contributors (40-70%) of urban NOx pollution, with diesel engine powered vehicles being the main culprit (as a result of higher operating temperatures). In fact, 85% of the total NOx released from mobile sources (mainly in the form of NO) are due to the diesel engines [55, 56]. These gases are responsible for a significant amount of environmental and health problems. NOx emissions cause photochemical smog, acid rain, and the formation of ozone. They also cause material loss as illustrated in the destruction of buildings, monuments and crops. They are considered as ground-level ozone precursors [49] and can react with other species in the atmosphere (VOC, for instance) to produce tropospheric ozone which is the main component of smoke around big cities. Tropospheric ozone formation reactions can be seen below [57]:

$$NO_2 + h\nu(\lambda < 415\ \text{nm}) \rightarrow NO + O^*$$

$$O_2 + O^* \rightarrow O_3$$

By the photochemical chain reactions of nitrogen oxides, other compounds like peroxyacetylene nitrates (PAN) can be formed too:

$NO_2 + hv \rightarrow NO + O^*$
$H_2O + O^* \rightarrow 2OH^*$
$CH_3\text{-}CHO + OH^* \rightarrow CH_3CO^* + H_2O$
$CH_3\text{-}CO^* + O_2 \rightarrow CH_3\text{-}CO^*$
$CH_3\text{-}CO^* + NO_2 \rightarrow CH_3\text{-}CO_3\text{-}NO_2$

The main source of these compounds are vehicles, as they are known as more harmful to living organisms than ozone because their contributions to photo-oxidizing pollution.

Because different atmospheric layers have different chemical compounds, the reactions that occur in them may vary for each layer has different compounds in various concentrations. Since a variety of molecules can be found in different layers (meso-, strato-, troposphere etc.) of the atmosphere, various types of wavelengths are absorbed subsequently followed by a wide range of solar radiations [48].

Many problems arise when pollutants build up in the atmosphere, one of which is known as acid rain. Acid rains can affect both terrestrial and aquatic systems. In recent years, the environment and other ecological ecosystems have been forced to cope with the deforestation of the northern hemisphere from water acidification. Acid rains are the main contributors of deforestation in which nitric oxides are oxidized by ozone while OH^* and HO_2 radicals are converted into NO_2, HNO_2 and HO_2NO_2. Generally, acid rain forms high up in the cloud where nitrogen oxides react with water, oxygen and other species. These compounds are converted into nitric acid which then acidifies rain, snow or fog because of its solubility in water. Thus, nitrogen oxide gases play a critical role in the photochemistry of stratosphere. Acid precipitation or accumulation can affect the organisms in aquatic ecosystem and can cause death in lakes and rivers. Chemical reactions (photochemical processes, thermal gas-phase processes, dry deposition, and heterogeneous reactions) of this transformation can be seen in Figure 2.4 and 2.5 [57].

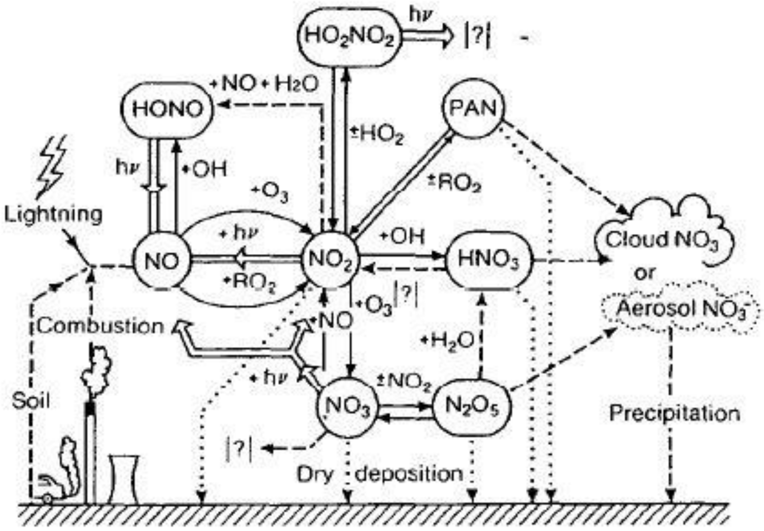

Figure 2. 4. Chemical transformation of nitrogen oxide species in the atmosphere [57]

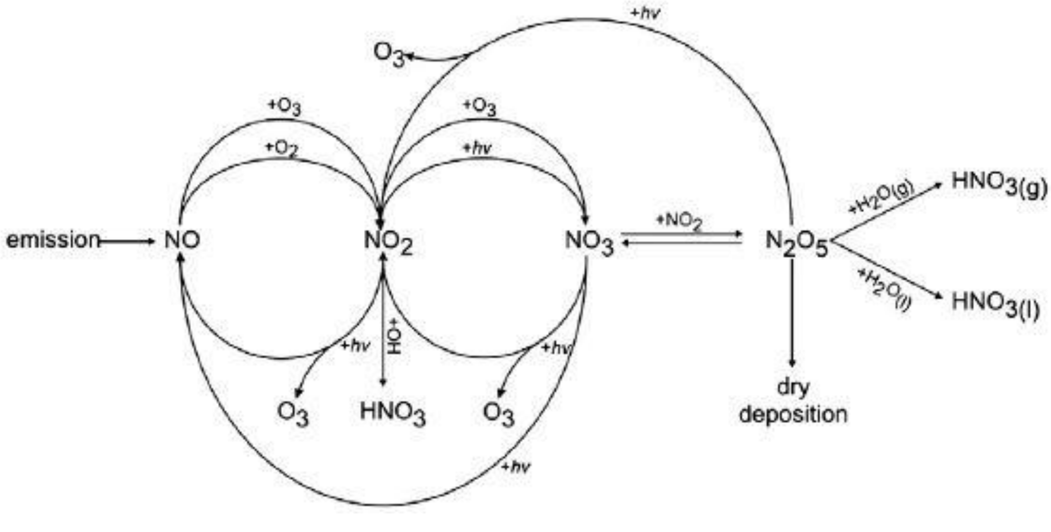

Figure 2. 5. Atmospheric NOx reactions cycle [49]

Recent studies in biological sciences show that NO is an essential messenger which transmits necessary information to the white corpuscles within the bloodstream to destroy tumor cells and assorted bacteria and, in a second role, to the neurotransmitters to dilate the blood vessels. However, while the biologically active NO is a poisonous product of the in vivo enzyme-catalyzed transformation of the amino acid, arginine, and is maintained only at beneficent concentrations, that emitted freely from a car engine presents a real hazard of toxicity. Studies show that exposure of oxides above 0.05 ppm over 24 h is enough to give significant damage to people in good health but this value is often exceeded in big cities with dense traffic or during summer [57].

Oxidation of NO to NO_2 is a very rapid process at high concentrations and the conversion is accelerated with the addition of sunlight and unburned hydrocarbons from fuel. Both of NO and NO_2 gases are considered toxic but nitrogen dioxide has a level of toxicity 5 times greater than nitrogen monoxide. Nitrogen monoxide causes eye and throat irritation. It is an unstable product like most radicals. It reacts with oxygen to form nitrogen dioxide which even the slightest inhalation or ingestion of may result in acute lung injury with pneumonitis and fulminant pulmonary edema, as well as irritate lungs, cause influenza, trigger respiratory allergies and even lead to lung cancer. Often, high nitrogen dioxide content is detected in residential areas where respiratory and cardiovascular diseases, and mortality is high [49].

2.1.7. European Emission Standards

The first regulation for diesel engines was introduced in 1988 but was mainly for particle emissions, due to the type of engine that was used in those years. However, with the beginning of the European Emission Standards, regulations related to hydrocarbons (HC) and NOx emissions were also taken into account. After 1996, regulations became even more stringent therefore the production of diesel engine without an exhaust after-treatment system became impossible [57].

Today, environmental protection has gained a lot of attention due to the increase in greenhouse gases and pollutants in the air. An increase in the amount of pollutants in the atmosphere galvanized the government to establish tighter regulations for the future. The first European Emission Standard (Euro 1) developed in 1993 has been progressively lowered to the current standard, called Euro 6. Emission standards for heavy duty diesel vehicles can be seen in Figure 2.6 [52].

Compared to the first emission standard, Euro 6 standard for carbon monoxide, unburned hydrocarbons, nitrogen oxide, and particular matter emissions were declined 66, 76, 95, and 98 %, respectively [52].

	CO (g/kWh)	HC (g/kWh)	NO_x (g/kWh)	PM (g/kWh)
Euro I	4.5	1.1	8.0	0.61
Euro II	4	1.1	7.0	0.15
Euro III	2.1	0.66	5.0	0.13
Euro IV	1.5	0.46	3.5	0.02
Euro V	1.5	0.46	2.0	0.02
Euro VI	1.5	0.13	0.4	0.01

Figure 2. 6. European Emission Standard for diesel-powered heavy duty vehicle [52]

Mechanical modifications like engine adjustment, electronically controlled fuel injection systems, and also fuel properties have dramatically increased the efficiency and cleanliness of these vehicles. However, these attempts have failed to meet the desired emission limits and after-treatment systems have been employed. Vehicles are rigged with engine control units (ECU) to meet desired emission requirements via controlling the fuel injection pressure and EGR fraction. Engine control unit can be defined as the brain of the engine, which can be developed by an external supplier or directly by the manufacturer itself. Previously, ECU used a feedback control loop where control parameters were chosen by an algorithm that processed input values from one or more sensors in the engine or tail pipe (exhaust gas stream). However, several years ago, this system changed to become a model based control where the control parameters were processed not only from sensor input but also from a matrix or model of the operating conditions of engine [58].

The ECU can generate various fuel injection methods for a specified engine. Higher injection pressures not only improve combustion in the engine cylinder but also lower nitrogen oxide emissions and particle formation. Thus, different injection methods applied by an ECU can create different emission characteristics. Moreover, to control the regeneration of particulate filters, lean NOx catalysts or NOx storage, fuel dosage after the expansion cycle can be increased up to 5 injections per combustion cycle [58].

2.2. Exhaust Gas After-Treatment Systems for Diesel-Powered Engines

Most of the research related to emission control has been performed to reduce NOx emission because nitrogen oxides are the most common pollutant in diesel exhaust gas. In order to eliminate NOx emission, exhaust gas recirculation (EGR), lean NOx trap (LNT) and selective catalytic reduction (SCR) technologies have been developed so far [52].

In the exhaust gas recirculation system, NOx emissions are lowered by recirculating combusted gases back into the combustion chamber so that they can, when mixed with fresh air, decrease combustion temperatures and thus, nitrogen oxide formation. Although this method reduces NOx emissions, a decrease in operating temperature in the engine cylinder worsens combustion efficiency, leading to an increase in hydrocarbon & carbon monoxide emissions as well as soot formation. This system alone cannot fulfill the requirements of the latest emission standards (i.e. Euro 6) [58].

LNT, or lean-NOx trap, aims to reduce nitrogen oxide emissions under lean burn conditions via storing NOx on the catalyst washcoat and then releasing and reacting it under rich burn conditions by conventional three-way catalyst reactions. Catalysts of this system include three main components: oxidation catalyst (Pt), NOx storage material (Ba or other oxides), and a reduction catalyst (Rh). Reaction mechanisms and pathway for LNT system can be seen in Figure 2.7. For oxidation reactions, the most used and effective catalysts are the ones with platinum content due to their low operating temperature and high stability when exposed to water and sulphur. However, this technology requires high operating cost (due to platinum) and still insufficient to fulfill desired regulation for heavy duty vehicles. The method applied in LNT is technically challenging, can entail a fuel penalty and requires very low sulfur amount in the fuel. Therefore, more research should be performed to full commercialization.

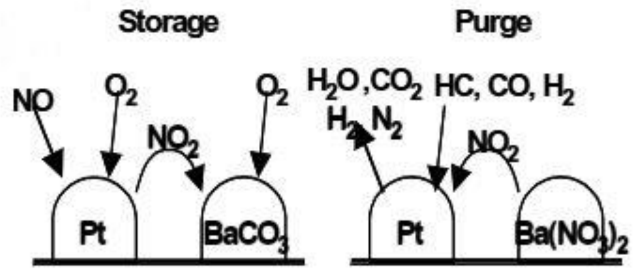

(a)

Oxidation

$$CO + \frac{1}{2}\ O_2 \rightarrow CO_2 \qquad (1)$$

$$C_xH_y + (x + y/4)O_2 \rightarrow xCO_2 + \frac{y}{2}H_2O \qquad (2)$$

Reduction

$$NO + H_2 \rightarrow \frac{1}{2}N_2 + H_2O \qquad (3)$$

$$NO + CO \rightarrow \frac{1}{2}N_2 + CO_2 \qquad (4)$$

$$(2x + y/2)NO + C_xH_y \rightarrow (x + y/4)N_2 + xCO_2 + \frac{y}{2}H_2O \qquad (5)$$

(b)

Figure 2. 7. LNT mechanism (a) [59] and reactions (b) [60]

Rather than these systems, selective catalytic reduction (SCR) technology can be used to fulfill current emission standards. SCR systems can meet Euro 6 standards even after 1000 hours accelerated aging of the catalyst [58].

Diesel powered heavy duty vehicles such as trucks and buses have an integrated system of DOC, DPF and SCR to reduce CO, unburned HC, PM, and NOx emissions. In the next section, emission control systems for heavy-duty vehicles are investigated separately.

2.2.1. Catalytic Emission Control Technologies for Diesel Heavy Duty Vehicles

2.2.1.1. Diesel Oxidation Catalyst (DOC)

The diesel oxidation catalyst (DOC) reduces hydrocarbon and carbon monoxide emissions without any feedback control system. In addition, it can oxidize nitrogen monoxides to nitrogen dioxides which then in turn accelerates the standard SCR reaction (fast SCR). However, NO_2 cannot be reduced to nitrogen due to the lean condition of DOC [52, 58].

The DOC is generally a monolith reactor with honeycomb structures made of cordierite (a type of ceramic) or metal. It consists of washcoated catalysts composed of aluminum oxide, cerium oxide, zirconium oxide supports, and active metals like platinum, palladium, and rhodium (with approximately 50–90 g/ft^3 loading). High surface area for active metals and lower amount of catalyst sintering is achieved by use of washcoated catalyst. A typical DOC can be seen in Figure 2.8 [52].

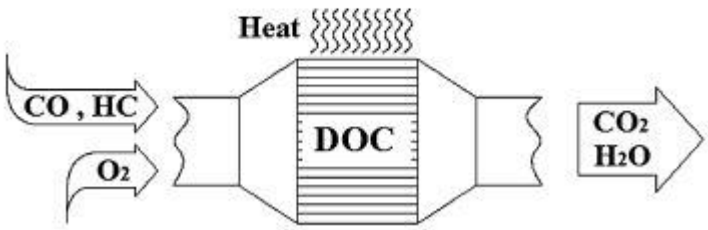

Figure 2. 8. Diesel Oxidation Catalyst [52]

Three main reactions occur in DOC [52]:

$CO + 1/2\ O_2 \rightarrow CO_2$

$C_3H_6 + 9/2\ O_2 \rightarrow 3\ CO_2 + 3H_2O$

$NO + 1/2\ O_2 \rightarrow NO_2$

Diesel exhaust gas includes unreacted oxygen from the combustion chamber around 2-17 % by vol. This amount is steadily consumed in the diesel oxidation catalyst. The DOC efficiency strictly depends on temperature. Effective oxidation of species can be achieved above light-off temperature, which is the temperature for the reactions to start. Light off temperatures can change depending on the velocity and the composition of the exhaust gas stream and also the catalyst type. Other parameters that can affect DOC efficiency can be listed as material tolerance to poisoning, channel density, dimensions of the monolith, wall thickness of the monolith channels, washcoat thickess, porosity, pore size, PGM loading, PGM particle size & distribution, and manufacturing cost.

Channel density and wall thickness are important because they designate mechanical stability and heat up response of the converter as well as the backpressure of the exhaust stream [52].

DOC can also be used as a heater since the oxidation reactions releases a considerable amount of heat. Released heat promotes diesel particulate filter regeneration via increasing the downstream temperature of the DOC. For every 1 % vol. of carbon monoxide oxidation, exit temperature increases around 90 °C. However, steep temperature gradients can lead to stress and deformation in the ceramic support and the catalyst. Increases in temperature to around 200-250 °C is permitted due to resulting stress on the system [52].

The DOC achieves around 60 to 90 % emission reduction for hydrocarbons and carbon monoxides. However, one of the main problems of the DOC is that it oxidizes SO_2 to SO_3, which generates sulfate and sulfuric acid via reacting with water in the exhaust gas stream. These species are very harmful for both the environment, organisms, and the after-treatment system itself. Also, there is no technology to eliminate these species completely. Using biodiesel or alcohol instead of diesel can be a solution to prevent generation of sulphur species [52].

2.2.1.2. Diesel Particulate Filter (DPF)

The diesel particulate filter (DPF) is a physical filter with a honeycomb-like structure made of cordierite or silicon carbide. It includes fine channels blocked at alternate ends where particulate matters are trapped while the other species pass through pores of the wall by diffusion. Channel wall thickness and cell density of the monolith vary between 300-400 μm and 100-300 cpsi, respectively [52]. A typical representation of DPF is shown in Figure 2.9.

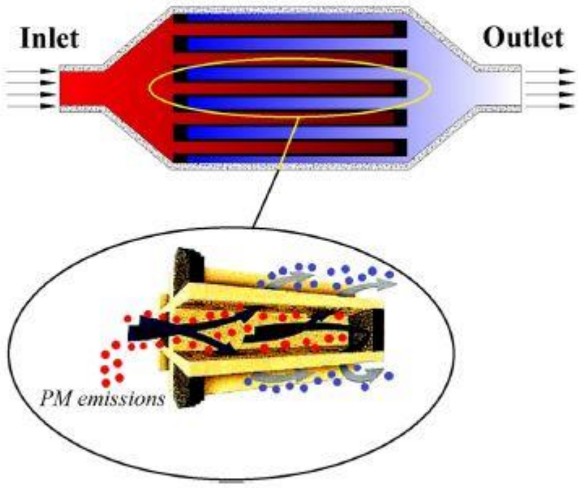

Figure 2. 9. Diesel Particulate Filter [52]

Exhaust gases can be enriched to combust PM. External cleaning is applied to remove particles in the DPF. The filter becomes saturated as particles accumulate on its surface but excessive saturation should be prevented to eliminate elevated backpressure on the engine. When it reaches around 45 % saturation, pressure drop across the filter increases, generate a signal and then regeneration process is started. Trapped particles are disposed of by burning to avoid high amounts of fuel consumption, engine failure, and stress originated from backpressure [52].

There are two types of regeneration in the DPF, which are known as active and passive regeneration. In active regeneration, trapped particles are oxidized periodically with oxygen at 550 °C or above by an external heat source like an electric heater of burner or DOC, while in passive regeneration, NO_2 based oxidation reactions of soot are accomplished. Deposition of an oxidation catalyst onto the filter facilitates NO to NO_2 conversion increasing the availability of NO2 for soot oxidation reactions and hence increases the filter efficiency. In the latter one, there is no need for an external heat supplier or additional fuel since the oxidation reactions take place at usual exhaust temperatures, at a temperature range of 200-450 °C [52].

DPF require ultra-low sulphur content in diesel fuel. In order to reduce PM emission, a fuel additive such as cerium can be used for light duty vehicles [58].

2.2.1.3. Selective Catalytic Reduction (SCR)

Selective Catalytic Reduction with ammonia is known as an efficient process for NOx abatement by means of a special monolith catalyst in heavy duty vehicles. In this process, NH_3, produced from an on board thermal decomposition of urea [2] is used as a reductant to reduce NOx in an excess oxygen environment. A combined system of DOC, DPF and SCR can be seen in Figure 2.10.

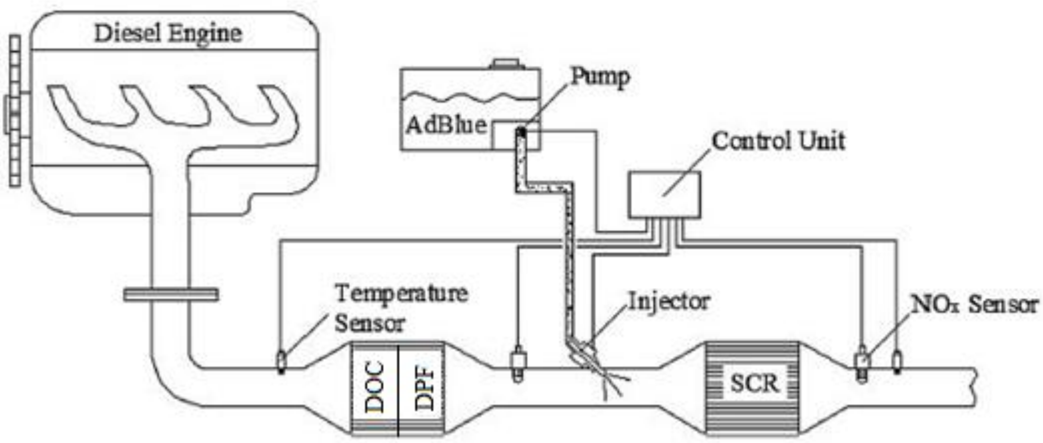

Figure 2. 10. After-treatment system for heavy duty vehicles (Adapted from İ.A. Reşitoğlu et al., 2015 [52])

2.3. Selective Catalytic Reduction Process

Selective catalytic reduction technology is an effective way to reduce nitrogen oxide emissions, especially for heavy duty diesel vehicles. In selective catalytic reduction, ammonia (NH_3) is used as a reductant to convert harmful nitrogen oxides to harmless nitrogen and water in an excess oxygen environment. In order to prevent the oxidation of ammonia before it reaches converter, it is provided from an aqueous solution of urea called Adblue. Adblue contains 33 wt. % urea ($(NH_2)_2CO$) and 67 wt. % water [52] and is thermally decomposed to urea [2] on board. Solid urea melts and is thermally decomposed according to the reaction below:

$$(NH_2)_2CO \rightarrow NH_3 + HNCO$$

Formed ammonia takes part in the SCR reactions while HNCO (isocyanic acid) is converted to ammonia and carbon dioxide via hydrolysis reaction [52].

$$HNCO + H_2O \rightarrow NH_3 + CO_2$$

At the end of the thermolysis and hydrolysis, 2 molecules of ammonia are produced. These two reactions are faster than SCR reactions and the efficiency of them highly depends on the temperature of the exhaust gas stream. Moreover, there is no consensus on the melting point of urea. Conversion of aqueous urea to ammonia starts at the time of injection but only half of it is converted at the entrance of the catalyst. Conversion efficiency is increased by the addition of a hydrolysis reaction which increases the temperature of the exhaust gas stream before the species arrive at the catalyst entrance [52].

Efficiency of the SCR also depends on the amount of ammonia stored and dosed. Precise injection of Adblue is very important to prevent or minimize the ammonia slip and to obtain lower operating cost [52, 61]. To obtain complete reaction between NH_3 and nitrogen oxides, the SCR should run at high temperatures since the adsorption and desorption of NH_3 occurs below 200 °C and 200 - 800 °C, respectively. The desired temperature range is achieved by arranging the ammonia dosage according to changing fuel mass flow rate. Researches on NOx emissions at different speeds reveal the fact that there is a linear relationship between fuel flow rates and nitrogen oxides. This simple control mechanism is applied in most of the vehicles with NH_3-SCR. The humidity and temperature of air, consumed fuel amount and exhaust gas temperature are some of the parameters that are considered to optimize ammonia dosage amount. Generally, ammonia slip can be minimized by setting NH_3/NOx values lower than one [60].

Urea delivery systems, catalyst injection solutions, and pressure and time are the crucial and complex parameters for SCR design as mentioned above. Research on the effects of urea quality on conversion efficiency reveal that urea dosage can affect conversion efficiency up to 10 %. Several amines such as methylamine, ethylamine, propylamine and butylamine were tested as alternate solutions, yet none of them provide the efficiency obtained by the urea solution (Adblue) as a reductant. In addition, hydrocarbons (HC) were also tested as reductants in the system (HC-SCR). Since the exhaust gas stream (passive mode) or fuel itself (active mode) include hydrocarbons, it is easier to apply HC-SCR to light duty vehicles. For diesel engines, some hydrocarbons like ethanol, propanol or acetone can be injected into the exhaust gas stream to promote nitrogen oxide reduction. In such systems, the $Ag\text{-}Al_2O_3$ is known as the most promising candidate as a HC-SCR catalyst [52].

One of the most attractive feature of SCR is that it includes a calibration to reduce PM as well as nitrogen oxides as shown in Figure 2.11. This strategy provides fuel economy in comparison to the Exhaust Gas Recirculation (EGR) technology [62].

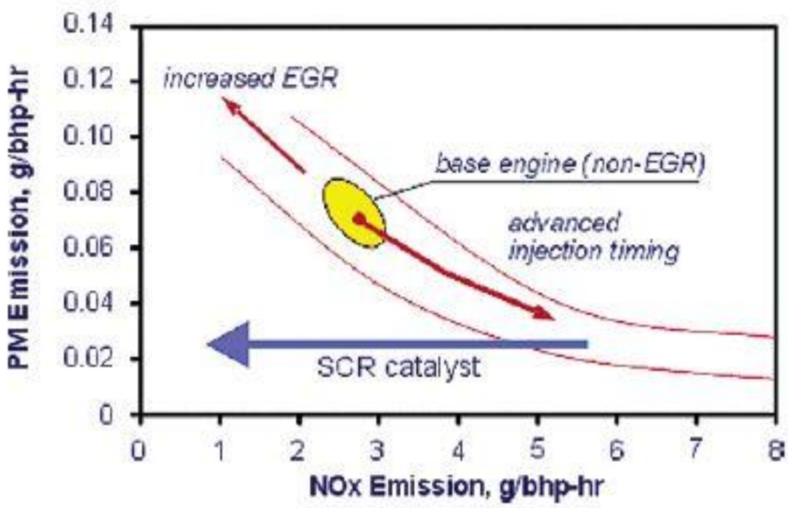

Figure 2. 11. Emission strategy for Selective Catalytic Reduction [62]

Three significant reactions occur in the SCR, which are named according to their rates of reaction. Above 90% of the nitrogen oxides in diesel exhaust are nitrogen monoxides (NO), which means that the main reaction of the NH_3-SCR is the standard SCR reaction [62].

Standard SCR: $4NO + 4NH_3 + O_2 \longrightarrow 4N_2 + 6H_2O$

Fast SCR: $NO + 2NH_3 + NO_2 \longrightarrow 2N_2 + 3H_2O$

NO_2 SCR: $6NO_2 + 8NH_3 \longrightarrow 7N_2 + 12H_2O$

SCR is a very effective technique to convert up to 98% of the total NOx emission in heavy-duty vehicles. Even after 200,000-300,000 km, the activity of the catalyst only reduced to 75-80 % of its initial value [45].

The standard SCR reaction occurs in the absence of NO_2 species. In the case of using a diesel oxidation catalyst before selective catalytic reduction, NO is converted to NO_2 and slow SCR reaction takes place. In this, the reaction rate declines and the conversion efficiency of NOx species decreases. However, when the size and metal loading amount of the DOC is optimized and a 1:1 of NO to NO_2 ratio is obtained, maximum performance is observed due to a higher reaction rate of fast SCR reaction [52].

In addition, several competitive and nonselective reactions can be observed in SCR systems. Reactions with oxygen can generate N_2O, NO, NH_4NO_3, NH_4-NO_2, NH_4HSO_4, and $(NH_4)_2SO_4$ emissions.

NH_4NO_3, or ammonium nitrate, is an explosive chemical that forms at 100-200 °C in liquid or solid form via reaction of nitrogen dioxide with ammonia. It causes temporary catalyst deactivation through the filling if pores of the catalyst [62].

$$2NH_3 + 2NO_2 \rightarrow N_2 + NH_4NO_3 + H_2O$$

By injecting less ammonia, NH_4NO_3 formation can be minimized. Moreover it can decompose to N_2O and water above 200 °C [2].

$$NH_4NO_3 \rightarrow N_2O + 2H_2O$$

NH_4HSO_4 and $(NH_4)_2SO_4$, or ammonium sulfates, form through the reaction between ammonia and sulphur trioxide which originates from the oxidation of sulphur dioxide in diesel fuel. Ammonium sulfates accumulate in the catalyst and then can induce catalyst deactivation and create some irreversible problems in the active sites [62].

Ammonia oxidation is the most important side reaction in the SCR since it competes with the SCR reactions. It prevents the reaction of ammonia with nitrogen oxides, thus it is considered as an undesired reaction. This reaction occurs above 300 °C on a copper- and iron-zeolite catalysts [2].

$4NH_3 + 3O_2 \longrightarrow 2N_2 + 6H_2O$

On the other hand, the oxidation of NO to NO_2 is a desirable reaction since it accelerates the standard SCR reaction via boosting the fast SCR reaction. This reaction occurs above 300 °C on copper- and iron-zeolite catalysts [2].

$NO + 1/2O_2 \longleftrightarrow NO_2$

SCR systems operate in the temperature range of 200-600 °C and maximum NOx conversion is observed around 350 °C. Depending on the catalyst used, the optimum temperature interval can slightly change but generally fits in this range. Above 600 °C can cause urea to burn and at temperatures below 200 °C, cyanide acid, biurea, melamine, amelide, and ameline can form due to urea decomposition. In order to eliminate the accumulation of these species, urea solutions are injected into the system after reaching 200 °C in the exhaust gas stream [52].

In general, two types of catalyst are used for this system so far. These are base metal oxides like vanadia based catalysts and metal exchanged zeolites such as Fe-ZSM-5 and Cu-SAPO-34. Differences and applications of these catalysts are discussed in the next sections.

2.4. SCR Catalysts

2.4.1. Vanadia-Based Catalysts

Base metal oxide catalysts were one of the first catalysts applied in the SCR system. The most common one was the vanadia-based catalyst which included the V_2O_5 active site promoted with the WO_3 and TiO_2 support. It was used in the form of powder obtained by crushing and then coated onto monolith bricks have a honeycomb structure. Effective temperature ranges for such a system are 300-400 °C [4]. The reaction mechanism starts with the adsorption of ammonia on active sites which are Bronsted acid sites (V^{5+}-OH) and then followed by the reaction with redox sites (V=O). After the ammonia activation, nitrogen and water is generated by the SCR reactions. V^{4+}-OH species were formed at the end of the reactions and were reduced with oxygen to complete the catalytic cycle [6]. Reaction scheme shown in Figure 2.12 can be used to define the SCR kinetics over V_2O_5/TiO_2 catalyst.

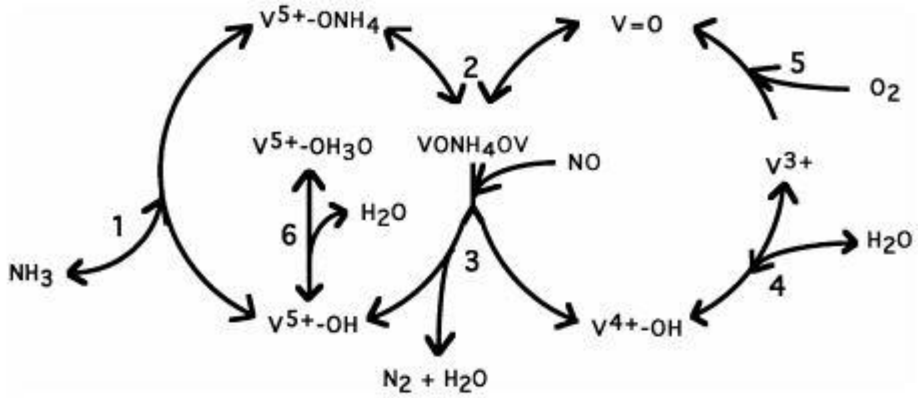

Figure 2. 12. SCR cycle over V_2O_5/TiO_2 promoted with WO_3 [6]

However, when they are compared to metal exchanged zeolites, vanadia-based catalysts generally exhibit poor hydrothermal stability, generate N_2O at high temperatures, have high activity for the undesired oxidation of SO_2 to SO_3 and formation of N_2O [18], and decrease in activity and selectivity at 550 °C [19, 20]. Therefore, succeeding research on SCR systems have focused on metal exchanged zeolite catalysts, both of which have high nitrogen oxide reduction abilities over broad temperature intervals.

2.4.2. Zeolites

Zeolites are the shape-selective solid catalysts with natural acidic property. Framework type and silicon to aluminum ratios are some of the most important catalytic parameters used to select the proper zeolite type. Catalytic properties can be improved by modifying these parameters, i.e. substitution of aluminum etc. Surface acidity of the zeolites can enhance the SCR activity via increasing the active metal sites [12].

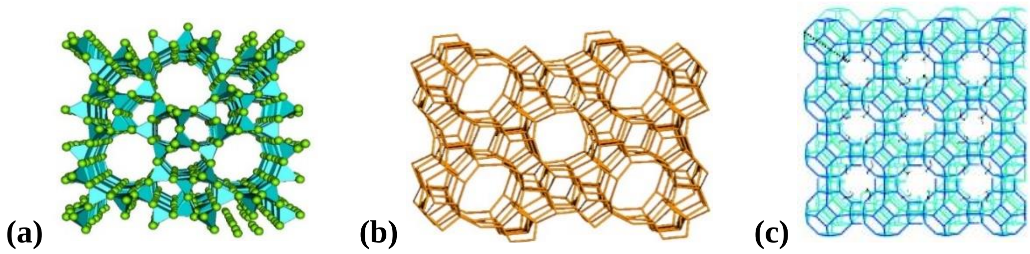

Figure 2. 13. Zeolite structures: (a) ZSM-5 (b) BETA (c) SSZ-13

Zeolites can be prepared by using several methods, yet ion exchanged zeolites generally have the highest activity. During ion exchange, extra framework cations (H^+, Na^+…) of the zeolite are exchanged with metal ions (Cu^{2+}, Fe^{3+}…) coming from a precursor solution [57]. The amount of metal loading (or cation exchanged) depends on the pH of the solution as well as the amount of the precursor, and is almost always independent of the temperature. These are used as a support for catalysts to obtain a well dispersion of the catalytically active species and to stabilize these components against sintering and other means of deactivation [63]. Zeolites are especially used for this system because they are unreactive, highly resistant to heat and chemicals, natural ion exchangers, have high surface area and acidic properties, crystalline in structure, available with a wide range of almost uniform pores of various sizes, and do not have any harmful effect on living organisms and environment. The crystal structure of some zeolites such as ZSM-5, mordenite, SSZ-13 and SAPO-34 can provide the necessary environment for the formation of the catalytically active sites for the SCR reaction [64].

2.4.3. Monolith Reactors

Monolith reactors are made of ceramic material (i.e. cordierite) in honeycomb structures and are used in SCR systems. These reactors have been found to be hydrodynamically better than other industrial/conventional reactors. In addition, they have excellent mass transfer characteristics [65]. SCR catalysts are washcoated inside the channels of the monolith bricks in order to prevent pressure drops, clogging of channels by ash and particulate matter, and also to increase the surface area for SCR reactions [7].

Monolith reactors used in the after treatment technologies mostly operate in a fully developed laminar flow regime. When flow passes through the monolith channels, species are transported to the thin washcoat of catalyst on the surface of the monolith wall where the SCR reactions take place.

2.4.3.1. Iron-Based Catalysts

Stricter NOx regulations, toxic properties of vanadium, and the decrease in activity of vanadium based catalysts at relatively low and high temperatures revealed the necessity of a new catalyst for SCR systems. The first metal exchanged catalysts for this system included iron as a metal active site and zeolite as a carrier. The catalyst in the form of powder was washcoated onto the monolith samples, like vanadium-based catalysts. Active iron sites consisted of isolated iron ions (monomeric species) and dimeric species. Although the catalyst surface included iron oxide clusters and larger oligomers (Fe_xO_y) with unknown nuclearity, these were not considered [9] since they only contributed to the activity at rather high temperatures (>500 °C) [21]. Moreover, monomeric sites ($[Fe(OH)_2^+]$) provided the most of the activity at temperatures below 300 °C yet with increasing temperature, contributions from dimeric species ($[HO{-}Fe{-}O{-}Fe{-}OH]^{2+}$) dominate [9]. Standard ammonia SCR cycle over iron based catalyst started with the adsorption of ammonia and then follows a redox mechanism as shown in Figure 2.13.

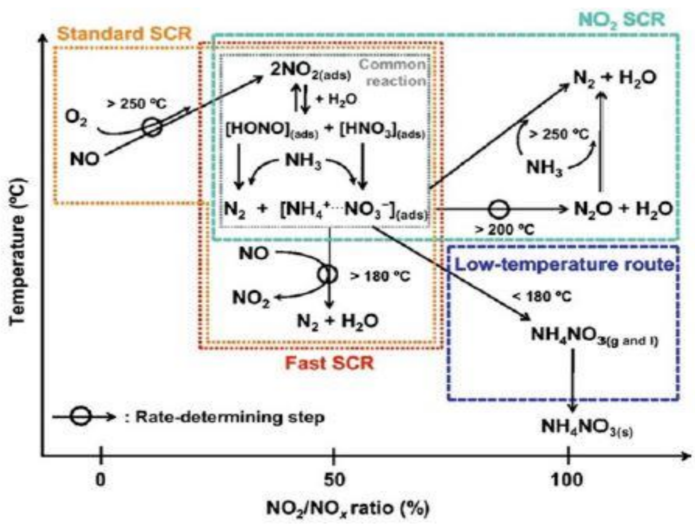

Figure 2. 14. SCR cycle over Fe-zeolite catalyst [21]

Even though iron-zeolites have been well known for their high N_2 selectivity [21] and high NOx removal ability at high temperatures (>350 °C) [2], their lower activity at low temperature range, relatively higher N_2O formation from the thermal decomposition of NH_4NO_3 [21] and lower ammonia uptake capacity than copper-zeolites [22] restrict their application.

2.4.3.2. Copper-Based Catalysts

Copper-zeolites with an excellent NH_3-SCR activity at low temperatures, N_2 selectivity [21] and ammonia uptake capacity [22] have received considerable attention in the past decade. A wide variety of copper containing zeolites with medium and large-pore sizes (i.e. Cu-MOR, Cu-BEA, and Cu-FAU) exist. Cu-ZSM-5 is the most widely known and studied copper-based catalyst. Although it has remarkable NO conversion activity and selectivity [14, 23], its low hydrothermal stability at high temperatures due to dealumination processes in the zeolite framework [24, 25] is a significant drawback. Nowadays, small-pore size zeolites with the chabazite (CHA) structure have been attracting increased attention due to their excellent catalytic activity for NO decomposition in the exhaust gas stream and enhanced hydrothermal stability with high hydrocarbon resistance [26-30]. Especially, Cu-SSZ/13 and Cu-SAPO/34 (zeolites with the CHA structure) have been shown to demonstrate superior performance due to their excellent catalytic activity for NO decomposition in exhaust gas streams and enhanced hydrothermal stability with high hydrocarbon resistance [26-30].

Activity of the catalyst strongly depends on the copper locations in the zeolite framework and the Cu loading amount. Reaction rates of NO oxidation, NH_3 oxidation and N_2O formation reactions per copper increase significantly with increasing copper loading while the rate of standard SCR reactions increases up to a certain Cu/Al ratio then decreases with increasing copper loading [66]. This suggests that there should be an optimum value for the metal loading amount [15]. The tetrahedral framework of SSZ-13 consists of 6-membered rings connected to form a cavity that is bound by six 8-membered and twelve 4-membered rings [67]. Interactions between copper and zeolites have been extensively studied to find an optimal location and loading amount for copper. It was suggested that the NOx conversion over Cu-SSZ-13 can be maximized by keeping copper loading around 40-60% and by placing the coppers in isolated positions in the 6-membered rings [15]. However, the locations of the copper species may slightly change upon the adsorption of ammonia, nitrogen monoxide, and water [68]. Conformational change in zeolite framework can be observed when the coppers move from 6-membered rings to the larger cages in case of contacting with ammonia at low temperatures (125 °C) Besides, the change in coordination geometry is permanent at higher temperatures [15]. It is also reported by many researchers that most of the copper is located in 8-membered rings of the chabazite framework. Hence, SCR reactions actually occur in the larger cages at high temperatures yet only the copper ions placed on/near to the smaller cages are active for the SCR reactions at low temperatures for copper-chabazite [68].

2.4.3.2.1. Reaction Kinetics and Mechanism for Cu-CHA Catalyst

Like iron-based zeolites, copper-zeolites usually have Brønsted acidity since the metal exchange procedure is frequently carried out in a certain degree which results in an incomplete exchange of metals leaving some of the protonic sites free. If the coppers are placed closely to the acid sites, ammonia on Brønsted site can directly interact with the NO_2 on a copper ion. It was revealed that SCR activity is independent of the number of Brønsted acid sites in Cu-MFI and Cu-CHA catalysts at 200 °C, therefore either these sites have no effect on SCR reactions or they are always saturated with NH^{4+} species during the reactions. Therefore, they are not that active but can either act as promoters for active metal sites or have an impact on the distribution of metal species. Therefore, the SCR reactions occur on the metal sites in copper-zeolites and the Brønsted acid sites can contribute to the catalytic activity slightly up to 200 °C via feeding NH_3 to the Cu sites where the reactions actually occur [68].

Distribution of framework Aluminum atoms may also affect the formation of copper dimers. It is known that copper atoms bound to oxygen atoms in Si-O-Al bridges have possibly Cu^{+2}-OH^- unit with a +1 charge. Cu-O-Cu structures bound to different framework of aluminum atoms can form between two adjacent Cu^{+2}-OH^- units. Recent studies show that activity per copper atom increases as the metal loading amount increases up to a certain Cu/Al ratio above which the turnover frequency drops; therefore formation of these dimers may have a role in the catalytic activity [68].

SCR reactions can be considered in two parts; oxidation step by $NO+O_2$ and reduction step by $NO+NH_3$. In reduction, first NO and NH_3 are adsorbed on Cu^{2+} sites. Then, formed ammonium nitrite or nitrate like components which then decompose to nitrogen and water. Here, Cu^{2+} ions are effectively reduced to Cu^{+} ions as this process continues over and over again. In the oxidation, activation of NO and restoration of catalytic parts can occur simultaneously; therefore another reaction is also required for this step, such as the oxidation of NO. In addition, the activation of NO to NO_2 is also critical to speed up the reactions (fast SCR). Adsorbed NO_2 species can react to give nitrite and nitrate via disprotonation of NO_2 molecules or reaction between NO and NO_2. Here, ammonium nitrate species form by further reactions, which then decompose to nitrogen and water at high temperatures [68].

Accordingly, following reaction scheme is proposed for SCR reactions that include NO activation step and the fast SCR reaction at 200 °C:

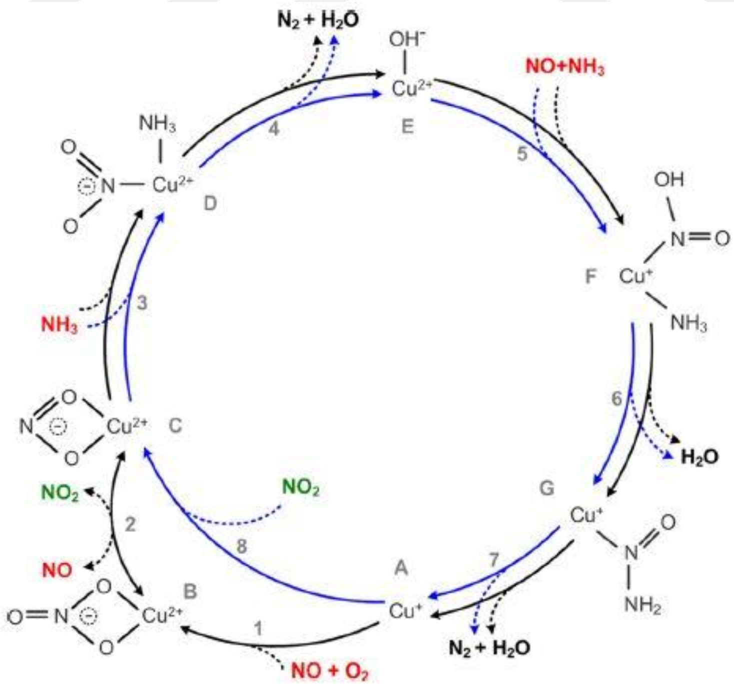

Figure 2. 15. SCR cycle over Cu-CHA catalyst (black: NO activation cycle, blue: fast SCR) [68]

However, higher temperatures can alter the monocopper active sites [68-70] of the Cu-chabazite catalyst and thus could change the standard SCR reaction mechanism. Recent studies reveal that dicopper or tricopper species could form on a number of Cu-zeolite families at temperatures above 400 ^{o}C [71-74]. First, it was suggested that Cu…Cu contribution is found for the O_2-activated over exchanged Cu-ZSM-5 sample, which are attributed as bis(μ-oxo)dicopper cores, i.e. $[Cu_2(\mu\text{-}O)_2]^{2+}$. In addition, catalysts retain their activity for NO decomposition reactions even after dehydration in Helium [71]. Hereafter, measurements revealed the fact that bis(μ-oxo)dicopper species are not thermodynamically stable and mono(μ-oxo)dicuprics are the real active sites [72]. Further, some studies showed that three or four copper containing sites may also be the active sites [75]. Grundner et al revelaed that trinuclear copper-oxo clusters have high activity towards methane oxidation reaction over Cu-MOR catalyst [74] and dicopper species could form in a dynamic fashion within the 8-membered ring of the SSZ-13 [33], and other studies suggested that copper oligomers could also be active for methane to methanol reaction over Cu-MOR catalyst [76].

2.5. Kinetic Modeling of Monolith Catalysts of SCR

Kinetic modeling of SCR reactors is a critical step to design and optimize the whole engine after treatment system to meet the desired emission level. Kinetics of the standard SCR reactions over a variety of catalyst have been extensively studied. Tronconi et al. [38] made one of the first mathematical models of monolith reactors for selective catalytic reduction of NOx by ammonia over a vanadia-based catalyst. In this study, they tried to produce 1-D and 2-D models by considering the effects of different channel geometries, NH_3/NO feed ratios, area velocity, and the size of monolith channels. First, 2-D models were generated and then the same assumptions are introduced to the 1-D model by taking the average values of the parameters (velocity, concentration etc.). They proposed a Sherwood number correlation to estimate mass transfer coefficients. This lumped parameter model almost gave the same results in a 2-D model, with the exception of only minor differences in the case of the triangular shaped monolith channels. However, this study only considers the standard SCR reaction on one site, at a certain temperature (380 °C) on a vanadia-based catalyst. Although a lot of kinetic model and mass transfer coefficient correlations are proposed after this one as stated in next sections, there is no comprehensive study which combines a multi-site kinetic modelling with mass transfer effects. In a recent study, Olsson et al. [15] developed a multi-site kinetic model for NH_3-SCR over Cu-SSZ-13. They showed a need for a multi-site model to describe the behaviors of ammonia adsorption, desorption, oxidation and SCR reactions at a high temperature range. Although this model is capable of describing the above mentioned reactions, the mass transfer part was not optimized separately, as they did not propose a correlation to estimate mass transfer correlation.

2.6. Mass Transfer in Monolith Reactors

In a single-phase system, conversion is only affected by the mixing quality of the reactants with homogeneous catalysts and with each other. However, in multiphase systems, process conditions should be designed such that particles are also transported efficiently across the solid-gas or solid-liquid interphases.

Monolith catalysts are solid ceramic or metallic bricks with many narrow, parallel channels. Catalysts are coated with a thin layer inside these channels to prevent pressure drops, the clogging of channels by ash and particulate matter, and also to increase the surface area for reactions as mentioned before. When the flow passes through these passages, radial mass transfer occurs via molecular diffusion from bulk phase to the surface of the washcoat and also from the catalyst’s surface to the active metal sites.

In these multi-phase reactors, mass transfer rates not only depend on operation temperature and pressure, but are also affected from kinetics, mass transfer conductance, and concentration gradients.

Generally, the overall reaction rate is either controlled by a mass transfer conductance, kinetics or both, and the slowest step becomes rate limiting. In the next section, mass transfer theories for the solid-gas or liquid-gas systems are investigated in detail.

2.6.1. Theories of Mass Transfer

2.6.1.1. The Thin Film Theory

This theory proposes that a stagnant, thin film layer occurs adjacent to the surface of the solid phase; therefore two phases are separated from each other by an interphase. This layer is almost hypothetical, yet gives an idea about the particle transportation in the interfacial region [77]. Mass transfer includes molecular diffusion across this layer; starting from high concentration to low concentration. The following assumptions are valid for this theory:

1) Bulk phase concentrations are homogeneous.
2) Steady state mass transfer occurs through the thin layer.
3) Species molar flux is small.
4) Mass transfer occurs at low concentration i.e. dilute mixture.

The concentration profile through the thin film is linear as shown in Figure 2.15.

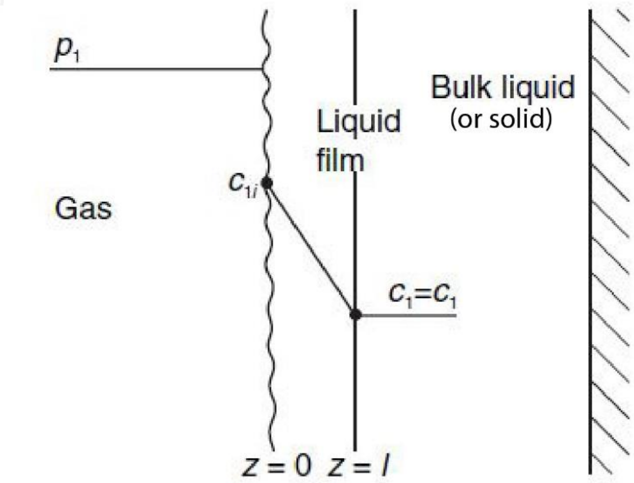

Figure 2. 16. Representation of thin film theory for mass transfer of particles [77]

The theory presents how resistance to mass transfer can arise near solid-fluid interface with a simple approach.

The steady-state mole flux across this layer can be written in terms of the mass transfer coefficient [77]:

$$N_1 = k_m (C_{1i} - C_1) \quad (1)$$

where N_1 indicates the mole flux to the interface, k is the mass transfer coefficient, and C_{1i} and C_1 are the concentrations at the interphase and bulk liquid, respectively.

Mole flux can be also defined by diffusion coefficient, which assumes total flux is equal to the diffusion flux (dilute solution).

$$N_1 = k_m (C_{1i} - C_1) = (D_{AB} / \Upsilon) (C_{1i} - C_1) \quad (2)$$

where Υ is the thickness of the thin film which is nearly never known.

Hence, the mass transfer coefficient depends on the diffusion coefficient and the thickness of the film layer whereas it seems independent of fluid velocity. This is not the case actually, because the change in the mass transfer coefficient with respect to fluid velocity is lumped into the film thickness which can be predicted by the measurements of k_m and D_{AB} [77].

2.6.1.2. Penetration Theory

This model proposes a mass transfer into a semi-infinite fluid unlike the thin film theory which is based on the mass transfer across the film layer [77]. Penetration theory is based on following assumptions:

1) The film layer is thick and unsteady state mass transfer occurs once the two phases are in contact.
2) Each particle in the solid or liquid phase stays in contact with the bulk phase (gas) for the same period of time.

3) The diffusion in the x direction is negligible compared to convection in this direction.
4) There is an equilibrium at the interphase.

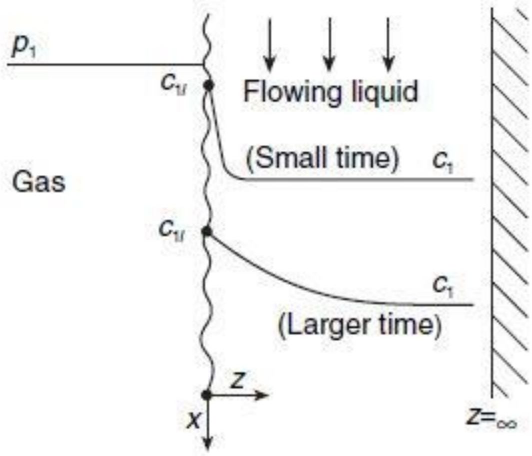

Figure 2. 17. Representation of penetration theory for mass transfer of particles [77]

2.6.1.3. Surface-Renewal Theory

This theory tries to use a mathematical approach as shown in the penetration theory yet by using a more logical physical representation.

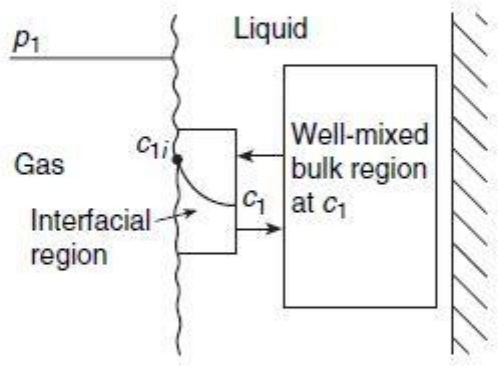

Figure 2. 18. Representation of surface renewal theory for mass transfer of particles [77]

The liquid part (it can be solid as well) is shown as two zones; a well-mixed bulk region and an interfacial region that acts as a thick film layer due to rapid surface renewal by liquid motion. Particles of the interfacial region are constantly exchanged with new ones from well-mixed bulk regions [77]. The following assumptions are valid for this theory:

1) Particles in the interphase are randomly exchanged by new ones from the bulk phase.
2) There is an equal chance for each particle at the interphase to be replaced by a fresh one.
3) Unsteady state conditions are applicable at the interphase.

2.6.2. External Mass Transfer

The overall reaction rate is controlled by the rate of diffusion of reactants from bulk gas phase to the surface of the catalyst when the reaction at the active site is so fast. In this case, concentration of the species j at the washcoat wall (C_j^w) becomes smaller than the average concentration in the bulk gas phase (C_j^b) [7].

When a flow passes through a surface of a solid catalyst, turbulence (depending on the Reynolds number) generally dominates the flow regime but there is a region (a thin film) very close to the catalyst surface where the flow is mostly laminar. When the distance from the surface increases, flow character alters gradually and becomes predominantly turbulent in the outermost parts. In the turbulent region, a portion of the fluid known as eddies, no longer move in an orderly manner. Instead, they carry with them dissolved matter in the bulk phase and hence contribute significantly to the mass transfer. Mass transfer in this region is much faster than that occurring in the thin film due to the rapid motion of eddies. Therefore, a smaller concentration gradient is observed in the turbulent region [78]. Since the laminar flow regime is applied for the after-treatment system mass transfer coefficients, and related correlations are investigated for fully developed laminar flow from now on.

2.6.2.1. External Mass Transfer Coefficient

Transportation of spontaneously mixed particles from relatively high concentration to lower concentration is known as diffusion. The rate constant for this process is shown by a mass transfer coefficient, which can be defined as the ratio between molar flux of species i at the interphase and concentration difference of species i at the interface and in the bulk solution. Physically, it is a rate constant used to demonstrate the movement of species from bulk phase to the boundary. A large value of mass transfer coefficient means fast mass transfer, while a small one implies slow mass transfer. It can be found experimentally or by some mathematical expressions found by the previous measurements of someone else. These expressions do not solely include the mass transfer coefficient itself but are instead reported as correlations of dimensionless numbers [77]. Some of the common dimensionless numbers used in mass transfer correlations can be listed as below:

$$Reynolds\ number = Re = \frac{inertial\ forces}{viscous\ forces} = \frac{d_h u \rho}{\mu} \tag{3}$$

$$Schmidt\ number = Sc = \frac{diffusivity\ of\ momentum}{diffusivity\ of\ mass} = \frac{\mu\rho}{D_{NO-air}} \tag{4}$$

$$Sherwood\ number = Sh = \frac{mass\ transfer\ velocity}{diffusion\ velocity} = \frac{k_m d_h}{D_{NO-air}} \tag{5}$$

In Equation 3 and 4, for ideal gases, the fluid density (ρ) can be expressed as a function of temperature and pressure, and fluid viscosity (μ) can be determined by Sutherland's formula:

$$\rho = \frac{p_t M_i}{RT} \tag{6}$$

$$\mu = \mu_0 \left(\frac{a}{b}\right) \left(\frac{T}{T_0}\right)^{3/2} \tag{7}$$

$$\text{where } a = T_0 + D \tag{8}$$

$$b = T + D \tag{9}$$

In the equations, the density and viscosity of nitrogen can be used since it constitutes a significant portion of the fluid mixture. Sutherland's constant (D), reference temperature (T_0) and viscosity (μ_0) values for nitrogen are 111, 27.4 °C [79] and 0.01781×10^{-3} Pa.s [79], respectively. By substituting Equation 6 and 7 into Equation 3 and 4, Reynolds and Schmidt numbers can be evaluated for all temperature ranges.

2.6.3. Internal Mass Transfer

Reactor performance can also be affected by the internal mass transfer resistances [7]. Two types of diffusion occur inside the washcoat layer. The first one is known as washcoat diffusion where reactants are transported by diffusion across the washcoat layer. In the second case, reactants diffuse inside the catalyst pores to the catalytic active site which is known as pore diffusion. Relatively longer internal diffusion paths in monolith catalysts may result in significant intraparticle mass transfer limitations. Internal diffusion may strongly affect the overall reaction rate when the reactant concentration approaches zero quickly throughout the pores. Uniform access of reactant species in the feed to the active sites may not be accomplished since the species are consumed within a short distance, while the inner portions of the catalyst layer remain dormant [7].

Effects of internal mass transfer resistance are investigated by using some parameters. Pores of the catalyst are not straight but rather are meandering paths with varying cross sectional areas with not all areas available for particle to diffuse. Accordingly, *effective diffusivity* is used to define the diffusion within each tortuous pathway separately. Effective diffusivity (De) can be related to binary diffusivity in accordance with the equation below [80]:

$$D_{eff,i} = \frac{D_{AB}\,\phi\,\sigma}{\tau} \tag{10}$$

where $D_{eff,i}$ is the effective diffusivity

D_{AB} is the binary diffusion coefficient

ϕ is the porosity

σ is the constriction factor that consider the change in the cross sectional area normal to the diffusion

τ is the tortuosity

2.6.5. Correlations for Mass Transfer Coefficients for Monolith Reactors

Mass transfer coefficients in monolith reactors are usually described by using a dimensionless parameter called Sherwood number, or *Sh*. This parameter is used to define the ratio between convective and molecular (diffusion) transport properties over the entire reactor length. The general form of mass transfer coefficient correlations for monolith reactors was firstly proposed by Hawthorn et al. [36] which is shown in Equation 11:

$$Sh = A(1 + B(Re)(Sc)(d_h/L))^{0.45} \qquad (11)$$

Constants *A* and *B* in Equation 11 are related to channel geometry and surface roughness, respectively [36] and *Re* and *Sc* indicate Reynolds and Schmidt numbers, respectively.

Table 2.1 shows mass transfer correlations in literature [36-43] proposed for monolith reactors. Most of them have the same general form; they typically include a Schmidt and Reynolds number. Schmidt number shows the characteristics of diffused species. On the other hand, Reynolds number is more complicated than the first one since the flow has two different physical sources which are forced and free convection. In the forced convection, flow is externally driven while in the free convection, the mass transfer of species induces a gradient in the surrounding solution [77].

Table 2. 1. Correlations for mass transfer coefficients from literature

Correlation Number	Sherwood Number Correlations	References
1	$Sh = 2.976(1 + 0.078Re\,Sc\,(d_h/L))^{0.45}$	Hawthorne [36]
2	$Sh = 0.705(Re\,(d_h/L))^{0.43}(Sc)^{0.56}$	Votruba [42]
3	$Sh = 0.077(1 + Re\,Sc\,(d_h/L))^{0.83}$	Bennett [37]
4	$Sh = 2.976 + 8.827(1000(LD_{NO-air}/{d_h}^2u))^{-0.545}\exp(-48.2(LD_{NO-air}/{d_h}^2u))$	Tronconi [38]
5	$Sh = 0.766(Re\,Sc\,(d_h/L)/L)^{0.483}$	Ullah [39]
6	$Sh = 2.696(1 + 0.139Re\,Sc\,(d_h/L))^{0.81}$	Uberoi [40]
7	$Sh = 3.53\,exp(0.0298Re\,Sc\,(d_h/L))$	Holmgren [41]
8	$Sh = 4.364$	Gundlapally [43]

Correlation 1 [36] was developed by combining experimental data with the analytical solutions proposed by Kays and London [81]. In Correlation 2 [42], external mass transfer coefficients associated with the vaporization of water & some hydrocarbons from washcoat layer in a monolith reactor were experimentally determined and correlated. Correlation 3 [37] was proposed for platinum-rhodium monolith catalysts used in exhaust emission treatment. Experimental data was obtained in both steady state and transient modes for $1 < (Re\ d_h/L) < 55$. In the experimental part, a mixture of air and propane were fed to a reactor continuously and runs were performed using 4 monolith reactors with different lengths to determine the Sherwood numbers in the mass transfer limited region. Correlation 4 [38] was derived from the quantitative analysis of an SCR reaction for circular, rectangular and triangular shaped monolith channels. For each channel geometry, a fully developed laminar flow condition was applied and the results were checked by comparing the values determined from Graetz-Nusselt problem with those in Shah and London [82]. Correlation 5 [39] was obtained from experimental data of CO oxidation reaction obtained under conditions that were suitable for automobile exhaust gas treatment applications ($1 < (Re\ d_h/L) < 100$). In Correlation 6 [40], a CO oxidation reaction was used to develop a correlation for mass transfer coefficient for square channel shaped titania-silica monolith catalysts. All experimental data was obtained from the region where external mass transfer limitations existed. Experiments were performed for $2 < (Re\ d_h/L) < 30$. Measured external mass transfer coefficients were combined with the Schmidt numbers and then correlation for mass transfer coefficients were obtained using the least square regression method. Correlation 7 [41] was developed using CO oxidation experiments at three different flow rates for square shaped monolith channels with rounded corners. In the experiments, data was acquired at 4 different reactor temperatures in the 250-400°C range. Reynolds numbers in the monolith channels were in the range of 300 to 1000, typical for an automotive exhaust emission systems [41]. In Correlation 8 [43], local Sherwood numbers were estimated for flows with slow and fast reactions and for all channel shapes. Proposed mass transfer coefficient correlations in that study only depended on the channel geometry. Actually, it was given with a position dependency term, yet this dependency is negligible for fully developed laminar flow and for uniform catalyst loading [43]. Although lots of mass transfer coefficient correlations were proposed for monolith reactors, all of them are very different from each other because the experimental conditions used to predict the correlations include wide ranges of chemical and physical properties. For instance, Reynolds number can vary 10,000 times or Schmidt number is around one for gases while around 1000 for liquids. Ranges of each parameters affect the reliability of the correlations, therefore one should not be pick a correlation and use for the design or modelling of full-scale equipment without necessary experimental checks [77].

Chapter 3

EXPERIMENTAL METHODOLOGY

3.1. Monolith Reactor Experiments

3.1.1. Catalyst Samples

The Cu-CHA catalyst used in this study was obtained from a commercial supplier in the form of a cordierite monolith with cell density of 300 cpsi. A cylindrical core with a 2.2 cm length and 1.9 cm of diameter was drilled from the monolith and used in the experiments.

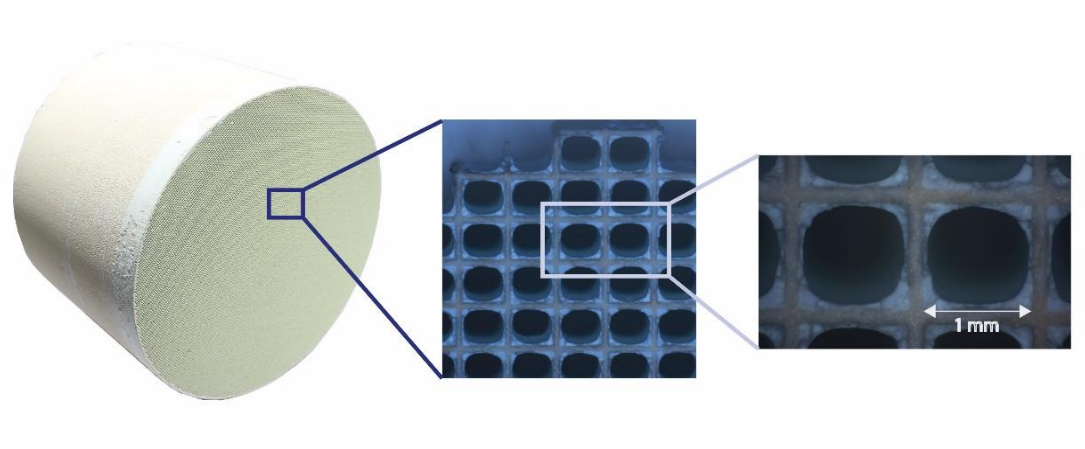

Figure 3. 1. Copper-chabazite catalyst washcoated monolith reactor

3.1.2. Monolith Reactor Experiments

The experiments were carried out in a synthetic gas bench, as shown in Figure 3.2. The entire set up can be divided into three main sections; a reactant gas dosing system,

the reactor (SCR system) and the exit gas analyzer (FTIR). In a typical run, the monolith reactor (300 cpsi, 2.2 cm in length, 1.9 cm of diameter) was first wrapped with a ceramic fiber paper, and then loaded into a quartz reactor, and placed in the isothermal zone of an electric tubular furnace (Thermo Scientific Lindberg Blue M). The reaction temperature was monitored using a J-type thermocouple placed 0.5 cm upstream of the catalyst. The feed gases needed for the measurement except NO (Elite Gas) were supplied by Air liquide. The grades of all the gases used were 5.0 or above. NH_3, NO, CO_2, O_2 and N_2 were dosed using mass flow controllers (Brooks Instruments). Before entering the reactor, CO_2, O_2 and N_2 were preheated to 150 °C over a pre-heater (Thermo Scientific Lindberg Blue M). Since H_2O was in the liquid form, it was dosed using a peristaltic pump (Gilson Minipuls 3) and then vaporized in the pre-heater. Nitrogen was used as a balance gas. The total mass flow rate is varied between 0.14 and 0.55 kg/h. All the gas lines before and after the reactor were heated to 190 °C. Initially, the catalyst was degreened at 600 °C using 5% H2O, 8% O_2, and 10% CO_2 in N_2 balance for 4h to remove the impurities deposited on the surface. After all of the experiments, the catalyst was exposed to 8% O_2 in N_2 balance at 600 °C for 30 min. to clean the surface of any N-containing residues. The species concentrations at the outlet of the reactor were continuously monitored using a FTIR spectrometer (MKS Multigas 2030) equipped with a 5.11 m multi-path gas cell (V = 240 ml) and a liquid nitrogen-cooled mercury cadmium telluride (MCT) detector.
The spectral resolution of FTIR was 0.5 cm^{-1}. The gas cell was always kept at 191 °C and exhaust gas from the device was released into a fume hood at atmospheric pressure.

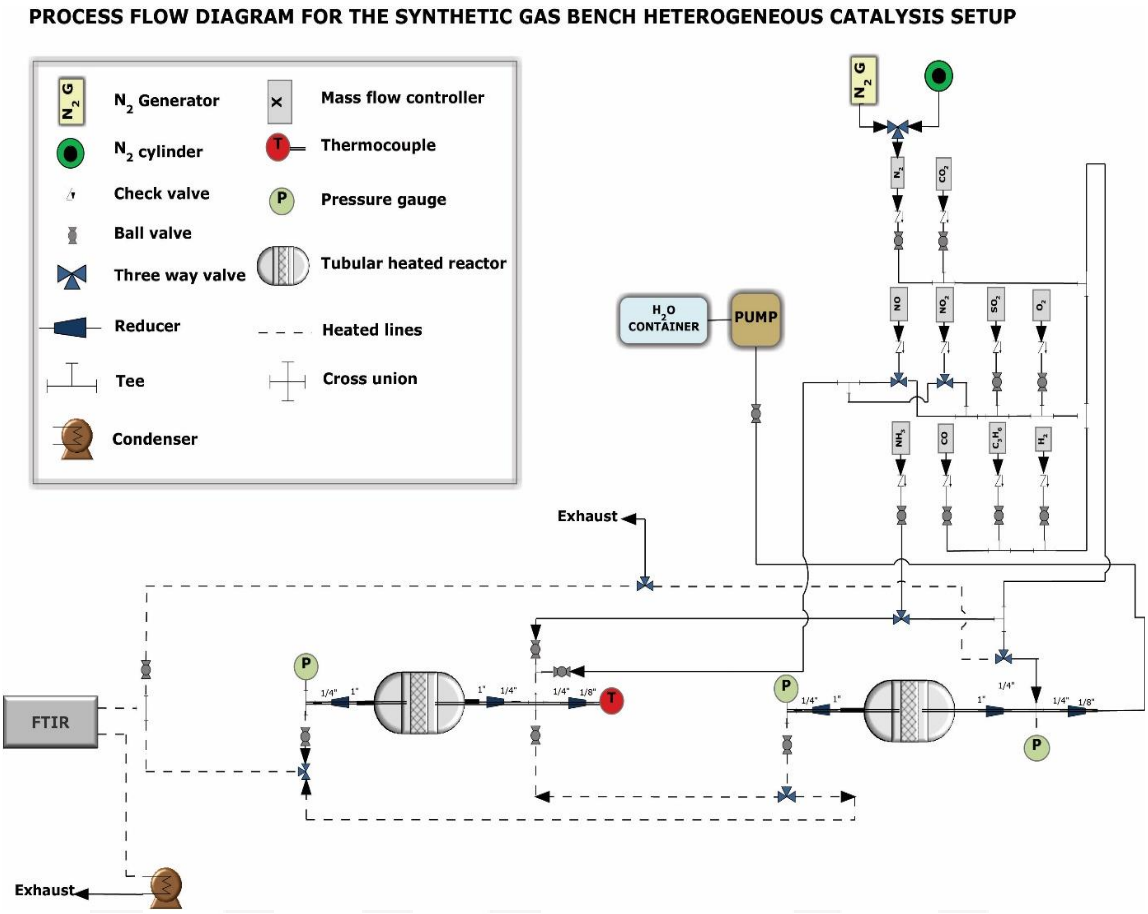

Figure 3. 2. Process flow diagram of experimental set-up

The first experiment, called NH_3 adsorption & desorption, consists of the adsorption, isothermal desorption, and temperature programmed desorption (TPD) parts. In a typical ammonia adsorption & desorption experiment, NH_3 was introduced to the reactor, which evidently resulted in an adsorption breakthrough curve. Once adsorption was completed NH_3 feed was cut off and isothermal desorption of weekly bound NH_3 started. After desorption of weakly bound ammonia was completed, temperature ramp was started with a rate of 10 ^oC/min. Adsorption was carried out at a desired temperature using a feed consisting of 500 ppm NH_3 , 5% H_2O, 10% CO_2 in a N_2 balance followed by an isothermal desorption phase where no NH3 was fed which was then followed by the TPD phase. Uptake values and the TPD peak center temperatures were tabulated to determine the site densities of each site.

In the NH_3 oxidation experiments, catalyst was exposed to 500 ppm NH_3, 10% CO_2, 8% O_2, 5 % H_2O and balance N_2 between 168 to 590 °C. In addition to transient experiment, NH_3 conversion at steady state data was measured in this temperature interval. The NO oxidation reaction was studied in a similar experiment using 300 ppm NO, 10% CO_2, 8% O_2, 5 % H_2O and balance N_2 between 160 to 590 °C. Then, NO conversion at steady state was also measured.

In a typical standard SCR experiment, the feed contained 300 ppm NH_3, 300 ppm NO, 10% CO_2, 8% O_2, 5 % H_2O and balance N_2 between 125 to 590 °C and also NO conversion at steady state data was measured

Experiments were carried out at different space velocities varying between 20,000 and 80,000 h^{-1} (STP).

Finally, low conversion experiments were carried out to construct the Arrhenius plots both for NH_3 oxidation and standard SCR using the same gas mixtures as mentioned above. This was performed in the temperature interval of 144 – 181 °C and 266-370 °C, respectively.

Chapter 4

MATHEMATICAL MODEL

4.1. One-Site Model for Standard SCR Reaction

4.1.1. External (Interphase) Mass Transfer

The steady state differential mass balance for the transportation of NO from bulk phase to the washcoat surface (bulk phase-solid interphase), in one channel is given by Equation 13. (see Figure 4.1)

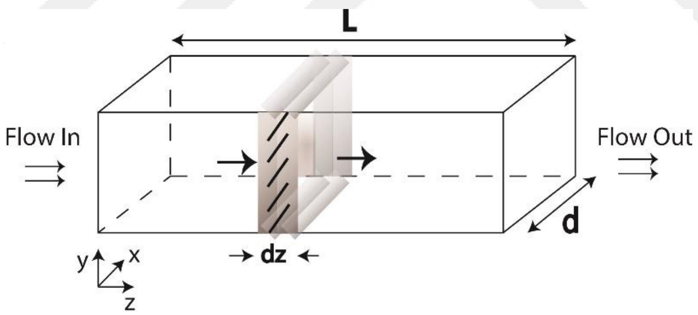

Figure 4. 1. One channel model for monolith reactors

$$-u\frac{dC_{NO}^{b}}{dz} = \frac{4}{d_h}k_m\left(C_{NO}^{b} - C_{NO}^{w}\right) \tag{13}$$

where u indicates the average fluid velocity, d_h is the hydraulic diameter and k_m is the external mass transfer coefficient. (C_{NO}^{b}) is the average concentration in the bulk gas phase and (C_{NO}^{w}) is the concentration of the nitric oxide at the surface of the washcoat layer. Overall reaction rate is controlled by the rate of diffusion of reactants from bulk phase to the surface of the catalyst when the reaction at the active site is fast. In this case, concentration of the nitric oxide species at the washcoat wall (C_{NO}^{w}) becomes smaller than the average concentration in the bulk gas phase (C_{NO}^{b}) [7].

For this equation, the assumptions are: a) negligible axial diffusion, b) identical conditions for each channel and c) negligible entrance length effects (assuming fully developed laminar flow). Non-uniform velocity, temperature and ammonia distribution can be observed in reactors of the after treatment systems of vehicles but this is not the case here, since the size of the monolith reactor used in the experiments was not to that scale. Therefore, single channel analysis is sufficient to describe entire reactor behavior.

As a boundary condition, the continuity of fluxes at the interphase imply that the mass transfer flux across the boundary layer is equal to the diffusive flux to washcoat according to:

$$k_m\left(C_{NO}^{b} - C_{NO}^{w}\right) = -D_{eff,NO}\left.\frac{dC_{NO}^{*}}{dx}\right|_{x=0} \tag{14}$$

In order to solve Equation 13 & 14 simultaneously, the right hand side of Equation 14 should be defined by solving the differential material balance within the washcoat.

4.1.2. Internal Mass Transfer

A concentration profile exists in the washcoat layer due to internal diffusion limitations which are quantified by a dimensionless number known as *Thiele Modulus, φ*. Equation 15 shows the ratio of surface reaction rate to rate of internal diffusion for first order reaction kinetics.

$$\varphi = t_w\sqrt{{k_c}^{*}/D_{eff,NO}} \tag{15}$$

where t_w is washcoat thickness, k_c^{*} is the intrinsic rate constant per washcoat thickness, and $D_{eff,NO}$ is the effective diffusivity of NO which is taken as $D_{NO\text{-}air}/10$, where $D_{NO\text{-}air}$ is the binary diffusion coefficient of NO in air [2].

The diffusivity of NO in air can be expressed by a modified Hirschfelder-Bird-Spotz equation [78] which is based on the kinetic theory of gases:

$$D_{NO-air} = \frac{10^{-4}(1.084-0.249\sqrt{1/M_{NO}+1/M_{air}})T^{3/2}\sqrt{1/M_{NO}+1/M_{air}}}{p_t(r_{NO-air})^2 f(\frac{kT}{\varepsilon_{NO-air}})} \quad (16)$$

where M_i is the molecular weight of species, p_t is the absolute pressure, $r_{NO\text{-}air}$ is the molecular separation at collision, $\varepsilon_{NO\text{-}air}$ is the energy of molecular attraction, k is the Boltzmann's constant, and f is the collision function.

Expressions for parameters in Equation 16 are given below [78].

$$r_{NO-air} = (r_{NO} + r_{air})/2 \quad (17)$$

where r_i is the molecular separation at collision and taken as 0.3711 nm for air and 0.3492 for NO [78].

$$\varepsilon_{NO-air} = \sqrt{\varepsilon_{NO}\varepsilon_{air}} \quad (18)$$

$$\varepsilon_{NO}/_k = 1.21T_{boiling,NO} \quad (19)$$

Lastly, the collision function is obtained from the "collision function for diffusion" chart [78] as 0.5.

In order to understand the effect of internal diffusion on reaction rate, another quantity, called the *effectiveness factor, η*, should also be defined as the ratio of reaction rate with washcoat diffusion to reaction rate without any diffusion limitations.

$$\eta = \frac{\overline{r_{NO}}|_{with\ diffusion}}{r_{NO}|_{without\ diffusion\ limitation}} \quad (20)$$

Since the rate of a reaction is proportional to the concentration of NO for a first order reaction, effectiveness factor, η, which is defined as the ratio of concentration of NO at the bulk phase to concentration of NO at the wall for a first order reaction, is a function of the Thiele Modulus.

$$\eta = \frac{C_{NO}^{b}}{C_{NO}^{w}} = \frac{\tanh(\varphi)}{\varphi} \tag{21}$$

The magnitude of the internal diffusion resistance depends on the Thiele Modulus given in Equation 15. For small φ, $\eta \approx 1$, therefore, there is negligible internal diffusion resistance. Large φ, $\eta \approx 1/\varphi$ means that reactants are depleted faster than the time necessary for them to reach the active sites due to strong internal diffusion effect [83]. When the monolith catalyst is approximated as a slab with washcoat thickness t_w, effectiveness factors for two regions mentioned above can be expressed as [7]:

$$\eta = 1 \qquad for\ small\ \varphi \tag{22}$$

$$\eta = \frac{1}{\varphi} = \frac{1}{t_w}\sqrt{\frac{D_{eff,NO}}{k_c^*}} \qquad for\ large\ \varphi \tag{23}$$

The steady state differential mass balance for the transportation of nitric oxide in the washcoat layer is given by Equation 24. (see Figure 4.2)

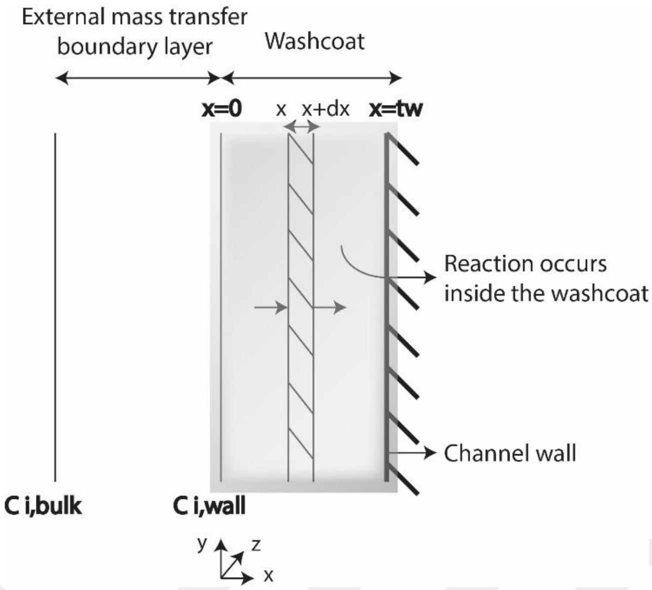

Figure 4. 2. External mass transfer boundary layer and washcoat inside a monolith channel

$$D_{eff,NO}\ \frac{d^2C_{NO}^*}{dx^2} - k_c^*(C_{NO}^*) = 0 \tag{24}$$

for an irreversible reaction with first-order kinetics; $-r_{NO} = k_c^{*}C_{NO}^{*}$

where k_c^* is the intrinsic rate constant per washcoat thickness, C_{NO}^* is the concentration of NO in the washcoat. The rate expression does not contain any terms on fractional coverage of the adsorbed species.

The boundary conditions are:

1. At x = 0, $C_{NO}^* = C_{NO}^w$
2. At x = t_w, $N_{NO,x} = 0$

The solution of Equation 24 is given by:

$$\frac{C_{NO}^*}{C_{NO}^w} = \frac{\cosh(\varphi(1-\left(\frac{x}{t_w}\right))}{\cosh(\varphi)} \tag{25}$$

The molar flux (N_{NO}) at x = 0 is:

$$N_{NO,x}\big|_{x=0} = -D_{eff,NO}\frac{dC_{NO}^{*}}{dx}\bigg|_{x=0} = \frac{C_{NO}^{w}D_{eff,NO}}{t_w}\ \varphi \tanh(\varphi) \tag{26}$$

The combination of Equation 13, 14, and 27 gives:

$$-u\frac{dC_{NO}^{b}}{dz} = \frac{4}{d_h}C_{NO}^{b}\left(k_m - \frac{{k_m}^2}{k_m+\frac{D_{eff,NO}\ \varphi\tanh(\varphi)}{t_w}}\right) \tag{27}$$

If an overall pseudo-first order reaction rate constant is defined as:

$$\frac{1}{k_{ov}} = \frac{1}{k_m} + \frac{1}{k_{app}} \tag{28}$$

Equations 27 and 28 can then be then combined to give an equation for overall pseudo-first order reaction rate constant:

$$-u\frac{dC_{NO}^{b}}{dz} = \frac{4}{d_h}k_{ov}C_{NO}^{b} \tag{29}$$

Parameters in Equation 28 represent the resistances affecting the overall reaction rate constant. Accordingly, if external mass transfer is the rate determining step, then $k_m << k_{app}$ and the chemical reaction and internal diffusion resistance ($1/k_{app}$) are negligible. If $k_{app} << k_m$, then the apparent reaction is the rate determining step and the overall reaction rate constant equals that of the apparent rate constant.

4.1.3. Determination of Apparent and Intrinsic Reaction Rate Constants

The monolith reactor can be operated in the kinetic regime at high flow rates and low temperatures due to the absence of external transport limitations. Apparent kinetic parameters were estimated in this regime where $(1/k_m) << (1/k_{app})$, therefore k_{ov} equals to k_{app}. Substitution of k_{app} for k_{ov} in Equation 29 with the condition of $(1/k_m) << (1/k_{app})$ gives:

$$-u\frac{dC_{NO}^{b}}{dz}=\frac{4}{d_h}k_{app}C_{NO}^{b} \tag{30}$$

The apparent rate constants were obtained by operating the monolith reactor at a high flow rate (SV: 80,000 h^{-1} STP) and in a low temperature range between 144 and 181 °C. In Section 4.1.2, the apparent rate constant is also determined as $D_{eff,NO}\ \varphi\tanh(\varphi)\ /\ (t_w)$ in Equation 27. Substituting the definition of the Thiele modulus into the apparent rate constant equation gives:

$$k_{app}=\sqrt{k_c{}^{*}D_{eff,NO}}\tanh(\sqrt{(t_w)^2k_c{}^{*}/D_{eff,NO}}) \tag{31}$$

Equation 21 and 31 are readily combined to give:

$$k_{app}=\eta k_c{}^{*}t_w \tag{32}$$

In the given temperature interval (144 and 181 °C), the reactor operates in the kinetic regime; therefore $k_c{}^{*}$ is defined by Equation 33:

$$k_c{}^{*}=k_{app}\ /t_w \tag{33}$$

$k_c{}^{*}$ can be expressed by the Arrhenius equation (Equation 34) where A_i is the pre-exponential factor and E_A is the activation energy.

$$k_c{}^{*}=A_i\exp(-\frac{E_A}{RT}) \tag{34}$$

4.2. Detailed Kinetic Model for SCR Reactions

4.2.1. Monolith reactor model

To develop a detailed mathematical model, kinetic and mass transfer characteristics of the catalyst should be investigated together. Accordingly, standard SCR, fast SCR, NH_3 oxidation, and NO oxidation experiments were considered in the model while NH_3 adsorption & desorption and TPD experiments were conducted to investigate the effect of external and internal mass transfer limitations of the catalyst.

A one channel model was used for the modelling of the NH_3-SCR reactions. A commercial software, called GT-POWER (version 2017) was used for the optimization of parameters and also to generate a mass transfer coefficient correlation. The optimization tool uses genetic algorithm for the parameter estimation. Basically, this algorithm tries to find kinetic parameters that minimize the total error over the duration of the simulation. Mass balance equations were derived for a system with multi-components and –reactions. Equations were divided into two parts which are bulk phase and washcoat species balances.

4.2.1.1. Bulk phase species balance

For the bulk phase, mass balance for any species i was shown by using the external mass transfer coefficient, $k_{m,i}$. The thin film theory was used to investigate the mass transfer of species from gas phase to the washcoat surface. GT-POWER [84] software was used for the modeling. Quasi-steady state assumption was made for both bulk phase and washcoat species balances due to short residence time of gas in the reactor compared to other time scales of interest.

$$-u\, \varepsilon\, \rho_i \frac{dw_i^b}{dz} = S k_{m,i}\left(W_i^b - W_i^w\right) \tag{35}$$

where S is the geometric surface area per unit reactor volume (GSA), and $k_{m,i}$ is the external mass transfer coefficient for species i were given by:

$$S\ (GSA) = 4 / d_h \qquad (36)$$

$$k_{m,i} = R_i/(S(W_i^b - W_i^w)) \qquad (37)$$

(The subscript i indicates the species in the reactor, such as NH_3, NO, NO_2, N_2O.)

For this equation, the assumptions are; a) negligible axial diffusion, b) identical conditions for each channel and c) negligible entrance length effects (assuming fully developed laminar flow (Re<100)).

The external mass transfer effects in the Cu-CHA catalyst was defined by a Sherwood number correlation, as shown below:

$$Sh = A(1 + B(Re)(Sc)(d_h/L))^C \qquad (38)$$

Constants *B* and *C* in Equation 38 are related to channel geometry and surface roughness, respectively [36] and *Re* and *Sc* indicate Reynolds and Schmidt numbers, respectively.

The internal mass transfer effects were quantified defining effective diffusivity of species in the exhaust gas mixture.

4.2.1.2. Washcoat species balance

Effect of internal mass transfer and the reactions in the washcoat were analyzed by following equations:

$$f_c \rho_s D_{eff,i} \frac{d^2 W_i}{dx^2} - R_i = 0 \qquad (39)$$

$$R_i(species\ rate) = M_i \sum_j a_j s_{ij} r_j \qquad (40)$$

where M_i is the molecular weight of species i

a_j is the active site density for reaction j

r_j is the rate of reaction of reaction j

s_{ij} is the stoichiometric coefficient of specie i of reaction j

f_c is the solid fraction of washcoat

with the continuity of fluxes at x = 0 (see Figure 4.2):

$$-u\,\mathcal{E}\,\rho_i \frac{dW_i}{dx}\bigg|_{x=0} = Sk_{m,i}\left(W_i^b - W_i^w\right) = \sum_j s_{ij} r_j \tag{41}$$

with $\frac{dW_i}{dx} = 0$ at x = δ, and $\delta = \frac{f_c}{S}$

where s_{ij} is the stoichiometric coefficient of species i for the reaction j.

Lastly, for the coverage of components on the surface, Equation 42 and 43 were used.

$$A_k \frac{d\theta_k}{dt} = \sum_j \sigma_{kj} a_j r_j \tag{42}$$

$$\sum_k \theta_k = 1 \tag{43}$$

where A_k is the active site density for coverage k

θ_k is the component of surface coverage

4.2.2. Kinetic model

The rate constants of the SCR reactions were defined by using Arrhenius equation:

$$k_i = A_i e^{-E_i/RT} \tag{44}$$

In previous studies [15, 85-89], it has been revealed that activation energy for NH_3 desorption can be described by Temkin-type isotherm. Thus, coverage dependent activation energy function was used to describe ammonia desorption behavior according to following equation:

$$E_i = E_{i,0}(1 - \alpha\theta_{NH_3,S}) \tag{45}$$

SCR reactions considered in this study and the rate expressions were shown in Table 4.1 with the corresponding kinetic parameters.

NH_3 adsorption and desorption is the first and key step in the kinetic modelling since NH_3 is stored in high amounts over zeolites [88, 90-92]. Olsson et al. [15] showed that a single site model is not sufficient to describe NH_3 activity over Cu-SSZ-13, therefore three types of ammonia storage and release sites were used in this model: two strong sites for chemisorbed ammonia and one site for loosely bound physisorbed ammonia. The first site (S1) is the main storage site where both copper and Bronsted acid sites were lumped together [15, 16, 85, 88]. S1 denotes moderately bound ammonia at low temperatures. The copper sites located on/near to six-membered rings of the chabazite are mostly the Bronsted and Lewis sites according previous studies [93]. The second site (S2) is the high temperature storage site [15, 94] where both copper and OH bridging Bronsted acid sites are found together as in S1. Moreover, it is suggested that copper ions may agglomerate in the larger cages of the chabazite structure as the temperature increases [ref], therefore the site S2 is also associated with the active copper-oxo clusters in the large cavities [15]. Apart from the chemisorption, ammonia can also be physisorbed which was described by site-3 (S3). The site densities of each site were found from NH_3 adsorption, desorption and TPD experiment which was described in detail in Section 5.2.1. This experiment showed that most of the ammonia adsorption occurs on the strong sites (S1 and S2), especially on S1. Sites S1 and S2 are the ones associated with active Cu sites where the SCR occurs [15]. The rate expressions for ammonia adsorption and desorption for the three sites was shown by reaction numbers 1-3 in Table 4.1. Kinetic parameters for NH_3 adsorption and desorption reactions, effective diffusivity of ammonia and the coefficients of the Sherwood number correlation were optimized using the experimental data via a genetic algorithm in the optimization tool of the GT-POWER software.

At high temperatures, significant amount of ammonia oxidation was observed, which was shown by reaction numbers 4 and 5 in Table 4.1. Kinetic parameters related to NH_3 oxidation reactions for the two sites were determined, during which the parameters obtained from previous optimization (NH_3 adsorption-desorption optimization) kept constant, and then incorporated into the overall model. Ammonia oxidation to N_2O reaction was not considered because very low amounts of N_2O were released during the experiments (around 1 ppm). Moreover, NO formation during NH_3 oxidation was not observed, which is why this reaction was ruled out in this study. Reaction orders for oxygen in ammonia oxidation reactions in both sites were optimized by GT-POWER. In addition, NO oxidation to NO_2 (reaction number 6) was also considered in the kinetic model by assuming the reaction proceeded in the gas phase as in several kinetic models [15, 85].

The rate expressions for standard SCR were shown in Table 4.1. In standard SCR reactions, it was assumed that strongly bound ammonia on the surface reacts with the NO in the gas phase. Accordingly, reactions were described between strongly bound ammonia on S1 and S2, and the gas phase NO. Reaction rate parameters and orders for O_2 in standard SCR reactions in both sites were optimized by keeping the parameters associated with previously optimized reactions (rxn. no: 1-6) constant .Effective diffusivity of NO were found and tabulated in Chapter 5.

Furthermore, formation of N_2O species was also incorporated into the kinetic model. Complex behavior of N_2O formation was described in two steps in earlier studies [15, 85, 95, 96]. Up to 225 °C, N_2O formation increased with increasing temperature due to the generation of ammonium nitrate type species and their reactions with oxygen (reaction number 10). Thereafter, decomposition of the ammonium nitrate type species started as the temperature increased further. Decline in the coverage of these types of species eliminated reaction 10, and therefore formation of N_2O up to 410 °C. However, after this point, N_2O formation increased again; that’s why reaction 11 was added to the model for the high temperature interval. Therefore, two reactions were suggested to describe the formation of N_2O from NO at low and high temperatures in this kinetic model. All reactions related to N_2O formation were suggested to occur on S2 because copper oxide clusters or coppers in the large cavities of chabazite are suggested to be active for N_2O formation reactions. Standard SCR experimental data was used for the optimization of parameters related to N_2O formation by keeping the parameters associated with the previously optimized reactions (rxn. no: 1-8) constant. Further, NO formation from the reaction of NH_3 and NO_2 was observed in the previous studies as well if the metal loading amount is high in the catalyst [85, 97]. However, this reaction was not considered in the kinetic model because it is only important for the aged samples [85]. Similarly, formation of nitrogen from the reaction between ammonia and NO due to copper oxide formation at high temperatures [85] was also ruled out since the all samples used in this study were fresh.

Each kinetic parameter of the individual reactions were determined by using an optimization software. Moreover, activation energies for standard SCR and NH_3 oxidation reactions on S1 were also found from Arrhenius plot.

Table 4. 1. Reactions and the rate expressions for three-site kinetic model.

Reaction	Rate expression	Reaction number
NH_3 + S1 ⇔ NH_3-S1	$r_1 = k_{1,f}C_{NH_3}\theta_{S1} - k_{1,b}\theta_{NH_3-S1}$	(1)
NH_3 + S2 ⇔ NH_3-S2	$r_2 = k_{2,f}C_{NH_3}\theta_{S1} - k_{2,b}\theta_{NH_3-S2}$	(2)
NH_3 + S3 ⇔ NH_3-S3	$r_3 = k_{3,f}C_{NH_3}\theta_{S1} - k_{3,b}\theta_{NH_3-S3}$	(3)
2S1-NH_3 + 1.5O_2 ⇒ N_2 + 3H_2O + 2S1	$r_4 = k_4{C_{O_2}}^{n_{NH_3-Ox,1}}\theta_{S1-NH_3}$	(4)
2S2-NH_3 + 1.5O_2 ⇒ N_2 + 3H_2O + 2S2	$r_5 = k_5{C_{O_2}}^{n_{NH_3-Ox,2}}\theta_{S2-NH_3}$	(5)
NO + 0.5O_2 ⇔ NO_2	$r_6 = k_{6,f}C_{NO}{C_{O_2}}^{0.5} - k_{6,b}\frac{C_{NO_2}}{K_{eq,NO}}$	(6)
4S1-NH_3 + 4NO + O_2 ⇒ 4N_2 + 6H_2O + 4S1	$r_7 = k_7C_{NO}{C_{O_2}}^{n_{std,1}}\theta_{S1-NH_3}$	(7)
4S2-NH_3 + 4NO + O_2 ⇒ 4N_2 + 6H_2O + 4S2	$r_8 = k_8C_{NO}{C_{O_2}}^{n_{std,2}}\theta_{S2-NH_3}$	(8)
S2-NH_3 + NO ⇔ S2-NH_3-NO	$r_9 = k_{9,f}C_{NO}\theta_{S2-NH_3} - k_{9,b}\theta_{S2-NH_3-NO}$	(9)
2S2-NH_3-NO + O_2 ⇒ N_2O + N_2 + 3H_2O + 2S2	$r_{10} = k_{10}C_{O_2}\theta_{S2-NH_3-NO}$	(10)
2S2-NH_3 + 2NO + O_2 ⇒ N_2O + N_2 + 3H_2O + 2S2	$r_{11} = k_{11}C_{O_2}C_{NO}\theta_{S2-NH_3}$	(11)

Chapter 5

RESULTS AND DISCUSSION

5.1. Results of the Single Reaction Model

5.1.1. Standard SCR Experiments

Figure 5.1 shows the variation of the NO conversion as a function of temperature in the 100-590 °C range at different space velocities. The maximum conversion (>98%) was observed in the temperature range 230-370 °C when the space velocity was in the 20,000-60,000 h^{-1} range while the maximum conversion at 80,000 h^{-1} (STP) was found to be slightly lower (>95%) in the same temperature range. The SCR activity was maintained up to 400 °C but NO conversion decreased at higher temperatures in agreement with the data in the literature [26, 28]. NOx reduction activity decreased since the consumption of ammonia in the ammonia oxidation reaction (which started above 350 °C) reduced the available ammonia for the standard SCR reaction. At 590 °C, NO conversion decreased up to 60% for 20,000 h^{-1} (STP) and 70% for 30,000 & 40,000 h^{-1} (STP). However, even at the highest temperature operated in this study, considerably high conversion (>80%) was obtained in the experiment with 80,000 h^{-1} (STP) as shown in Figure 5.1. The maximum NO conversion for the highest flow rate was obtained at the high temperature interval (>400 °C). Therefore, the reactor operates in the kinetic regime at high flow rates and at low temperatures whereas external mass transfer limitations are present at high temperatures.

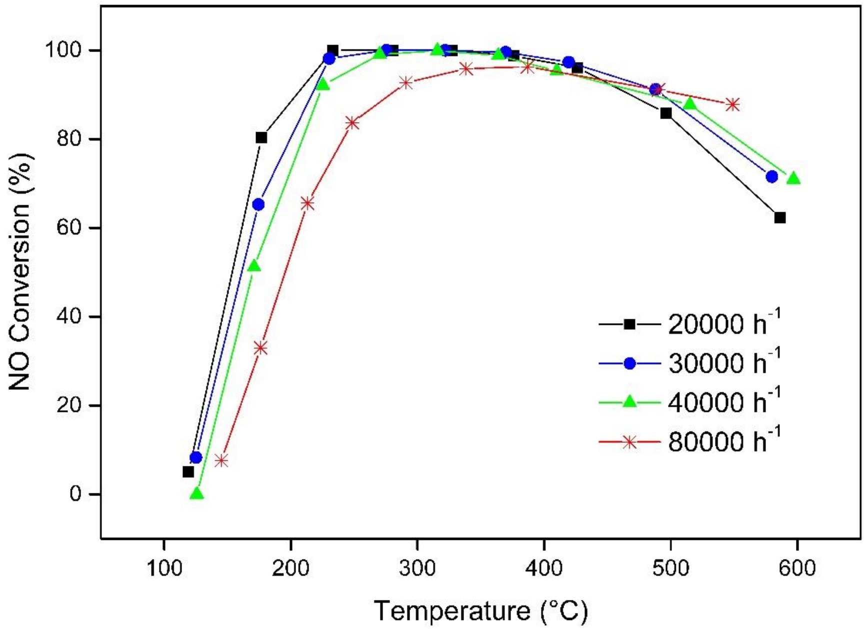

Figure 5. 1. Steady state NO conversion as a function of temperature during standard SCR. Reactant feed contains 300 ppm NH_3, 300 ppm NO, 10% CO_2, 8% O_2, 5 % H_2O, and balance N_2 at GHSV of 20000-80000h^{-1}(STP) range

In order to obtain the kinetic parameters of a standard SCR reaction, the reactor was operated at a high flow rate (SV: 80,000 h^{-1}) and in the low temperature (144 to 181 °C) with the feed condition of 300 ppm NH_3, 300 ppm NO, 10% CO_2, 8% O_2, 5 % H_2O and balance N_2 from. The activation energy and pre-exponential factor for this reaction were found using the Arrhenius Plot (see Figure 5.2). Kinetic parameters of a standard SCR reaction were used to determine external mass transfer coefficients in the region where overall rate was controlled by mass transfer.

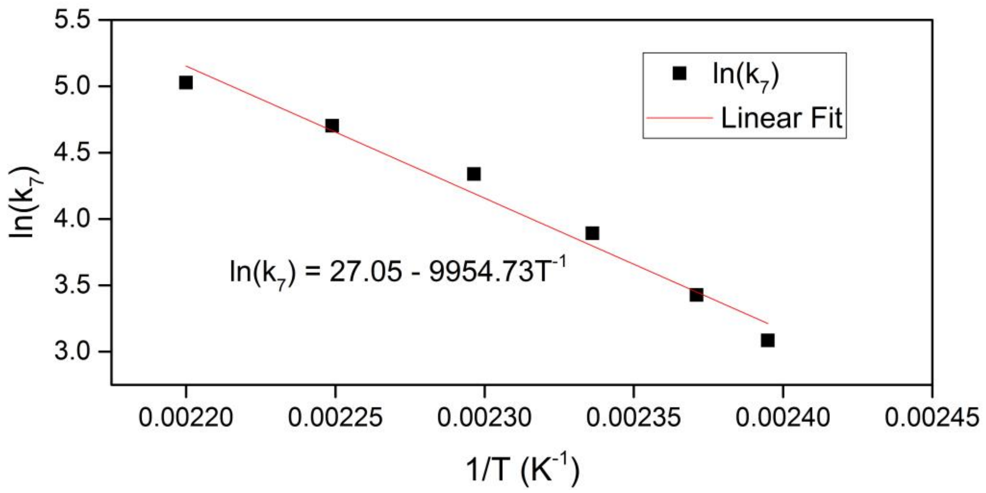

Figure 5. 2. Arrhenius plot for standard SCR. Reactant feed contains 300 ppm NH_3, 300 ppm NO, 10% CO_2, 8% O_2, 5 % H_2O, and balance N_2 at a GHSV of 80000h^{-1}(STP)

5.1.2. Evaluation of Mass Transport and Surface Reaction Resistances

Overall reaction rate constants over entire temperature interval for standard SCR reaction were evaluated using Equation 29 for each of the space velocities, while apparent reaction rate constants were determined from Equation 31. Then, the external mass transfer coefficients were extracted from the relation between resistances (Equation 28).

We obtained a similar trend for the effects of each resistances in the specified temperature intervals of each flow rate. Overall reaction rate was controlled by the apparent reaction rate and the internal diffusion limitation was negligible up to 230 °C. Theoretical calculations and Thiele Modulus criteria (Weisz–Prater criterion) supported the experimental findings. Moreover, external mass transfer resistances were very small when compared to apparent reaction resistance in the same temperature interval. Therefore, the overall reaction rate was controlled by the surface reaction kinetics in the low temperature zone (<230 °C) for 20,000 and 30,000 h^{-1} (STP). Between 230 and 330 °C, both chemical reactions, internal, and external mass transfer resistances were significant, thus this temperature interval could be ascribed as a mixed regime. Above 330 °C, the effects of external mass transfer on overall reaction resistance began. Thiele Modulus criteria proved the existence of internal diffusion limitation at higher temperatures. In this temperature zone, the surface reaction was very fast when compared to external diffusion. Hence, the magnitude of $1/k_{app}$ became much smaller than $1/k_m$. It can be concluded that the external diffusion limitations were present for the standard SCR reaction after 330 °C for 20,000 and 30,000 h^{-1} (STP).

At higher flow rates, similar results were observed with slight differences. The overall reaction rate was controlled by surface reactions up to 225 °C and 213 °C for 40,000 and 80,000 h^{-1} (STP), respectively. There was a mixed region, where overall reaction rates were controlled by both mass transport and kinetic resistances, between 225-360 °C for 40,000 h^{-1} and between 213-380 °C for 80,000 h^{-1} (STP). Above these temperatures, external mass transfer rate controlled the overall reaction rate but the magnitude of the mass transfer resistances were lower at these flow rates. As the flow rate increased, the transportation of NO from bulk phase to the surface of the catalyst became much slower than the reaction at the active site. Therefore, the effect of interphase diffusion resistance ($1/k_m$) became smaller.

As a consequence, at lower temperatures (below ≈210 °C) the effect of external mass transfer resistance was insignificant, therefore the overall reaction rate only depended on the surface kinetics. However as the temperature increased, the effect of interphase diffusion became significant, particularly for the lower flow rates. In this zone, an increase in the flow rate resulted in a higher external mass transfer coefficient (k_m) or lower resistances to external mass transfer ($1/k_m$). Therefore, very low space velocities and high temperatures (above ≈350 °C) were necessary to operate purely in external mass transfer controlled regions. The result related to the external mass transfer limited region was also in line with the experimental result shown in Figure 5.1.

5.1.3. Comparison of the External Mass Transfer Coefficients of Standard SCR Reaction with Those in the Literature

Sherwood numbers given in Section 2.6.5 were calculated for 2.2 cm length monolith catalysts for the range of experimental conditions. External mass transfer coefficients were calculated from average Sherwood number equation according to:

$$k_m = \frac{Sh\, D_{NO-air}}{d_h} \tag{12}$$

External mass transfer coefficients were calculated using various correlations from the literature and those obtained experimentally in this study for standard SCR at 80,000 h^{-1}, (STP) shown in Figure 5.3. Coefficients were extracted from data in the 210-550 °C temperature range, since the reactor operated in the kinetically controlled region for the temperatures below 210 °C. Coefficients increased as the temperature increased from 210 to 390 °C as shown in Figure 5.3. This was due to the increase of the diffusivity of NO with the increase in temperature since the external mass transfer coefficients were proportional to the diffusion coefficient. For temperatures between 210 and 390 °C, calculated external mass transfer coefficients were in good agreement with the trends from the literature. Our k_m values were lower than those determined by Gundlapally [43], Holmgren [41], Uberoi [40], Hawthorn [36], and Troconi [38], higher than Bennett's correlation [37], and slightly higher than the models of Votruba [42] and Ullah [39].

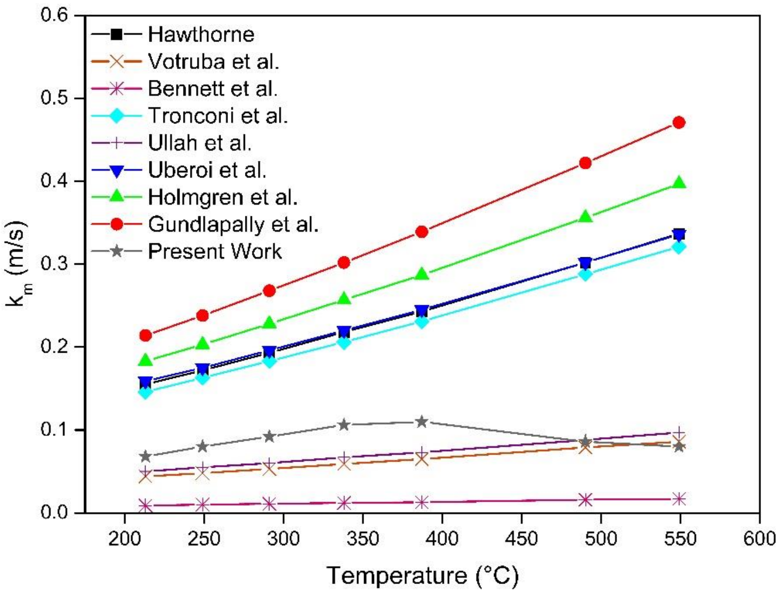

Figure 5. 3. External mass transfer coefficients against temperature for standard SCR 80000 h^{-1} (STP)

The reason for lower external mass transfer coefficients obtained from Bennett, Votruba and Ullah can be attributed to their experimental conditions that were used to derive mass transfer correlations. [41]. In Bennett et al., experiments were conducted in the 407-527 °C temperature interval and the measured reaction rate was considerably lower than expected. The authors attributed the reason for the low reaction rate to the effect of mass transfer limitations. However, analysis of Hayes and Kolaczkowski [98] proved that the surface reaction prevailed the mass transfer effects at 407-527 °C range, therefore the monolith reactor operated in the kinetic controlled region while the mass transfer coefficients were extracted. Regarding the study by Votruba et al, their correlation was obtained from the evaporation of water and hydrocarbons from monolith reactors, hence experiments were conducted under non-reacting conditions. The reason of the divergence between Votruba and our work can be illustrated by the fact that Votruba et al. used larger monolith channels up to 1 cm which may affect the extracted mass transport parameters. Experiments of Ullah et al. were analyzed by Hayes and Kolaczkowsk [98] and revealed that the overall reaction rate was kinetically controlled when they determined the Sherwood numbers. Moreover, internal mass transfer rates can be the rate-determining step for the temperature ranges where they were used to measure external mass transfer coefficients. [41]. Hayes and Kolaczkowsk [98] also found out that the Ullah model was only applicable for a restricted range of monolith length, since this correlation did not express the asymptotic values like the Votruba model. Asymptotic value of Sherwood number correlation was obtained when the distance required to attain fully developed profiles were reached in the reactor [98]. Furthermore, channels of the monolith reactor used in that study were varying in size which may have caused velocity, temperature, and concentration profile, thus different reactant conversions in each channel.

The discrepancy between the Hawthorn model and present work may come from the unconventional behavior during their experiments. Previous studies revealed that sudden increases were observed in Sherwood numbers during the transient carbon monoxide oxidation experiments when unexpected light-off arose [98]. Similar results were obtained when correlations from Uberoi and Tronconi were used. The reason of divergence in coefficients obtained from Uberoi was analyzed by Holmgren et al. [41]. Theoretical values from Uberoi were valid for laminar flow regime. However, in real case, some turbulence occurs naturally at reactor entrances, which increased the mass transfer rate [41]. Accordingly, the Holmgren model considered the turbulent flow generated at the inlet but at very high flow rates. Like in Figure 5.3 (80,000 h^{-1} (STP)), this turbulence increases and results in a substantial increase in the calculated coefficients.

As shown in Figure 5.3, k_m values calculated in our work increased up to 390 °C after which they decreased slightly. The reason of the decline in external mass transfer coefficients was that the intrinsic kinetic parameters obtained at low temperatures could not account for SCR activity at higher temperatures. This may have been due to a change in the mechanism with increasing temperature. Higher temperatures could alter the monocopper active sites [68-70] of the Cu-chabazite catalyst. This may have changed the standard SCR reaction mechanism, as it was well known that dicopper or tricopper species could form on a number of Cu-zeolite families at temperatures above 400 ^{o}C [71-74]. Furthermore, for the temperatures higher than 350 °C, NO conversion started decreasing as shown in Figure 5.1 due to ammonia oxidation reaction. In this region, it was hard to extract the external mass transfer coefficient values because the ammonia oxidation reaction was not considered in the governing equations.

As a consequence, when the same conditions were applied for the correlations in the literature, external mass transfer coefficients were calculated as 0.24 m/s [36], 0.06 m/s [42], 0.01 m/s [37], 0.23 m/s [38], 0.07 m/s [39], 0.25 m/s [40], 0.29 m/s [41], and 0.34 m/s [43] for eight different correlations from the literature. These findings revealed that correlations in the literature are not appropriate for this system and there is a need to develop a detailed kinetic model which accounts for all mass transfer effects.

5.2. Results of the Detailed Kinetic Model for SCR Reactions

5.2.1. NH_3 adsorption - desorption

In NH_3-TPD experiment where first 500 ppm of NH_3 was fed to the reactor in the presence of 5% H_2O, 10% CO_2 and balance N_2 at 150 °C. Once the adsorption breakthrough was reached, NH_3 was removed from feed stream and then temperature was linearly increased with a ramp of 10 °C/min up to 600 °C. Uptake values and TPD peak center temperatures were used to determine site densities. NH_3-TPD experiment at 100 °C was used to determine the site densities of S1, S2 and S3. The site density for loosely bound ammonia (S3) was found using the amount of ammonia desorbed during the isothermal phase and released ammonia at the low temperature TPD phase. The amount of ammonia released during the TPD phase was used to detect the site densities of strongly bound ammonia (S1 and S2). Multiple peaks that overlap with each other in the TPD part was deconvoluted by the addition of two more Gaussian peaks. Raw data and fitted peaks were shown in Figure 5.4.

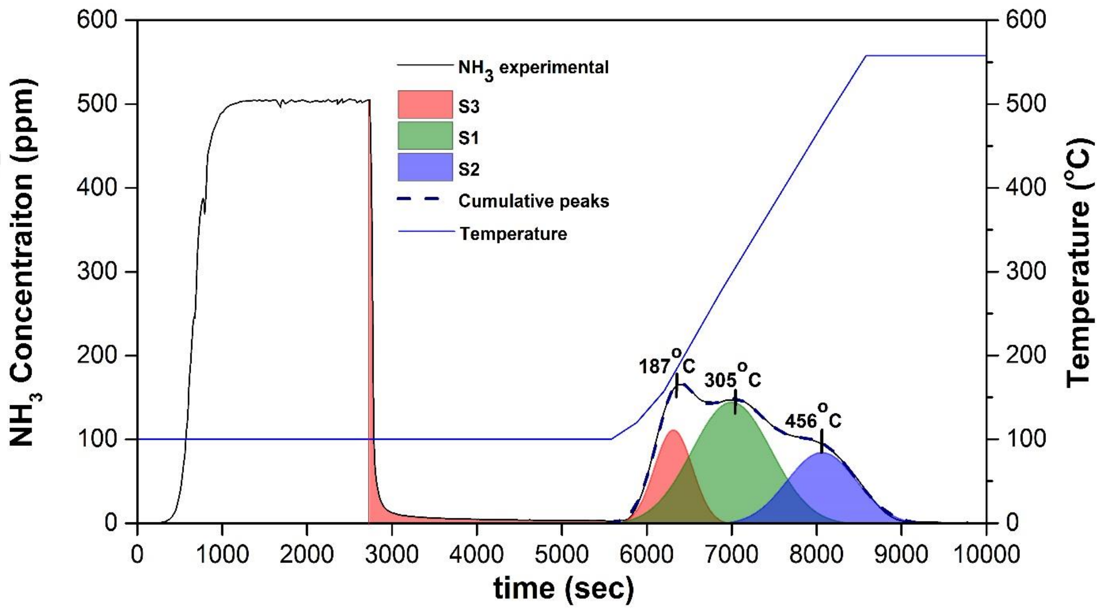

Figure 5. 4. NH_3 adsorption and TPD experiment. Reactant feed contains 500 ppm NH_3, 10% CO_2, 0% O_2, 5 % H_2O and balance N_2 at GHSV of 40,000h^{-1}(STP). Temperature of isothermal adsorption phase = 100 °C, T-ramp = 10 °C/min. (Colored peaks were obtained from deconvolution)

Exit ammonia concentration from the experiment and simulation were shown in Figure 5.4. Ammonia was first adsorbed on the surface thereafter it reached the NH_3 feed value. After the catalyst was fully saturated, the ammonia feed was terminated which resulted in desorption of loosely bound ammonia between t = 47 and t = 80 min. When the temperature was increased, three-site model resulted in two distinct desorption peaks in the TPD phase where the first ammonia desorption peak was seen with a maximum at about 290 °C. A second peak for desorption of strongly bound ammonia was observed at around 433 °C as the temperature was increased further. The model gave an excellent representation of ammonia storage, isothermal release, and the TPD phase due to the implementation of Temkin-type (coverage dependent) desorption kinetics and multi-site kinetic model.

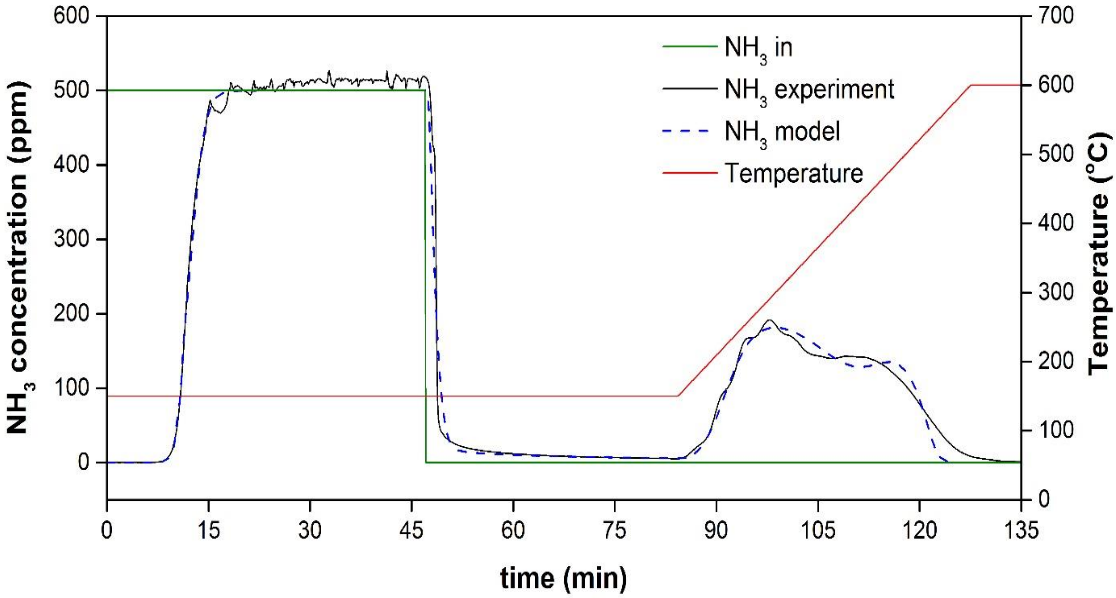

Figure 5. 5. NH_3 adsorption and TPD, solid line: experimental & dashed line: kinetic model. Reactant feed contains 500 ppm NH_3, 10% CO_2, 0% O_2, 5 % H_2O and balance N_2 at GHSV of 40,000h^{-1}(STP). Temperature of isothermal adsorption phase = 150 °C, T-ramp = 10 °C/min.

Furthermore, parameters for Sherwood number correlation were optimized using NH_3 adsorption-desorption experiment at 150 °C and tabulated in Table 5.1. Presented correlation in this study was compared with the various correlations for monolith reactors from literature in next section.

By using the same experiment, effective diffusivity of ammonia (D_{eff,NH_3}) in the washcoat was optimized and found 6.6 x 10^{-6} m^2/s using the ammonia adsorption and desorption experimental data. Effective diffusivity for each species can vary depending on the catalyst used in the experiments and the method applied, that’s why estimation of $D_{eff,i}$ was necessary. In the literature, different values were used for the effective diffusivity of ammonia over the metal-exchanged zeolite catalysts. Chatterjee et al. [17] and Olsson et al. [15] used a value of 5 x 10^{-6} m^2/s for Cu-SSZ-13 while Metkar et al.

[99] used a value in the range of 10^{-6} – 10^{-7} m^2/s in Cu-CHA. Huang et al. [100] used a value of 10^{-8} m^2/s for Fe-ZSM-5, and Metkar et al. [2] reported a value in the range of 10^{-8} – 10^{-9} m^2/s over Cu-ZSM-5 and Fe-ZSM-5 samples. Since there is no consensus for the value of effective diffusivity of ammonia, it is optimized with the kinetic parameters of the Reaction 1, 2 and 3.

Table 5. 1. Effective diffusivities of NH_3, NO, N_2O and optimized parameters for mass transfer coefficient correlation

Internal mass transfer parameters:	
Species	*Effective diffusivity, $D_{eff,I}$ (m^2/s)*
NH_3	6.54 x 10^{-6}
NO	4.72 x 10^{-6}
N_2O	6.51 x 10^{-6}
External mass transfer parameters:	
A	3.744
B	1.206
C	0.719
Mass transfer coefficient correlation:	$Sh = A(1 + B(Re)(Sc)(d_h/L))^C$

5.2.1.1. Comparison of mass transfer coefficient correlation with those in literature

Mass transfer coefficients in reactors are usually described by a dimensionless parameter called Sherwood number, or *Sh*. Table 5.1 shows mass transfer correlations proposed for monolith reactors in literature [36-43]. Catalyst and flow properties used in this study were applied to eight different correlations to make a comparison. The highest flow rate employed in the experiments was chosen (GHSV of 80,000 h^{-1} (STP)) for the calculation of Reynolds numbers. External mass transfer coefficients were calculated for

210 - 550 °C temperature interval since the reactor operates in the kinetically controlled region at lower temperatures [101].

Table 5. 2. Correlations for monolith reactors from literature

Correlation Number	Sherwood Number Correlations	References
1	$Sh = 2.976(1 + 0.078Re\ Sc\ (d_h/L))^{0.45}$	Hawthorne [36]
2	$Sh = 0.705(Re\ (d_h/L))^{0.43}(Sc)^{0.56}$	Votruba [42]
3	$Sh = 0.077(1 + Re\ Sc\ (d_h/L))^{0.83}$	Bennett [37]
4	$Sh = 2.976 + 8.827(1000(LD_{NO-air}/{d_h}^2u))^{-0.545}\exp(-48.2(LD_{NO-air}/{d_h}^2u))$	Tronconi [38]
5	$Sh = 0.766(Re\ Sc\ (d_h/L)/L)^{0.483}$	Ullah [39]
6	$Sh = 2.696(1 + 0.139Re\ Sc\ (d_h/L))^{0.81}$	Uberoi [40]
7	$Sh = 3.53\ exp(0.0298Re\ Sc\ (d_h/L))$	Holmgren [41]
8	$Sh = 4.364$	Gundlapally [43]

Variation of external mass transfer coefficients and Sherwood numbers with temperature were shown in Figure 5.6. Decline in the external mass transfer coefficients at high temperature interval (see Figure 5.3) was fixed by the implementation of additional sites for SCR reactions and side reactions. Here, we showed that mass transfer resistances in a monolith reactor can be affected by the side reactions. Addition of these reactions increased the deNOx ability of the SCR reactor, corrected the reaction mechanism and then resulted in a consummate multi-site kinetic model.

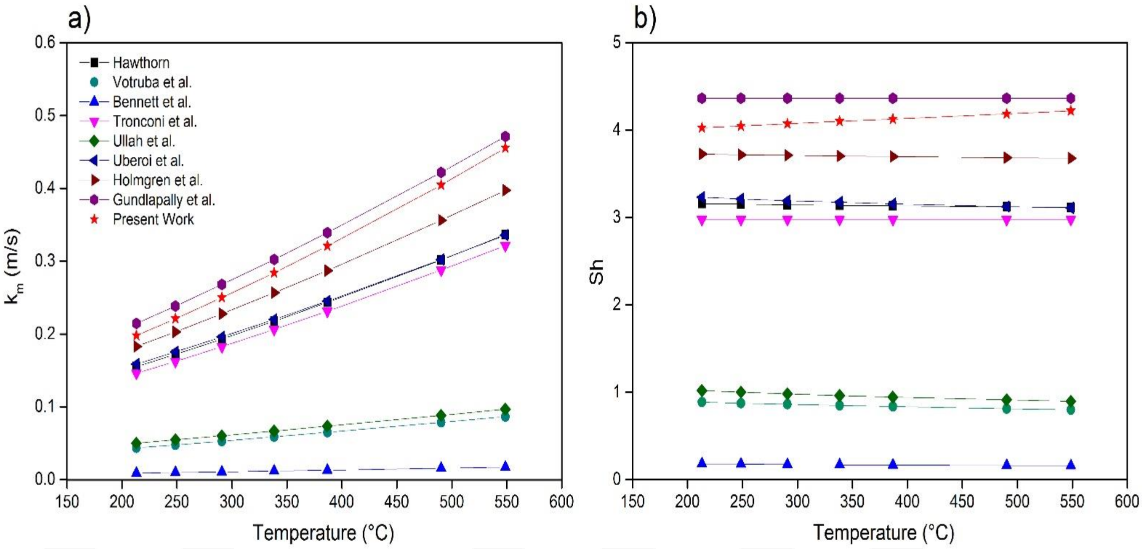

Figure 5. 6. Comparison of k_m and Sh numbers with literature (a) external mass transfer coefficients against temperature for standard SCR 40000 h^{-1} (STP), (b) Sh numbers against temperature for standard SCR 40000 h^{-1} (STP)

Once again, widely diverging results were obtained when the same experimental conditions were employed to the correlations in Table 5.2. In previous part [101], we discussed the possible reasons of discrepancies between the correlations. The clear difference between the correlations of Bennett, Votruba, Ullah and the others were attributed to some mistakes in their experimental conditions while measuring the external mass transfer coefficients. Results indicate that the mass transfer coefficient correlations from literature cannot be directly employed to every system, therefore they should be evaluated at conditions of interest.

5.2.2. NH_3 oxidation

NH_3 oxidation is the most important side reaction which competes with the main SCR reactions for ammonia. This reaction proceeds at high temperatures and decreases the NOx reduction selectivity. Therefore, it is very important to investigate the ammonia oxidation reaction in the kinetic model.

In the experiment, the catalyst was exposed to 500 ppm NH_3, 10% CO_2, 8% O_2, 5 % H_2O and balance N_2 and NH_3 conversion was measured between 168 to 590 °C. Experimental results and the model was shown in Figure 5.7. In the beginning of the experiment, first ammonia uptake and then break through were observed thereafter NH_3 oxidation started due to desorption of ammonia as the temperature increased stepwise. Ammonia conversion was first seen at about 270 °C with a low rate and the maximum conversion was observed at 500 °C and higher temperatures. These findings are in line with the values reported in literature [15, 85]. In the past, two sites were proposed for ammonia oxidation to occur on the copper-exchanged catalyst with different activation energies at low and high temperature intervals [15, 102]. Accordingly, ammonia oxidation reaction was described on both S1 and S2 in this study.

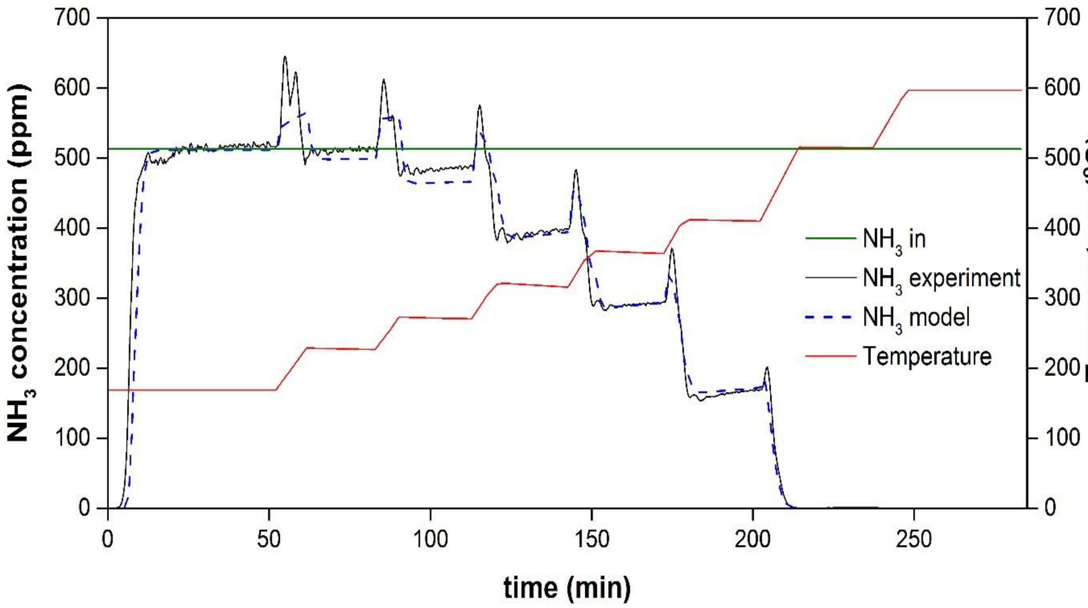

Figure 5. 7. NH_3 oxidation, solid line: experimental & dashed line: kinetic model. Reactant feed contains 500 ppm NH_3, 10% CO_2, 8% O_2, 5 % H_2O and balance N_2 at GHSV of 40,000h^{-1}(STP). Temperature of isothermal adsorption phase = 100 °C, T-ramp = 10 °C/min.

The model described the ammonia oxidation reaction very well due to the implementation of the second site at high temperatures. Negligible amount of N_2O (~1 ppm) was observed yet NO was not formed during the ammonia oxidation experiment. Previous studies revealed that reaction rates did not only depend on the ammonia coverages in each site but also depended on the oxygen concentration [15, 85, 99, 103].

Furthermore, a low conversion experiment was performed with 500 ppm NH_3, 10% CO_2, 8% O_2, 5 % H_2O, and balance N_2 from 266 to 370 °C to determine the activation energy for S1 and compare this value with the result from optimization tool. For selected temperature range, 14% maximum conversion was obtained and corresponding steady state data was shown in Figure 5.8. Activation energy for low temperature range was calculated from the Arrhenius plot, which is in an excellent agreement with the activation energy value optimized for the NH_3 oxidation reaction occurring on S1.

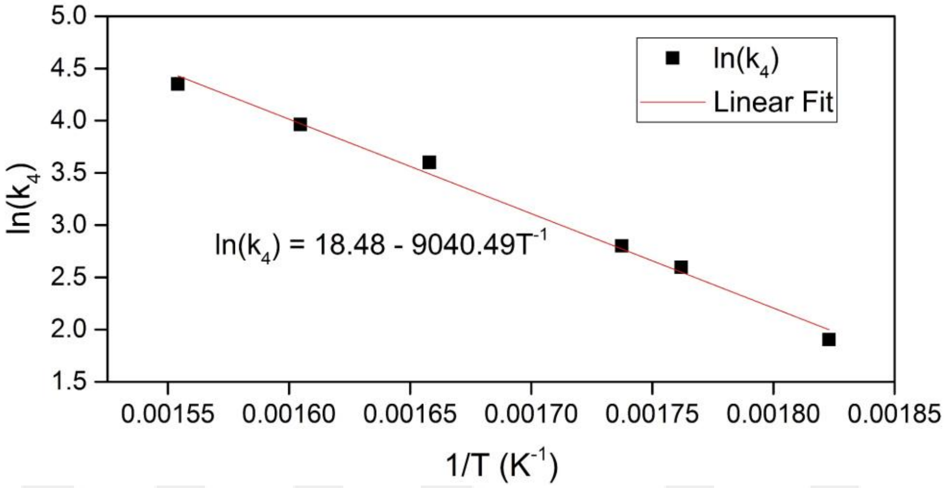

Figure 5. 8. Steady state NH_3 conversion as a function of temperature (266-370 °C) during NH_3 oxidation. Reactant feed contains 500 ppm NH_3, 10% CO_2, 8% O_2, 5 % H_2O and balance N_2 at a GHSV of 80,000h^{-1}(STP)

5.2.3. NO oxidation

NO oxidation is one the key steps which is considered as the slowest step among the reactions considered in this study. We used a Cu-CHA catalyst with 300 ppm NO, 10% CO_2, 8% O_2, 5 % H_2O and balance N_2 from 160 to 590 °C to study NO oxidation reaction as mentioned before. The model fitted to the experimental data is in line for the downstream NO and NO2 concentrations as shown in Figure 5.9. In a typical run, NO_2 formation increased as the temperature increased because the forward reaction is kinetically controlled at lower temperatures [88, 99]. As the temperature increased further, it was expected to observe a decline in NO conversion, since the reverse reaction (NO_2 decomposition) became important after 450-500 °C [88, 99]. Accordingly, this behavior was observed after 500 °C and the model showed a good agreement with the experimentally observed NO & NO_2 concentration profiles. NO oxidation reaction rate was expressed by a global rate equation which considers the equilibrium phenomena [104].

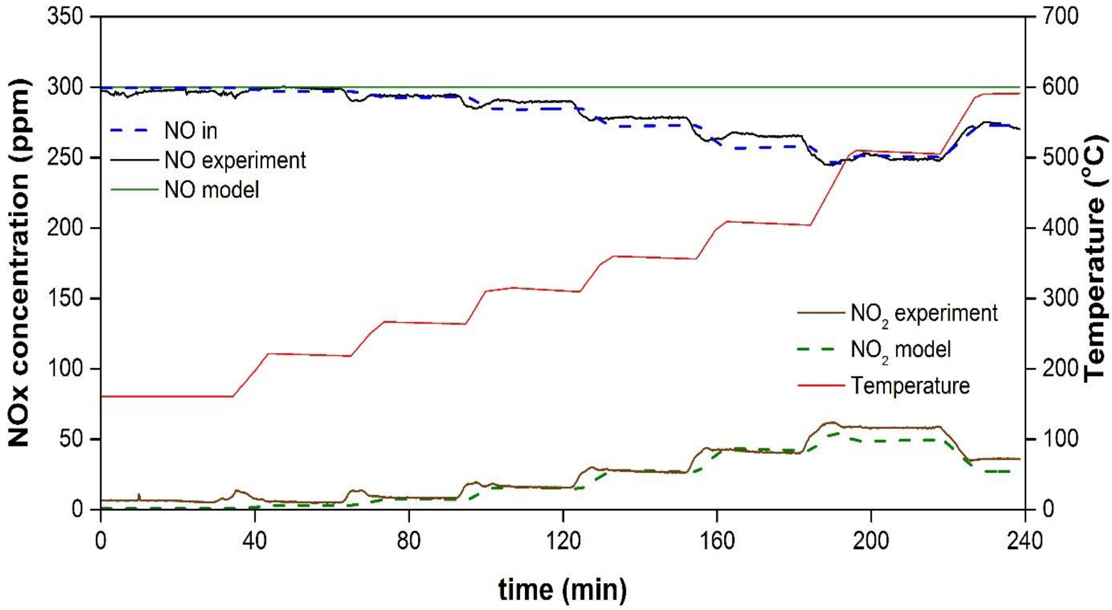

Figure 5. 9. NO oxidation, solid lines: experimental & dashed lines: kinetic model. Reactant feed contains 300 ppm NO, 10% CO_2, 8% O_2, 5 % H_2O and balance N_2 at GHSV of 40,000h^{-1}(STP). Temperature of isothermal phase = 160 °C, T-ramp = 10 °C/min.

5.2.4. Standard SCR with N_2O formation

In the standard SCR experiment, the catalyst was exposed to 300 ppm NH_3, 300 ppm NO, 10% CO_2, 8% O_2, 5 % H_2O and balance N_2 while the temperature was increased from 125 to 590 °C and NO conversion was measured. The results from experiment, and model as well as the inlet concentrations for NH_3, NO, NO_2 and N_2O were shown in Figure 5.10. In the beginning of the experiment, ammonia was stored on the catalyst and then began to desorb as the temperature increased. A previous study by Olsson et al. [15] revealed the fact that a high temperature ammonia storage site (S2) is necessary for the accurate modelling of the SCR behavior. Accordingly, standard SCR reactions were represented on both S1 and S2 in order to describe the SCR activity over the entire temperature range.

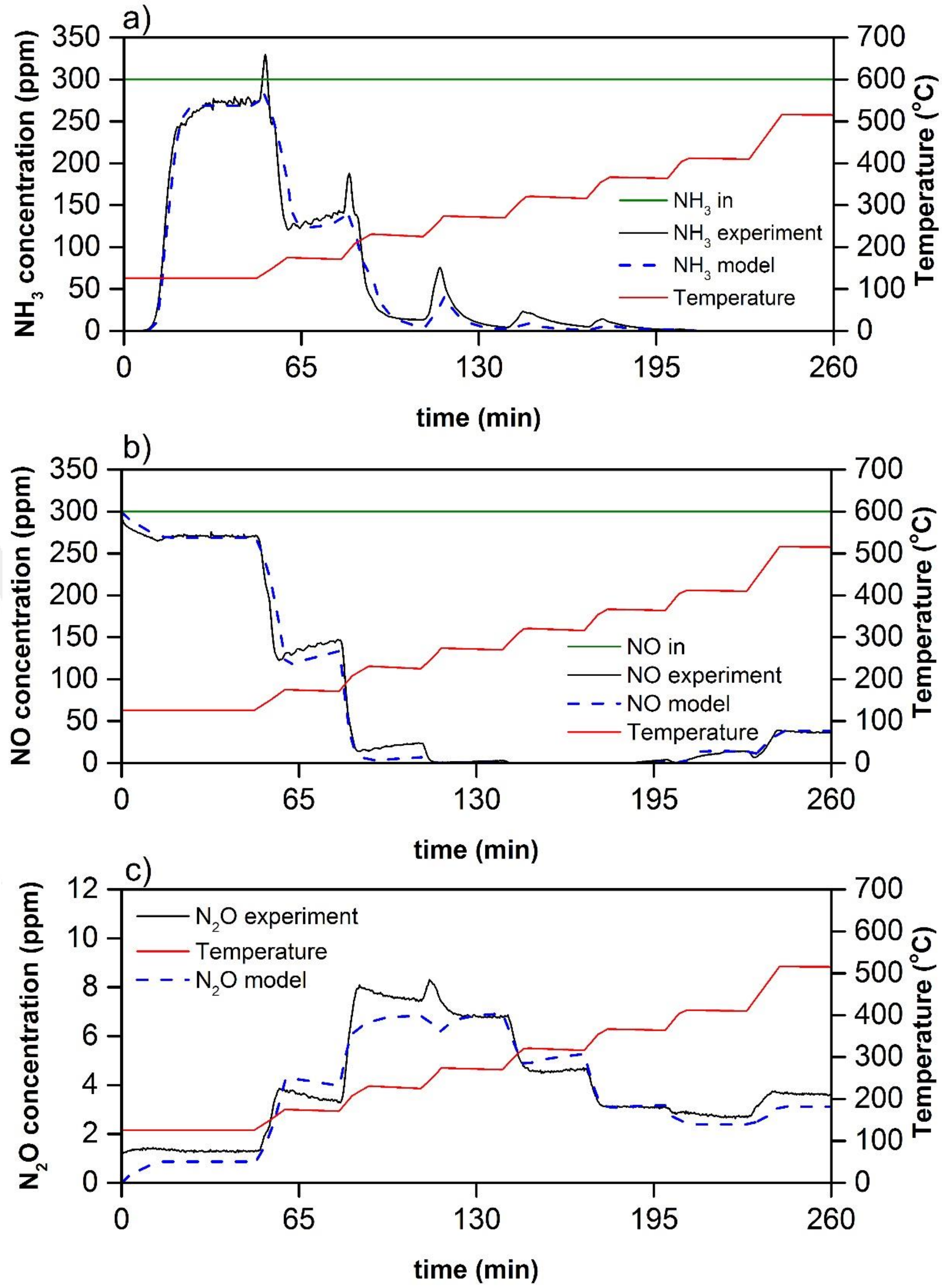

Figure 5. 10. NH_3-SCR (standard SCR), solid line: experimental & dashed line: kinetic model where (a) shows the NH_3 concentration, (b) NO and (c) NO_2 & N_2O concentrations. Reactant feed contains 300 ppm NH_3, 300 ppm NO, 10% CO_2, 8% O_2, 5 % H_2O and balance N_2 at GHSV of 40,000h^{-1}(STP). Temperature of isothermal adsorption phase = 126 °C, T-ramp = 10 °C/min.

Furthermore, N_2O formation during the SCR reactions were also included in the kinetic model. First, formation increased at low temperature range but as the temperature increased, its formation decreased. However, when the temperature was increased further, N_2O formation started to increase again. The same phenomena was also observed in previous studies [15, 85, 95, 96]. It is therefore likely that there are two different routes for the formation of N_2O for low and high temperature intervals over Cu-CHA as stated by Olsson et al. [15]. Its formation at low temperatures is related to ammonium nitrate formation and decomposition [96, 105]. Up to 200 °C, ammonium nitrate type species are formed from NO (reaction number 9a) which reacts to give N_2O according to reaction 10. At this point, N_2O reaches its maximum. After 200 °C, decomposition of ammonium nitrate type species started and decrease in their coverage yields to decline in N_2O formation. Further increase in temperature initiates additional reaction which was shown by reaction number 11. These experimental findings are in line with studies performed by Colombo [104], Olsson [15] and Supriyanto et al. [85]. Model showed a good agreement with the experimental data, verifying the necessity of an additional site for standard SCR reactions at high temperatures, and also the incorporation of N_2O formation reactions.

Further, like in the ammonia oxidation, a low conversion experiment at a space velocity of 80,000 h^{-1} was performed as stated in Section 5.1.1. Activation energy for S1 was determined using Arrhenius plot (see Figure 5.2). Calculated Ea value for low temperature range was used to check the accuracy of the optimization.

Table 5. 3. Diffusivity ratios for NH_3, NO and N_2O

	NH_3	**NO**	**N_2O**
D_{ab}/D_{eff}	13	17	10

By using the standard SCR experiment, effective diffusivities of NO and N_2O were also optimized and the results were shown in Table 5.3. D_{ab}/D_{eff} ratios for each species were calculated to check the accuracy of optimized D_{eff} values. This ratio should be in the same order of magnitude for NO, NH_3 and N_2O because effective diffusivity is a function of binary diffusion coefficient and fixed catalyst properties such as tortuosity and porosity. Since the catalyst properties are same for each species in the reactor, the ratio between binary diffusion coefficient and effective diffusion coefficient for each species should be very similar. We can check the accuracy of optimized D_{eff} values by considering the magnitudes of D_{ab}/D_{eff} ratios. Accordingly, D_{ab}/D_{eff} ratio of around 10 have been found for each species which is in good agreement with a previous study by Joshi et al. [103].

5.2.4.1. Coverage fractions during standard SCR reaction

Coverage fractions of each site during standard SCR reaction were also controlled and showed in Figure 5.11. Accordingly, we predicted high initial coverage for NH_3 on S1 and S2 while some ammonia on S3 in the isothermal phase. In the same temperature zone, surface coverage of S2-NH_3-NO reached its maximum. When the temperature was increased to 200 °C, the surface coverage of NH_3 on S1 and S2 remained high but the ammonia coverage on S3 decreased up to 0.1. This result was expected since the ammonia was strongly bound to those sites with high coverage even in the higher temperatures yet it was loosely bound to S3. Moreover, a low amount of NH_3-NO was continued to observe on S2. When the temperature was increased further, the amount of ammonia on S3 and NH_3-NO on S2 decreased dramatically. Almost all of the loosely bound ammonia was desorbed from the surface at 230 °C. When the temperature reached to 300 °C, coverage of NH_3-NO on S2 approached to zero since the dissociation of these species (reaction 9b) started above 200 °C. After this point, coverage of NH_3 on S1 and S2 continued to decrease, yet high amount of ammonia was maintained on S2 even in the 350°C. This high coverage retained SCR activity at high temperature interval therefore it was curial to add reaction 8 to the kinetic model. Further increase in the temperature caused in a very low amount of coverage on both S1 and S2, freeing up the sites and stop the standard SCR reactions (see Appendix-A), which resulted in an increase in NO concentration at high temperature interval (Figure 5.10.b and Figure B.1/Appendix-B).

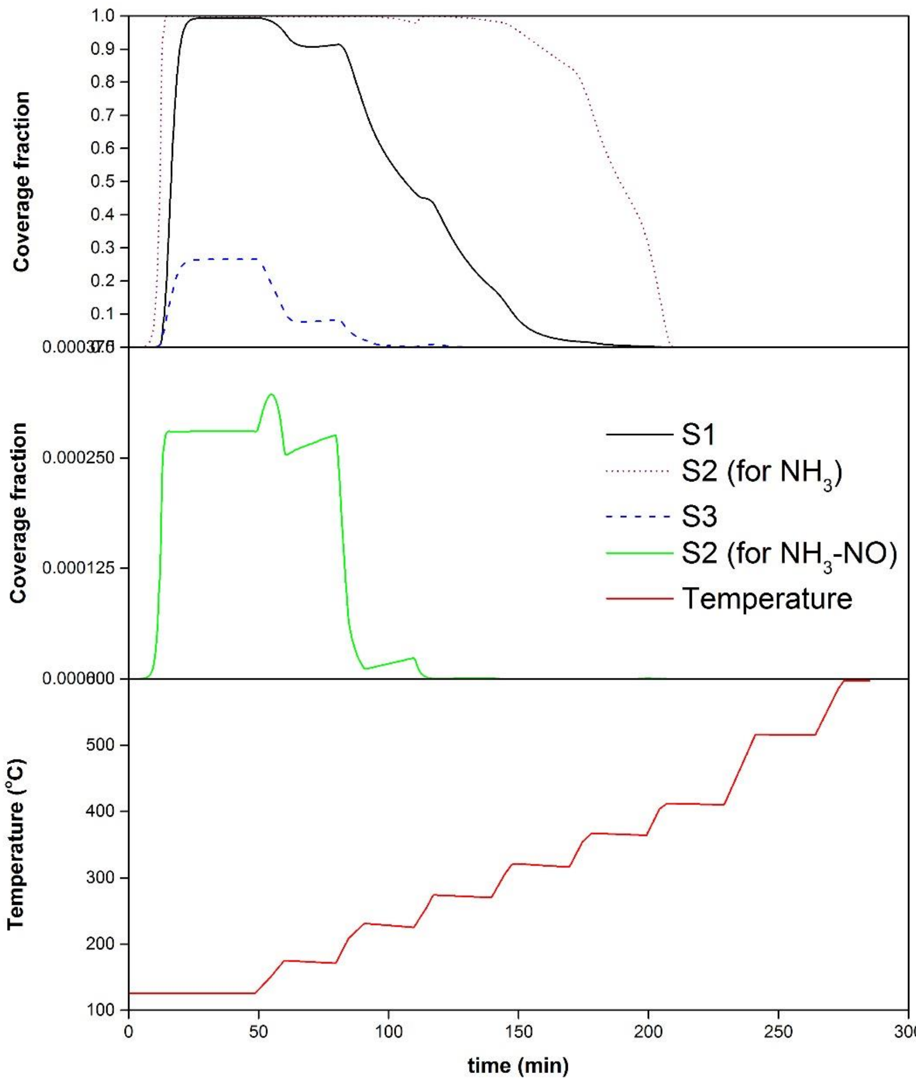

Figure 5. 11. Coverage fractions of S1, S2 and S3 during standard SCR reaction

5.2.5. Validation

The kinetic model described in this study also predicted very well standard SCR reactor effluent composition at different flow rates, which were not considered during the parameter estimation. Two standard SCR experiments with different flow rates were performed for the validation of estimated kinetic parameters. In the first experiment, catalyst was subjected to same feed conditions as those described in standard SCR experiment at 90 °C and 30,000 h^{-1} (STP) and then temperature was stepwise increased up to 500 °C. In the second experiment, same procedure was applied at 100 °C and 80,000 h^{-1} (STP). The exit concentrations of NO, NH_3 and N_2O were shown in Figure 5.12.

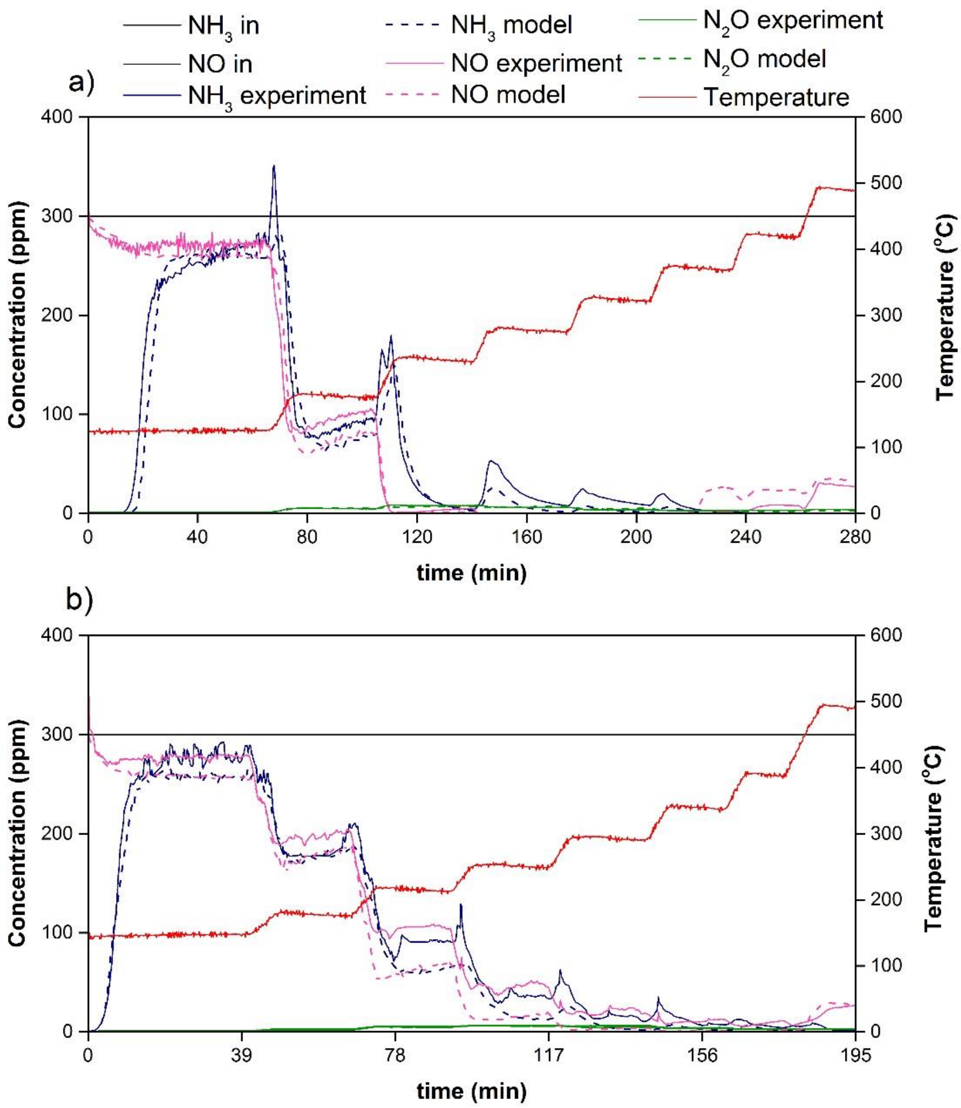

Figure 5. 12. NH_3-SCR (standard SCR) with different flow rates, solid line: experimental & dashed line: kinetic model where (a) shows the NH_3, NO, NO_2 & N_2O concentrations at GHSV of 30,000h^{-1} (STP) (b) shows the NH_3, NO, NO_2 & N_2O concentrations at GHSV of 80,000h^{-1} (STP). Reactant feed contains 300 ppm NH_3, 300 ppm NO, 10% CO_2, 8% O_2, 5 % H_2O and balance N_2. Temperature of isothermal adsorption phase = 90 °C for (a) and 100 °C for (b), T-ramp = 10 °C/min.

Our model well describes the concentrations of each species for 30,000 h^{-1} (STP) space velocity up to 375 °C (Figure 5.12.a). In between 375 and 415 °C, the model gave slightly lower NO conversion but the difference between the model and experimental data was around 20 ppm even in the region where the highest gap was observed between two data. For 80,000 h^{-1} (STP) standard SCR experiment, we obtained fairly good agreement between the model and the experimental data (Figure 5.12.b). The model slightly under-predicted the outlet NH_3 and NO concentrations between 210 and 290 °C. Nevertheless, concentration profiles of each species was successfully captured by the three-site model for both cases.

Chapter 6

CONCLUSIONS

Selective catalytic reduction of NOx with ammonia (NH_3-SCR) is an effective NOx abatement technology for lean-burn heavy duty vehicles. Development of a detailed kinetic model for NH_3-SCR is important for design and optimization of engine after treatment systems to meet stringent emissions standards. In this study, we developed a kinetic model by considering the external and internal mass transfer limitations on ammonia SCR over a commercial copper-chabazite (Cu-CHA) washcoated monolith catalyst. In the first part of this study, mass transfer limitations for standard SCR reaction in a monolith reactor over a commercial Cu-CHA catalyst were investigated using a one site model. Experiments with varying space velocities (20,000-80,000 h^{-1} (STP) range) were carried out to identify the regions with external mass transfer limitations. NO conversion decreased with increasing flowrate up to 230 °C yet at higher temperatures (>400°C) maximum conversion was obtained at the highest flow rate in the experiments. Therefore, external diffusion limitations are significant for higher temperatures and lower flow rates and the reactor operates in the kinetically controlled region at high flow rates and at low temperatures. Activation energy and pre-exponential factor for the standard SCR reaction were obtained at low temperature interval where no mass transfer limitation exists. Intrinsic kinetic parameters obtained at low temperatures were used to extract external mass transfer coefficients in the mass transfer controlled region. Calculated external mass transfer coefficients are in good agreement with the values obtained from different mass transfer correlations from literature at low temperatures. However, these intrinsic kinetic parameters cannot account for SCR activity at higher temperatures. Accordingly, in the second part, a multi-site kinetic model, in combination with internal and external mass transfer effects, was developed for ammonia SCR of NOx over Cu-CHA. A wide temperature interval (100 to 600 °C) was used in the monolith reactor experiments which include NH_3 adsorption & desorption, NH_3 oxidation, NO oxidation and standard SCR reactions as well as the N_2O formation reactions. NH_3 adsorption and desorption profiles showed good agreement with a kinetic model based on three different sites for ammonia storage on Cu-CHA. These three sites are believed to be sites on which ammonia binds loosely (S3), mono- or di-copper species located near/on 8-membered ring of the chabazite structure and Brönsted sites (S1), and active copper-oxo sites for the high temperature range which consist of copper-oxo oligomers that may form via the increased mobility of copper ions at high temperatures along with the high temperature fraction of the Brönsted sites (S2). Site densities and coefficients of the mass transfer coefficient correlation for square channeled cordierite honeycomb monoliths, ($Sh = A(1 + B(Re)(Sc)(d_h/L))^C$), were regressed from NH_3 adsorption breakthrough and temperature programmed desorption data. The parameters A, B and C in the mass transfer coefficient correlation were found as 3.744, 1.206 and 0.719, respectively. When the same conditions were applied for the presented correlation and correlations in the literature, external mass transfer coefficient results revealed that the mass transfer correlations in the literature are not appropriate for this system. Kinetic parameters for each SCR reactions were also extracted from experimental data. The three site kinetic model is in excellent agreement with the experimental data at a wide temperature range (100 to 600 °C). The three site model also described very well standard SCR reactor effluent composition at different flow rates, which were not considered during the parameter estimation. The findings in this study emphasize the importance of evaluation of mass transfer coefficients from experiments at conditions of interest when testing the SCR reactor performance.

BIBLIOGRAPHY

[1] A. Russell, W.S. Epling, Diesel oxidation catalysts, Catalysis Reviews, 53 (2011) 337-423.

[2] P.S. Metkar, V. Balakotaiah, M.P. Harold, Experimental study of mass transfer limitations in Fe-and Cu-zeolite-based NH 3-SCR monolithic catalysts, Chemical engineering science, 66 (2011) 5192-5203.

[3] I. Nova, L. Lietti, E. Tronconi, P. Forzatti, Transient response method applied to the kinetic analysis of the DeNO x–SCR reaction, Chemical Engineering Science, 56 (2001) 1229-1237.

[4] C. Ciardelli, I. Nova, E. Tronconi, D. Chatterjee, B. Bandl-Konrad, M. Weibel, B. Krutzsch, Reactivity of NO/NO 2–NH 3 SCR system for diesel exhaust aftertreatment: identification of the reaction network as a function of temperature and NO 2 feed content, Applied Catalysis B: Environmental, 70 (2007) 80-90.

[5] G. Madia, M. Koebel, M. Elsener, A. Wokaun, Side reactions in the selective catalytic reduction of NO x with various NO2 fractions, Industrial & Engineering Chemistry Research, 41 (2002) 4008-4015.

[6] J. Dumesic, N.-Y. Topsøe, H. Topsøe, Y. Chen, T. Slabiak, Kinetics of selective catalytic reduction of nitric oxide by ammonia over vanadia/titania, Journal of Catalysis, 163 (1996) 409-417.

[7] E. Tronconi, A. Beretta, The role of inter-and intra-phase mass transfer in the SCR-DeNO x reaction over catalysts of different shapes, Catalysis Today, 52 (1999) 249-258.

[8] H. Sjövall, R.J. Blint, A. Gopinath, L. Olsson, A Kinetic Model for the Selective Catalytic Reduction of NO x with NH3 over an Fe− zeolite Catalyst, Industrial & Engineering Chemistry Research, 49 (2009) 39-52.

[9] F. Gao, Y. Zheng, R.K. Kukkadapu, Y. Wang, E.D. Walter, B. Schwenzer, J. Szanyi, C.H. Peden, Iron Loading Effects in Fe/SSZ-13 NH3-SCR Catalysts: Nature of the Fe Ions and Structure–Function Relationships, ACS Catalysis, 6 (2016) 2939-2954.

[10] A. Grossale, I. Nova, E. Tronconi, Study of a Fe–zeolite-based system as NH 3-SCR catalyst for diesel exhaust aftertreatment, Catalysis Today, 136 (2008) 18-27.

[11] M. Schwidder, S. Heikens, A. De Toni, S. Geisler, M. Berndt, A. Brückner, W. Grünert, The role of NO 2 in the selective catalytic reduction of nitrogen oxides over Fe-ZSM-5 catalysts: active sites for the conversion of NO and of NO/NO 2 mixtures, Journal of Catalysis, 259 (2008) 96-103.

[12] K. Rahkamaa-Tolonen, T. Maunula, M. Lomma, M. Huuhtanen, R.L. Keiski, The effect of NO 2 on the activity of fresh and aged zeolite catalysts in the NH 3-SCR reaction, Catalysis Today, 100 (2005) 217-222.

[13] P.S. Metkar, V. Balakotaiah, M.P. Harold, Experimental and kinetic modeling study of NO oxidation: Comparison of Fe and Cu-zeolite catalysts, Catalysis today, 184 (2012) 115-128.

[14] H. Sjövall, L. Olsson, E. Fridell, R.J. Blint, Selective catalytic reduction of NO x with NH 3 over Cu-ZSM-5—the effect of changing the gas composition, Applied Catalysis B: Environmental, 64 (2006) 180-188.

[15] L. Olsson, K. Wijayanti, K. Leistner, A. Kumar, S.Y. Joshi, K. Kamasamudram, N.W. Currier, A. Yezerets, A multi-site kinetic model for NH 3-SCR over Cu/SSZ-13, Applied Catalysis B: Environmental, 174 (2015) 212-224.

[16] A. Pant, S.J. Schmieg, Kinetic Model of NOx SCR Using Urea on Commercial Cu−Zeolite Catalyst, Industrial & Engineering Chemistry Research, 50 (2011) 5490-5498.

[17] D. Chatterjee, T. Burkhardt, B. Bandl-Konrad, T. Braun, E. Tronconi, I. Nova, C. Ciardelli, Numerical simulation of ammonia SCR-catalytic converters: Model development and application, in, SAE Technical Paper, 2005.

[18] R.Q. Long, R.T. Yang, Superior Fe-ZSM-5 catalyst for selective catalytic reduction of nitric oxide by ammonia, Journal of the American Chemical Society, 121 (1999).

[19] M. Moliner, C. Franch, E. Palomares, M. Grill, A. Corma, Cu–SSZ-39, an active and hydrothermally stable catalyst for the selective catalytic reduction of NO x, Chemical Communications, 48 (2012) 8264-8266.

[20] S. Brandenberger, O. Kröcher, A. Tissler, R. Althoff, The State of the art in selective catalytic reduction of NOx by ammonia using metal‐exchanged zeolite catalysts, Catalysis Reviews, 50 (2008) 492-531.

[21] F. Liu, L. Xie, X. Shi, H. He, Emerging Applications of Environmentally Friendly Zeolites in the Selective Catalytic Reduction of Nitrogen Oxides, in: Zeolites in Sustainable Chemistry, Springer, 2016, pp. 393-434.

[22] A. Shishkin, H. Kannisto, P.-A. Carlsson, H. Härelind, M. Skoglundh, Synthesis and functionalization of SSZ-13 as an NH 3-SCR catalyst, Catalysis Science & Technology, 4 (2014) 3917-3926.

[23] M.Y. Kustova, S.B. Rasmussen, A. Kustov, C.H. Christensen, Direct NO decomposition over conventional and mesoporous Cu-ZSM-5 and Cu-ZSM-11 catalysts: Improved performance with hierarchical zeolites, Applied Catalysis B: Environmental, 67 (2006) 60-67.

[24] M. Berggrund, H.H. Ingelsten, M. Skoglundh, A.E. Palmqvist, Influence of synthesis conditions for ZSM-5 on the hydrothermal stability of Cu-ZSM-5, Catalysis letters, 130 (2009) 79-85.

[25] J. Yan, W. Sachtler, H. Kung, Effect of Cu loading and addition of modifiers on the stability of Cu/ZSM-5 in lean NOx reduction catalysis, Catalysis today, 33 (1997) 279-290.

[26] J.H. Kwak, R.G. Tonkyn, D.H. Kim, J. Szanyi, C.H. Peden, Excellent activity and selectivity of Cu-SSZ-13 in the selective catalytic reduction of NOx with NH 3, Journal of Catalysis, 275 (2010) 187-190.

[27] X. Hu, M. Yang, D. Fan, G. Qi, J. Wang, J. Wang, T. Yu, W. Li, M. Shen, The role of pore diffusion in determining NH 3 SCR active sites over Cu/SAPO-34 catalysts, Journal of Catalysis, 341 (2016) 55-61.

[28] F. Gao, J.H. Kwak, J. Szanyi, C.H. Peden, Current understanding of Cu-exchanged chabazite molecular sieves for use as commercial diesel engine DeNOx catalysts, Topics in Catalysis, 56 (2013) 1441-1459.

[29] F. Gao, N.M. Washton, Y. Wang, M. Kollár, J. Szanyi, C.H. Peden, Effects of Si/Al ratio on Cu/SSZ-13 NH 3-SCR catalysts: Implications for the active Cu species and the roles of Brønsted acidity, Journal of Catalysis, 331 (2015) 25-38.

[30] S.A. Bates, A.A. Verma, C. Paolucci, A.A. Parekh, T. Anggara, A. Yezerets, W.F. Schneider, J.T. Miller, W.N. Delgass, F.H. Ribeiro, Identification of the active Cu site in

standard selective catalytic reduction with ammonia on Cu-SSZ-13, Journal of Catalysis, 312 (2014) 87-97.
[31] J. Xue, X. Wang, G. Qi, J. Wang, M. Shen, W. Li, Characterization of copper species over Cu/SAPO-34 in selective catalytic reduction of NOx with ammonia: Relationships between active Cu sites and de-NOx performance at low temperature, Journal of catalysis, 297 (2013) 56-64.
[32] S.T. Korhonen, D.W. Fickel, R.F. Lobo, B.M. Weckhuysen, A.M. Beale, Isolated Cu 2+ ions: active sites for selective catalytic reduction of NO, Chemical Communications, 47 (2011) 800-802.
[33] C. Paolucci, I. Khurana, A.A. Parekh, S. Li, A.J. Shih, H. Li, J.R. Di Iorio, J.D. Albarracin-Caballero, A. Yezerets, J.T. Miller, Dynamic multinuclear sites formed by mobilized copper ions in NOx selective catalytic reduction, Science, 357 (2017) 898-903.
[34] P.S. Metkar, N. Salazar, R. Muncrief, V. Balakotaiah, M.P. Harold, Selective catalytic reduction of NO with NH 3 on iron zeolite monolithic catalysts: steady-state and transient kinetics, Applied Catalysis B: Environmental, 104 (2011) 110-126.
[35] I. Nova, D. Bounechada, R. Maestri, E. Tronconi, A.K. Heibel, T.A. Collins, T. Boger, Influence of the substrate properties on the performances of NH3-SCR monolithic catalysts for the aftertreatment of diesel exhaust: an experimental and modeling study, Industrial & Engineering Chemistry Research, 50 (2010) 299-309.
[36] R. Hawthorn, Afterburner catalysts-effects of heat and mass transfer between gas and catalyst surface, in: AIChE Symp. Ser, 1974, pp. 428-438.
[37] C. Bennett, R. Hayes, S. Kolaczkowski, W. Thomas, An experimental and theoretical study of a catalytic monolith to control automobile exhaust emissions, in: Proceedings of the Royal Society of London A: Mathematical, Physical and Engineering Sciences, The Royal Society, 1992, pp. 465-483.
[38] E. Tronconi, P. Forzatti, Adequacy of lumped parameter models for SCR reactors with monolith structure, AIChE Journal, 38 (1992) 201-210.
[39] U. Ullah, S. Waldram, C. Bennett, T. Truex, Monolithic reactors: mass transfer measurements under reacting conditions, Chemical Engineering Science, 47 (1992) 2413-2418.

[40] M. Uberoi, C.J. Pereira, External mass transfer coefficients for monolith catalysts, Industrial & engineering chemistry research, 35 (1996) 113-116.

[41] A. Holmgren, B. Andersson, Mass transfer in monolith catalysts–CO oxidation experiments and simulations, Chemical engineering science, 53 (1998) 2285-2298.

[42] J. Votruba, O. Mikuš, K. Nguen, V. Hlaváček, J. Skřivánek, Heat and mass transfer in honeycomb catalysts—II, Chemical Engineering Science, 30 (1975) 201-206.

[43] S.R. Gundlapally, V. Balakotaiah, Heat and mass transfer correlations and bifurcation analysis of catalytic monoliths with developing flows, Chemical engineering science, 66 (2011) 1879-1892.

[44] X. Cheng, X.T. Bi, A review of recent advances in selective catalytic NO x reduction reactor technologies, Particuology, 16 (2014) 1-18.

[45] J. Kašpar, P. Fornasiero, N. Hickey, Automotive catalytic converters: current status and some perspectives, Catalysis Today, 77 (2003) 419-449.

[46] M. Kulazynski, Selective Catalytic Reduction NO by Ammonia Over Ceramic and Active Carbon Based Catalysts, in: Heat Analysis and Thermodynamic Effects, InTech, 2011.

[47] J. Li, H. Chang, L. Ma, J. Hao, R.T. Yang, Low-temperature selective catalytic reduction of NO x with NH 3 over metal oxide and zeolite catalysts—a review, Catalysis Today, 175 (2011) 147-156.

[48] M. Radojevic, Reduction of nitrogen oxides in flue gases, Environmental Pollution, 102 (1998) 685-689.

[49] K. Skalska, J.S. Miller, S. Ledakowicz, Trends in NO x abatement: a review, Science of the Total Environment, 408 (2010) 3976-3989.

[50] S. Roy, M. Hegde, G. Madras, Catalysis for NOx abatement, Applied Energy, 86 (2009) 2283-2297.

[51] K. Packham, Lean-burn engine technology increases efficiency, reduces NOx emissions, Technical Information from Cummins Power Generation, Power Topic, 7009 (2007) 2.

[52] İ.A. Reşitoğlu, K. Altinişik, A. Keskin, The pollutant emissions from diesel-engine vehicles and exhaust aftertreatment systems, Clean Technologies and Environmental Policy, 17 (2015) 15-27.

[53] J.A. Raub, M. Mathieu-Nolf, N.B. Hampson, S.R. Thom, Carbon monoxide poisoning—a public health perspective, Toxicology, 145 (2000) 1-14.
[54] D.B. Kittelson, Engines and nanoparticles: a review, Journal of aerosol science, 29 (1998) 575-588.
[55] T. Lee, J. Park, S. Kwon, J. Lee, J. Kim, Variability in operation-based NO x emission factors with different test routes, and its effects on the real-driving emissions of light diesel vehicles, Science of the Total Environment, 461 (2013) 377-385.
[56] X. Wang, D. Westerdahl, J. Hu, Y. Wu, H. Yin, X. Pan, K.M. Zhang, On-road diesel vehicle emission factors for nitrogen oxides and black carbon in two Chinese cities, Atmospheric Environment, 46 (2012) 45-55.
[57] A. Fritz, V. Pitchon, The current state of research on automotive lean NOx catalysis, Applied Catalysis B: Environmental, 13 (1997) 1-25.
[58] D. Bauner, S. Laestadius, N. Iida, Evolving technological systems for diesel engine emission control: balancing GHG and local emissions, Clean Technologies and Environmental Policy, 11 (2009) 339-365.
[59] Y.-W. Kim, J. Sun, I. Kolmanovsky, J. Koncsol, A phenomenological control oriented lean NOx trap model, in, SAE Technical Paper, 2003.
[60] P. Granger, V.I. Parvulescu, Catalytic NO x abatement systems for mobile sources: from three-way to lean burn after-treatment technologies, Chemical Reviews, 111 (2011) 3155-3207.
[61] Z. Liu, S. Ihl Woo, Recent advances in catalytic DeNOx science and technology, Catalysis Reviews, 48 (2006) 43-89.
[62] F. Klingstedt, K. Arve, K. Eränen, D.Y. Murzin, Toward improved catalytic low-temperature NO x removal in diesel-powered vehicles, Accounts of chemical research, 39 (2006) 273-282.
[63] E. Marceau, X. Carrier, M. Che, O. Clause, C. Marcilly, Ion exchange and impregnation, Handbook of Heterogeneous Catalysis, (2008).
[64] F.-S. Xiao, X. Meng, Zeolites in Sustainable Chemistry: Synthesis, Characterization and Catalytic Applications, Springer, 2015.
[65] S. Roy, T. Bauer, M. Al‐Dahhan, P. Lehner, T. Turek, Monoliths as multiphase reactors: a review, AIChE journal, 50 (2004) 2918-2938.

[66] J.H. Kwak, D. Tran, J. Szanyi, C.H. Peden, J.H. Lee, The effect of copper loading on the selective catalytic reduction of nitric oxide by ammonia over Cu-SSZ-13, Catalysis letters, 142 (2012) 295-301.

[67] J.-S. McEwen, T. Anggara, W. Schneider, V. Kispersky, J. Miller, W. Delgass, F. Ribeiro, Integrated operando X-ray absorption and DFT characterization of Cu–SSZ-13 exchange sites during the selective catalytic reduction of NO x with NH 3, Catalysis today, 184 (2012) 129-144.

[68] T.V. Janssens, H. Falsig, L.F. Lundegaard, P.N. Vennestrøm, S.B. Rasmussen, P.G. Moses, F. Giordanino, E. Borfecchia, K.A. Lomachenko, C. Lamberti, A consistent reaction scheme for the selective catalytic reduction of nitrogen oxides with ammonia, ACS Catalysis, 5 (2015) 2832-2845.

[69] E. Borfecchia, K. Lomachenko, F. Giordanino, H. Falsig, P. Beato, A. Soldatov, S. Bordiga, C. Lamberti, Revisiting the nature of Cu sites in the activated Cu-SSZ-13 catalyst for SCR reaction, Chemical Science, 6 (2015) 548-563.

[70] K.A. Lomachenko, E. Borfecchia, C. Negri, G. Berlier, C. Lamberti, P. Beato, H. Falsig, S. Bordiga, The Cu-CHA deNO x Catalyst in Action: Temperature-Dependent NH3-Assisted Selective Catalytic Reduction Monitored by Operando XAS and XES, Journal of the American Chemical Society, 138 (2016) 12025-12028.

[71] M.H. Groothaert, J.A. van Bokhoven, A.A. Battiston, B.M. Weckhuysen, R.A. Schoonheydt, Bis (μ-oxo) dicopper in Cu-ZSM-5 and its role in the decomposition of NO: A combined in situ XAFS, UV− Vis− Near-IR, and kinetic study, Journal of the American Chemical Society, 125 (2003) 7629-7640.

[72] J.S. Woertink, P.J. Smeets, M.H. Groothaert, M.A. Vance, B.F. Sels, R.A. Schoonheydt, E.I. Solomon, A [Cu2O] 2+ core in Cu-ZSM-5, the active site in the oxidation of methane to methanol, Proceedings of the National Academy of Sciences, 106 (2009) 18908-18913.

[73] E.M.C. Alayon, M. Nachtegaal, A. Bodi, M. Ranocchiari, J.A. van Bokhoven, Bis (μ-oxo) versus mono (μ-oxo) dicopper cores in a zeolite for converting methane to methanol: an in situ XAS and DFT investigation, Physical Chemistry Chemical Physics, 17 (2015) 7681-7693.

[74] S. Grundner, M.A. Markovits, G. Li, M. Tromp, E.A. Pidko, E.J. Hensen, A. Jentys, M. Sanchez-Sanchez, J.A. Lercher, Single-site trinuclear copper oxygen clusters in mordenite for selective conversion of methane to methanol, Nature communications, 6 (2015).

[75] D. Palagin, A.J. Knorpp, A.B. Pinar, M. Ranocchiari, J.A. van Bokhoven, Assessing the relative stability of copper oxide clusters as active sites of a CuMOR zeolite for methane to methanol conversion: size matters?, Nanoscale, 9 (2017) 1144-1153.

[76] P. Tomkins, A. Mansouri, S.E. Bozbag, F. Krumeich, M.B. Park, E.M.C. Alayon, M. Ranocchiari, J.A. van Bokhoven, Isothermal Cyclic Conversion of Methane into Methanol over Copper‐Exchanged Zeolite at Low Temperature, Angewandte Chemie, 128 (2016) 5557-5561.

[77] E.L. Cussler, Diffusion: mass transfer in fluid systems, Cambridge university press, 2009.

[78] R.E. Treybal, Mass transfer operations, New York, (1980).

[79] R.C. Weast, M.J. Astle, W.H. Beyer, CRC handbook of chemistry and physics, CRC press Boca Raton, FL, 1988.

[80] H.S. Fogler, Elements of chemical reaction engineering, (1999).

[81] W.M. Kays, A.L. London, Compact heat exchangers, (1984).

[82] R.K. Shah, A.L. London, Laminar flow forced convection in ducts: a source book for compact heat exchanger analytical data, Academic press, 2014.

[83] O. Levenspiel, C. Levenspiel, Chemical reaction engineering, Wiley New York etc., 1972.

[84] GT-SUITE exhaust aftertreatment application manual, in, Gamma Technologies, 2016.

[85] K. Wijayanti, A. Kumar, S. Joshi, K. Kamasamudram, N.W. Currier, A. Yezerets, L. Olsson, Global kinetic modeling of hydrothermal aging of NH 3-SCR over Cu-zeolites, Applied Catalysis B: Environmental, 163 (2015) 382-392.

[86] S. Malmberg, M. Votsmeier, J. Gieshoff, N. Söger, L. Mußmann, A. Schuler, A. Drochner, Dynamic phenomena of SCR-catalysts containing Fe-exchanged zeolites–experiments and computer simulations, Topics in Catalysis, 42 (2007) 33-36.

[87] E. Tronconi, I. Nova, C. Ciardelli, D. Chatterjee, B. Bandl-Konrad, T. Burkhardt, Modelling of an SCR catalytic converter for diesel exhaust after treatment: Dynamic effects at low temperature, Catalysis Today, 105 (2005) 529-536.

[88] L. Olsson, H. Sjövall, R.J. Blint, A kinetic model for ammonia selective catalytic reduction over Cu-ZSM-5, Applied Catalysis B: Environmental, 81 (2008) 203-217.

[89] H. Sjövall, R.J. Blint, L. Olsson, Detailed kinetic modeling of NH3 and H2O adsorption, and NH3 oxidation over Cu-ZSM-5, The Journal of Physical Chemistry C, 113 (2009) 1393-1405.

[90] K. Kamasamudram, N.W. Currier, X. Chen, A. Yezerets, Overview of the practically important behaviors of zeolite-based urea-SCR catalysts, using compact experimental protocol, Catalysis Today, 151 (2010) 212-222.

[91] M. Colombo, I. Nova, E. Tronconi, A comparative study of the NH 3-SCR reactions over a Cu-zeolite and a Fe-zeolite catalyst, Catalysis Today, 151 (2010) 223-230.

[92] H. Sjövall, E. Fridell, R.J. Blint, L. Olsson, Identification of adsorbed species on Cu-ZSM-5 under NH3 SCR conditions, Topics in Catalysis, 42 (2007) 113-117.

[93] D. Wang, L. Zhang, K. Kamasamudram, W.S. Epling, In situ-DRIFTS study of selective catalytic reduction of NO x by NH3 over Cu-exchanged SAPO-34, Acs Catalysis, 3 (2013) 871-881.

[94] Q. Zhu, J.N. Kondo, T. Tatsumi, S. Inagaki, R. Ohnuma, Y. Kubota, Y. Shimodaira, H. Kobayashi, K. Domen, A comparative study of methanol to olefin over CHA and MTF zeolites, The Journal of Physical Chemistry C, 111 (2007) 5409-5415.

[95] N. Wilken, K. Wijayanti, K. Kamasamudram, N.W. Currier, R. Vedaiyan, A. Yezerets, L. Olsson, Mechanistic investigation of hydrothermal aging of Cu-Beta for ammonia SCR, Applied Catalysis B: Environmental, 111 (2012) 58-66.

[96] O. Mihai, C.R. Widyastuti, A. Kumar, J. Li, S.Y. Joshi, K. Kamasamudram, N.W. Currier, A. Yezerets, L. Olsson, The Effect of NO2/NOx Feed Ratio on the NH3-SCR System Over Cu–Zeolites with Varying Copper Loading, Catalysis letters, 144 (2014) 70-80.

[97] T.C. Watling, M.R. Ravenscroft, G. Avery, Development, validation and application of a model for an SCR catalyst coated diesel particulate filter, Catalysis Today, 188 (2012) 32-41.

[98] R. Hayes, S.T. Kolaczkowski, Mass and heat transfer effects in catalytic monolith reactors, Chemical Engineering Science, 49 (1994) 3587-3599.
[99] P.S. Metkar, M.P. Harold, V. Balakotaiah, Experimental and kinetic modeling study of NH 3-SCR of NOx on Fe-ZSM-5, Cu-chabazite and combined Fe-and Cu-zeolite monolithic catalysts, Chemical engineering science, 87 (2013) 51-66.
[100] H. Huang, R. Long, R. Yang, Kinetics of selective catalytic reduction of NO with NH 3 on Fe-ZSM-5 catalyst, Applied Catalysis A: General, 235 (2002) 241-251.
[101] G.H. Karadag, S.E. Bozbag, D. Sanlı, O. Demir, B. Ozener, G. Hisar, C. Erkey, Mass Transfer Effects in SCR Reactor for NOx Abatement in Diesel Engines, in: I. Dincer, C.O. Colpan, O. Kizilkan (Eds.) Exergetic, Energetic and Environmental Dimensions, Elsevier Science & Technology Books, 2017.
[102] F. Gao, E.D. Walter, E.M. Karp, J. Luo, R.G. Tonkyn, J.H. Kwak, J. Szanyi, C.H. Peden, Structure–activity relationships in NH 3-SCR over Cu-SSZ-13 as probed by reaction kinetics and EPR studies, Journal of catalysis, 300 (2013) 20-29.
[103] S.Y. Joshi, A. Kumar, J. Luo, K. Kamasamudram, N.W. Currier, A. Yezerets, Combined experimental and kinetic modeling study of the bi-modal NO x conversion profile on commercial Cu-SAPO-34 catalyst under standard SCR conditions, Applied Catalysis B: Environmental, 165 (2015) 27-35.
[104] M. Colombo, I. Nova, E. Tronconi, Detailed kinetic modeling of the NH 3–NO/NO 2 SCR reactions over a commercial Cu-zeolite catalyst for diesel exhausts after treatment, Catalysis Today, 197 (2012) 243-255.
[105] O. Mihai, C.R. Widyastuti, S. Andonova, K. Kamasamudram, J. Li, S.Y. Joshi, N.W. Currier, A. Yezerets, L. Olsson, The effect of Cu-loading on different reactions involved in NH 3-SCR over Cu-BEA catalysts, Journal of Catalysis, 311 (2014) 170-181.

APPENDIX-A

RATE OF REACTIONS WITH TIME

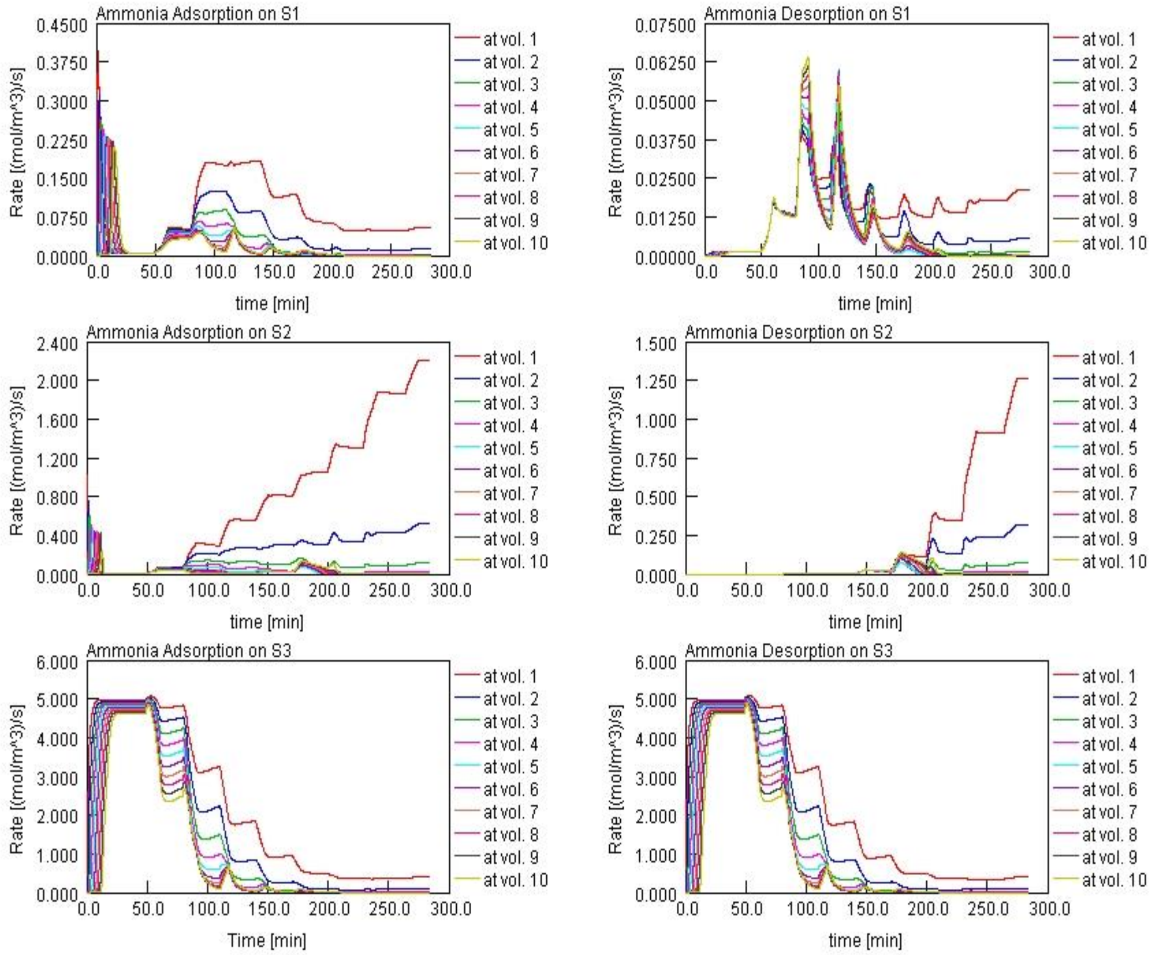

Figure A. 1. Rate of ammonia adsorption and desorption reactions with time (according to the species with stoichiometric coefficient of one)

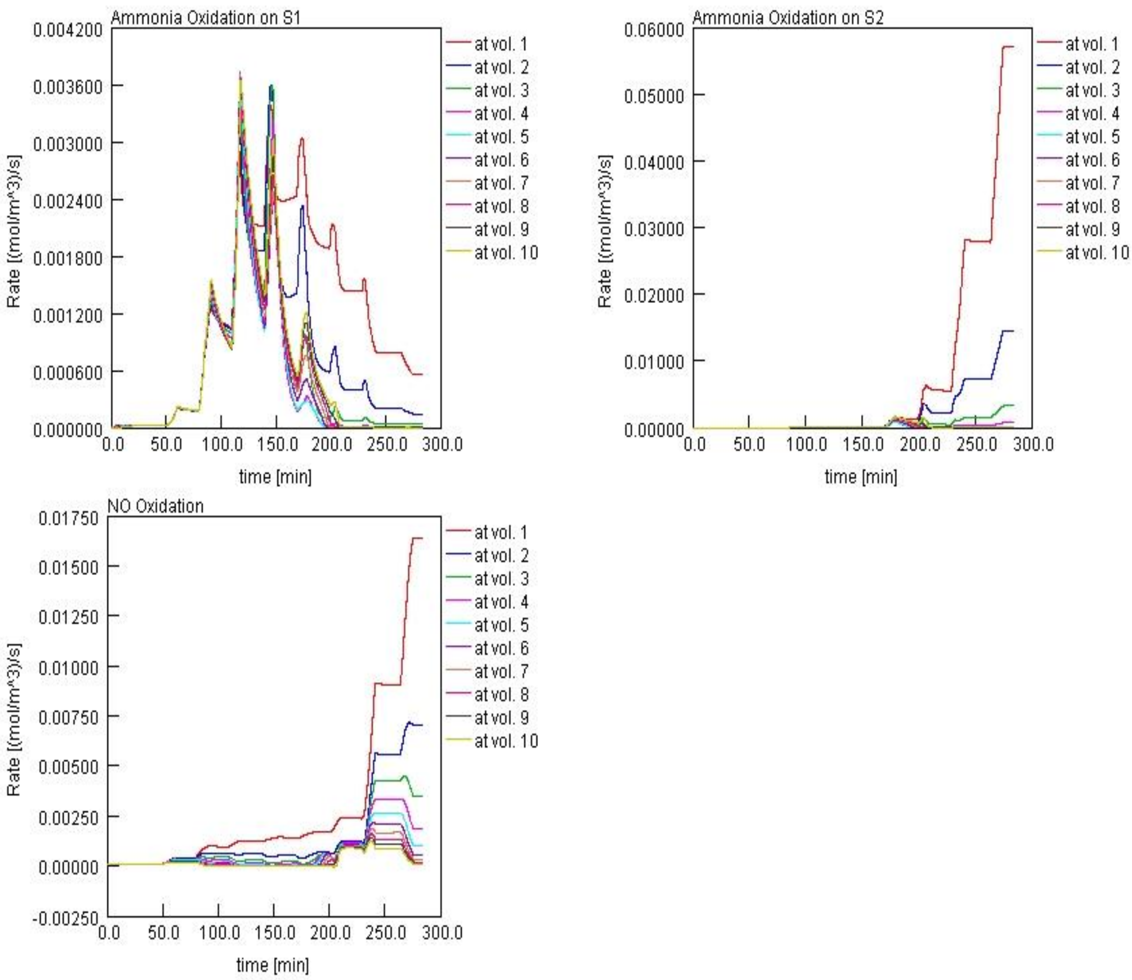

Figure A. 2. Rate of ammonia and NO oxidation reactions with time (according to the species with stoichiometric coefficient of one)

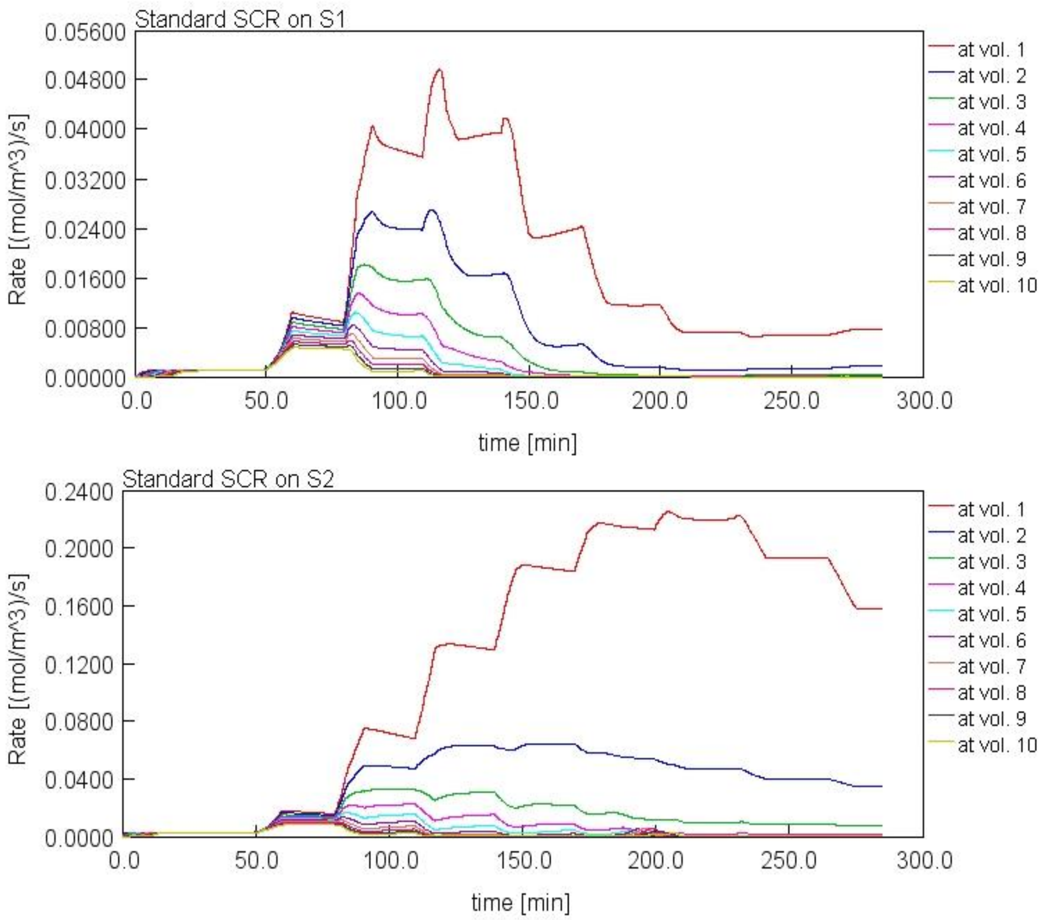

Figure A. 3. Rate of standard SCR reactions with time (according to the species with stoichiometric coefficient of one)

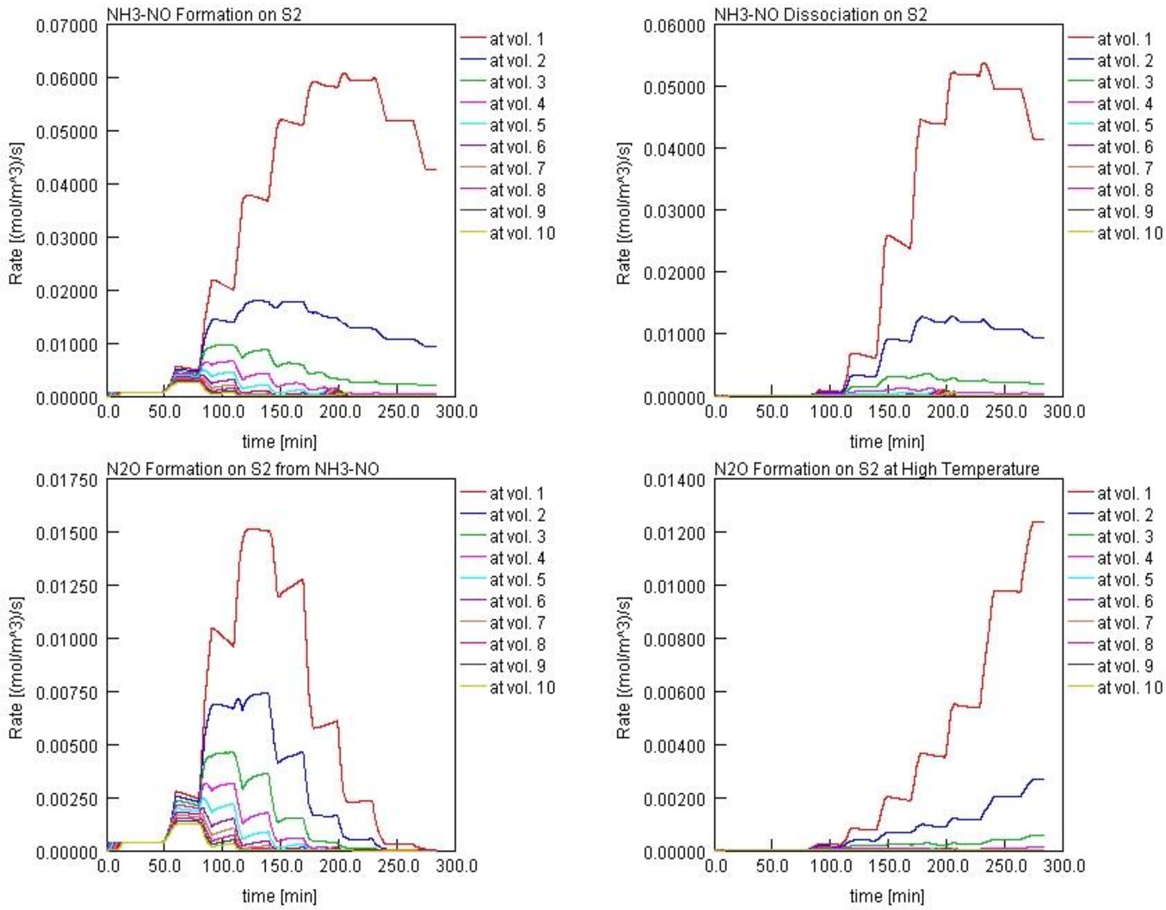

Figure A. 4. Rate of ammonium nitrate type species formation, dissociation and N_2O formation reactions with time (according to the species with stoichiometric coefficient of one)

APPENDIX-B

CHANGE OF CONCENTRATIONS OF SPECIES IN WASHCOAT DURING STANDARD SCR REACTION

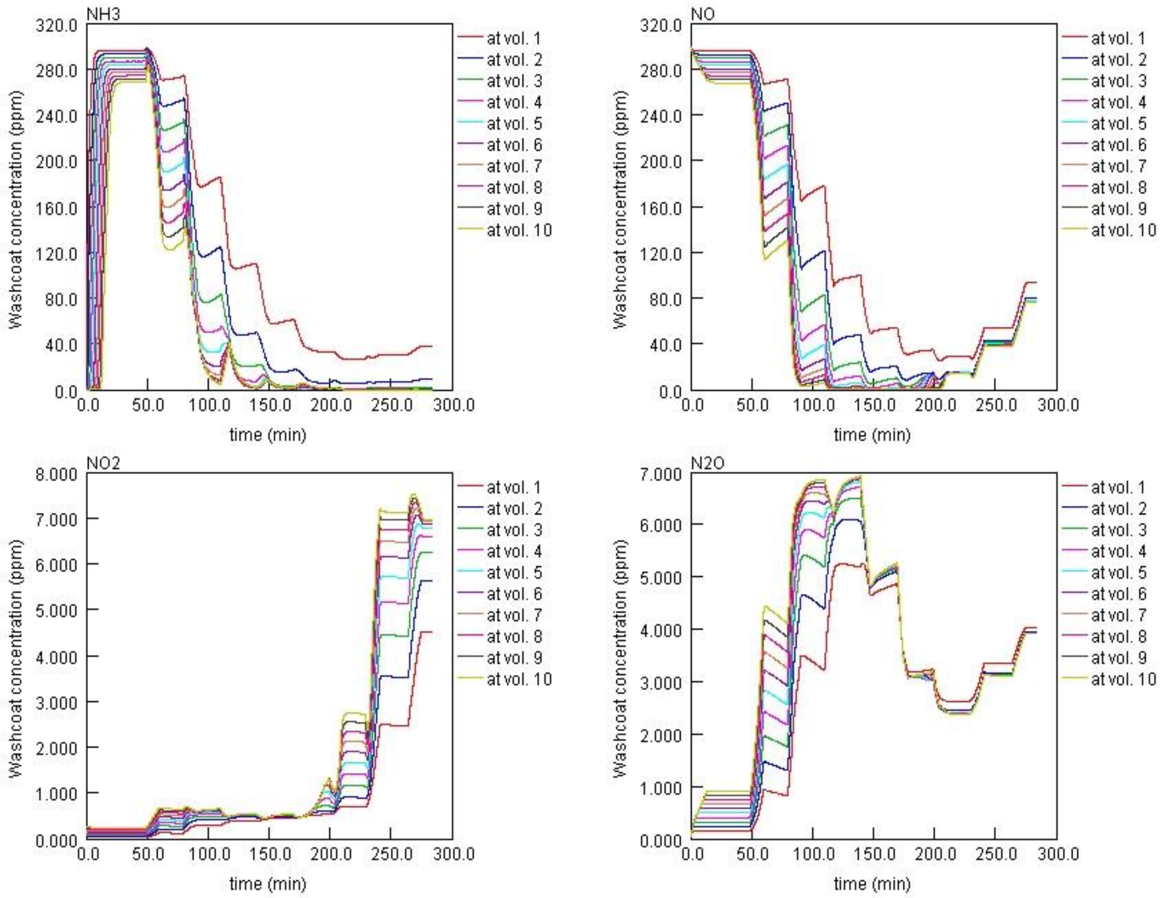

Figure B. 1. Change of concentrations of species (NH_3, NO, NO_2, N_2O) in washcoat during standard SCR reaction